POLITECNICO DI MILANO

Facoltà di Ingegneria Industriale

Corso di Laurea Specialistica in
Ingegneria Spaziale

Optimal Low-Thrust Transfers in Two-Body and Three-Body Dynamics

Relatore: Prof. Franco Bernelli Zazzera
Correlatore: Dr. Roberto Armellin
Dr. Pierluigi Di Lizia

Tesi di laurea di:
Mirco Rasotto Matr. 753683

Anno Accademico 2011 - 2012

Optimal Low-Thrust Transfers in Two-Body and Three-Body Dynamics

Mirco Rasotto

Abstract

The objective of this dissertation is the development of an efficient and robust optimal control algorithm for the design of fuel-optimal low-thrust interplanetary transfers. The solution is obtained with an indirect optimization approach, which has been selected to minimize the number of unknowns and to limit the computational effort. The optimization algorithm can deal with different intermediate conditions, such as flybys, rendezvous, or multiple gravity assists. Moreover, within the formulation adopted, no a priori knowledge of the control structure is required. The application of calculus of variations leads to a Multi Point Boundary Value Problem (MPBVP), characterized by complex inner constraints, which has been solved by means of an indirect multiple shooting method. Some effective techniques to increase the robustness of the algorithm and to overcome numerical difficulties are introduced, followed by the presentation of some test cases to assess the overall performances of the software-tool. Test cases include low-thrust transfers in both two-body and three-body dynamical frameworks.

Keywords: Trajectory Optimization, Low-Thrust, Optimal Control, Multi-Point Boundary Value Problem, Two-Body and Three-Body Dynamics.

Optimal Low-Thrust Transfers in Two-Body and Three-Body Dynamics

Mirco Rasotto

Estratto della Tesi di Laurea

Lo scopo principale di questa tesi è lo sviluppo di un algoritmo efficiente e robusto, per la progettazione e l'ottimizzazione di trasferimenti a bassa spinta, nella dinamica a due e a tre corpi.
Nella prima parte della tesi viene adottata una dinamica a due corpi, largamente utilizzata nella prima fase di progettazione della maggior parte delle missioni spaziali. Utilizzando infatti l'approssimazione patched conics, basata sul concetto di sfere di influenza, è possibile ottenere risultati accettabili anche per quelle traiettorie che coinvolgono più gravity assist. A partire dalle più generali relazioni valide per un sistema a n corpi, vengono quindi ricavate, attraverso opportune semplificazioni, le equazioni di moto per un sistema a due corpi e le relative condizioni al contorno.
Successivamente viene introdotto il problema di controllo ottimo, il cui scopo è quello di ottimizzare il consumo di propellente, ossia minimizzare una funzione di costo $\mathcal{J}$, opportunamente definita. Tuttavia, tale ottimizzazione risulta essere vincolata dalla dinamica stessa del sistema, oltre che, ovviamente, dai vincoli al contorno e da eventuali limiti imposti sull'azione di controllo. In ogni caso, il problema di ottimizzazione vincolata può essere tradotto in uno non vincolato, aggiungendo tali vincoli alla funzione di costo. In particolare il set di equazioni differenziali, rappresentante la dinamica degli stati del sistema, viene aggiunto alla funzione $\mathcal{J}$ attraverso i cosiddetti moltiplicatori di Lagrange o costati, funzioni del tempo. Semplici costanti moltiplicative aggiuntive, sono invece richieste per le condizioni al contorno.
Considerando a questo punto la variazione prima della funzione di costo così aumentata, e uguagliandola a zero, si ottengono le condizioni necessarie per minimizzare tale indice. In primo luogo, si ricavano le condizioni di ottimalità, che definiscono cioè la legge di controllo: nel caso specifico, questa risulta essere di tipo "bang-bang" e la switching function ad essa correlata, dipende sia dagli stati che dai costati. Dall'annullamento di $\delta\mathcal{J}$, si ricava inoltre un nuovo set di

equazioni differenziali, che descrivono la dinamica dei costati e che si aggiungono a quelle per la dinamica degli stati. Pur non essendo di grande rilevanza dal punto di vista fisico, tali equazioni devono essere integrate simultaneamente in quanto il controllo è funzione di entrambi. Da ultimo, si ottengono delle condizioni di trasversalità, che definiscono le condizioni al contorno sui costati. Queste, specialmente per quanto riguarda quelle relative agli incontri intermedi, possono essere di diversi tipi, ed è necessario effettuare un'attenta analisi delle possibili situazioni e dei corrispondenti vincoli da soddisfare.
Il problema di controllo ottimo derivante dal calcolo delle variazioni risulta molto complesso e pertanto sono indispensabili alcune semplificazioni. A questo proposito alcune variabili, come ad esempio la data di lancio e i tempi di volo, vengono mantenute fisse all'interno di tale formulazione, in modo da evitare la nascita di altre condizioni aggiuntive, spesso difficili da valutare e che potrebbero inficiare l'efficienza dell'algoritmo risolutivo. L'ottimizzazione di tali variabili, può in ogni caso essere ottenuta per via numerica, inserendo il problema di controllo ottimo in un problema di ottimizzazione parametrica. Una prima stima di tali variabili di ottimizzazione è quindi necessaria, e a questo proposito, viene utilizzato uno strumento di ottimizzazione di traiettorie che fa uso di algoritmi genetici, già disponibile presso il Dipartimento, in grado di generare una soluzione di primo tentativo.
Per quanto riguarda il problema di controllo ottimo, innestato all'interno del problema di ottimizzazione parametrica, esso viene risolto con un metodo multiple shooting indiretto. Più specificamente, la traiettoria viene divisa in nodi, coincidenti tipicamente ai punti di incontro con i vari corpi celesti, ma che possono, più in generale, comprendere dei punti generici, definiti dall'utente per migliorare la convergenza dell'algoritmo. Ad ogni nodo intermedio è associato un set di variabili di ottimizzazione, un set di condizioni iniziali e uno di vincoli finali. Il problema viene quindi risolto cercando i valori delle variabili di ottimizzazione e delle condizioni iniziali che annullano le violazioni dei vincoli finali. Tale approccio, di fatto trasforma il problema di controllo ottimo in un ulteriore problema di ottimizzazione parametrica, in cui le variabili sono rappresentate dalle incognite corrispondenti a ciascun nodo. Pertanto è possibile inglobare il tutto in un unico problema di ottimizzazione parametrica, risolto poi per mezzo della funzione *fmincon* dell'optimization tool di Matlab.

A questo punto, il problema è discontinuo e genera pertanto delle difficoltà nell'integrazione delle equazioni dinamiche e quindi nel processo di ottimizzazione stesso. Allo scopo di superare tali problematiche, viene utilizzato un metodo di continuazione. In particolare, viene dapprima introdotto e risolto un problema di minima energia, caratterizzato cioè, da un controllo continuo in termini di accelerazione, piuttosto che di spinta discontinua, e da una funzione di costo leggermente diversa rispetto a quella originale. Ciò di fatto, ne facilita la risoluzione. Tale soluzione a minima energia, viene quindi utilizzata come condizione iniziale per la risoluzione del problema di minimo consumo di propellente, caratterizzato da un controllo in termini di spinta, dipendente dal parametro di continuazione p. Il controllo è tuttora continuo, ma all'aumentare di tale parametro, viene gradualmente approssimato il comportamento discontinuo della spinta. L'ultimo passo riguarda la soluzione del problema effettivamente discontinuo.
Le prestazioni dell'algoritmo presentato sono state valutate in una fase intensiva di test, che ne ha dimostrato l'efficacia nel trovare soluzioni accurate. In particolare i test effettuati mostrano come il processo di ottimizzazione implementato sia utilizzabile per progettare diversi tipi di traiettorie di crescente complessità, senza modificarne l'architettura e risultando pertanto applicabile in molte situazioni pratiche.
Nell'ultima parte della tesi, l'approccio è stato esteso alla dinamica dei tre corpi per allargare il ventaglio di missioni progettabili con il software. Orbite come quelle Halo ad esempio, stanno acquisendo sempre maggior interesse dal punto di vista scientifico, a causa della loro particolarità di mantenersi a una distanza fissata dai primari, ideale ad esempio per satelliti di telecomunicazioni o telescopi spaziali. Tuttavia la generazione di tali orbite richiede necessariamente un modello a tre o più corpi, mentre non sono ammissibili in un modello a due corpi.
Il cambiamento delle equazioni di moto, si traduce inevitabilmente in una modifica delle equazioni per i costati e le relative condizioni al contorno, mentre le condizioni sul controllo risultano invariate.
Anche l'approccio risolutivo differisce leggermente da quello introdotto nel caso di dinamica a due corpi, almeno nelle fasi iniziali. La prima fase di ottimizzazione globale, infatti, viene completamente eliminata dal processo risolutivo, in quanto l'algoritmo precedentemente utilizzato, disponibile presso il Politecnico di Milano, non include la dinamica a tre corpi. E' stato verificato inoltre,

che la soluzione di un problema a minima energia risulta scarsamente efficace se utilizzata come soluzione di primo tentativo per il problema di minimo consumo di propellente. Tuttavia, per ottenere la convergenza, rimane comunque forte l'esigenza di avere dei valori di primo tentativo piuttosto accurati, soprattutto per quanto riguarda i valori iniziali dei costati. Questi infatti non sono facilmente intuibili, dato lo scarso significato fisico che ricoprono e pertanto, è necessario un metodo alternativo per la loro determinazione. A questo proposito viene utilizzato un approccio recentemente sviluppato, basato sull'introduzione di nuove variabili di ottimizzazione: gli angoli α e β, indicanti l'orientamento del vettore di spinta rispetto a quello della velocità, le loro rispettive derivate, il valore iniziale della norma dei moltiplicatori di Lagrange per la velocità, λ_{v0} e la sua derivata. Queste quantità, sicuramente dotate di maggior significato fisico, permettono di ottenere, attraverso opportune trasformazioni e sostituzioni, i valori iniziali di $\boldsymbol{\lambda_r}$ e $\boldsymbol{\lambda_v}$. Una volta inizializzati tali parametri, è possibile procedere direttamente alla risoluzione del problema di minimo consumo di propellente, facendo uso, ancora una volta, del metodo di continuazione, per approssimare man mano l'andamento discontinuo della spinta. Il passo finale è quello relativo alla risoluzione del problema discontinuo vero e proprio, come visto già in precedenza. Anche in questo caso, vengono riportati alcuni esempi, per lo più volti a verificare la robustezza dell'algoritmo e valutarne le prestazioni.

Chiaramente, l'algoritmo implementato non è esente da ulteriori possibili miglioramenti. Per esempio, il calcolo analitico dello Jacobiano dei vincoli potrebbe migliorare la convergenza, specialmente per problemi di grandi dimensioni. La formulazione utilizzata, infatti, porta ad una struttura semplificata dello Jacobiano che può quindi essere realizzato fornendo le derivate parziali richieste per via analitica. Il set di vincoli intermedi può essere ulteriormente esteso comprendendo ad esempio i powered gravity assist o le manovre di spazio profondo. In tal caso è necessaria un'attenta analisi delle rispettive condizioni di trasversalità sui costati. Inoltre, potrebbero essere inclusi eventuali vincoli di percorso aggiuntivi, sia sulle variabili di stato sia su quelle di controllo, come ad esempio la possibilità di avere un sistema di propulsione a spinta variabile, a seconda della potenza disponibile.

Infine, il metodo di ottimizzazione proposto nel caso di modello a tre corpi, non fa uso esplicito degli invariant manifolds, pertanto, un ulteriore sviluppo potrebbe

riguardare l'integrazione di queste strutture, al fine di ottenere una soluzione che combini i vantaggi associati ad un trasferimento a bassa energia con quelli tipici dei trasferimenti a bassa spinta.

Parole chiave: Ottimizzazione di traiettorie, propulsione low-thrust, controllo ottimo, dinamica a due e tre corpi.

Acknowledgments

I would like to thank my advisor, prof. Franco Bernelli Zazzera, for his support and for having inspired this work, introducing me to the problem of low-thrust trajectory optimization.

Many thanks to Dr. Roberto Armellin and Dr. Pierluigi Di Lizia. I truly appreciated the amount of time and energy that you invested in guiding me throughout this work, the many precious advices and enriching scientific discussions, your continuing support and your enthusiasm in sharing your knowledge.

I extend my appreciation and sincere thanks to all the professors that I had the pleasure to learn from during the whole study period.

I'm grateful to all my fellow students with whom I have shared these years of both intense study and fun. Among them a special thank goes to Fiorangelo, for being a very good friend rather than simply a colleague; to Cristina and Laura, for your contagious cheerfulness, for inviting me to your wonderful dinners and for your incredible hospitality; to Davide and Alessandro, for having shared with me the alternate fortunes of students life; to all the members of the Apeiron team, for the time spent together and for having made pleasant even the most difficult moments.

Finally I would like to thank those closest to me. A very special thank goes to my family for all the moral and loving support and for their unshakable condifidence in my abilities. Lastly, I would thank all my friends for sharing with me some of the most important moments of my life.

Mirco

Contents

List of Figures

List of Tables

Chapter 1

Introduction

Deep-space exploration missions require large velocity increments and therefore demand for sophisticated and capable propulsion technologies. Most of the missions, carried out so far, have been designed using state-of-the-art high-thrust propulsion technologies (such as chemical propulsion systems) in combination with gravity assist maneuvers, which, however, typically feature inflexible mission profiles, based on isolated, singular events.

In the last few years a growing interest for low-thrust propulsion systems has taken place: first of all their higher specific impulse, compared to the traditional chemical propulsion, allows an increased spacecraft payload ratio. This means also a considerably decreased spacecraft volume, which consequently turns into a reduction of launch vehicle size. Secondary, low-thrust propulsion systems could enhance mission feasibility: by expoiting continuous thrust arcs rather than instantaneous ones, the duration of control increases and the propellant can be used more efficiently.

The recent successful launches of the Deep Space 1 [47], SMART-1 [53], Hayabusa [31] and Dawn [50] missions show that electric propulsion will likely be the preferred option for solar system exploration in the near future, in particular to small bodies.

1.1 Trajectory Optimization for Low-Thrust Space Travel

Spacecraft trajectories in general are obtained from a numerical integration of a set of differential equation describing the system dynamics. These differential equations typically account for inertial force terms as well as force terms due to control variable

inputs.
The optimization problem is to find a control law that minimizes - or equivalently maximizes - an objective function and simultaneously satisfy mission constraints. Generally, optimality is defined with respect to the overall propellant consumption, so the optimal preliminary trajectory design problem aims at reducing the propellant mass required to accomplish the transfer. The performance index is

$$\mathcal{J}_{m_p} = \int_{t_0}^{t_f} \dot{m}_p dt = m_p(t_f) - m_p(t_0), \tag{1.1}$$

where m_p is the propellant mass. Obiouvsly, other performance indices can be defined to include the minimization of the transfer time, or the minimization of hyperbolic excess velocity relative to the arrival or the flyby of a celestial body, or the minimization of the value of the Jacobi constant of a spacecraft in a circular restricted three-body system. Throughout this thesis, however, we faced with the minimum-fuel problem only, so the performance index $\mathcal{J}$ that will be considered, is the one presented in (1.1).

Different strategies can be used to solve the trajectory optimization problem, depending on the spacecraft propulsion system. Traditional chemical propulsion system generates instantaneous high thrust, consequently the duration of control is usually short in comparison of mission time: thrust arcs are therefore modeled as isolated, singular events, justifying the use of discrete optimization theory. Low-thrust propulsion system, on the other side, operates for a significant part of overall trajectory and the control variable needs to be modeled as continuous functions to solve optimal control problem adequately. Therefore, the design and optimization of suitable trajectories is rather difficult for a mission where low-thrust propulsion system is employed, and this represents one of the major challenges for mission designers.

Despite the numerous techniques that have been developed over the years, the methods used to solve the optimal control problem can be summarized in two different philosophies: direct and indirect approaches.

Direct methods parameterize the optimal control problem through discretization and then use nonlinear programming (NLP) to find out the optimal solution. However, the number of design variables for direct methods can become very large, and therefore these problems are limited by current NLP techniques.
Additionally, because direct methods require discretization of a continuous problem, the solution is considered sub-optimal, although the accuracy is generally sufficient for conceptual design. The main advantages of direct method techniques are their increased

computational efficiency and their robust convergence. The solution is not very sensitive to the initial guesses and those initial guesses are physically intuitive. A variety of different direct approaches exist, based on the method used to discretize the problem, including collocation, direct transcription, and differential inclusion [6, 25, 18].

Indirect methods formulate the optimal control problem as a two-point boundary value problem (TPBVP), converted from unconstrained control problems by using the calculus of variations or from constrained control problem by employing Pontryagin's maximum principle (PMP). If a solution to the TPBVP is obtained, the resulting trajectory is the optimal solution for those particular initial conditions and targeting constraints. Indirect methods generally produce more accurate solutions than direct methods, but the convergence domain of trajectory optimization techniques based on calculus of variation tends to be small and heavily depends on the quality of the initial guess of optimization parameters and costate variables, which are generally not physically intuitive [30].
Adding intermediate gravity assists, frequently encountered in mission design of deep space exploration, further increases the sensitivity to the initial guesses and further decreases the convergence domain, since complex inner costraints are added to the problem.

A hybrid formulation, which combines the advantages of both direct and indirect methods, is also possible. As in direct methods, the optimal control problem is first converted in a nonlinear programming problem through a parameterization of all the continuous variables. The approximate solution, provided by the direct method, represents a good first guess to be used in the indirect method: in particular, an approximation of the costates variables (that do not explicitly appear in the direct formulation) can also be obtained according to [62] with an accuracy sufficient to yield the convergence of the indirect method.

1.2 State of the Art

A considerable amount of work has been done in the past concerning the theory and the applications of the optimal control problem: the goal of this section is to give a brief presentation of the most important works related in the field of optimal trajectory optimization along with the most relevant results.

1.2.1 Trajectory Optimization via Indirect Methods

Before the advent of the modern computers, the only optimal control problems that could realistically be solved where those with analytic solutions. The low-thrust trajectory design problem is generally not amenable to analytic solutions and therefore cannot be solved in any practical sense without numerical methods.

Then, in the 1950s and 60s, when the first computers started to appear, the optimal control problem regained interest and many efforts were accomplished by Lawden [33], Marec [34], Jezewsky [28], Sauer [52] and others to apply the well-estabilished principles of calculus of variations [8] specifically to the low-thrust spacecraft trajectory problem.

In 1962, Pontryagin published a work [45] in which he presented the so-called "Pontryagin Minimum Principle"[1] (PMP), that certainly represented a leap forward in the solution of optimal control problem. Indeed it was at the basis, together with the calculus of variations, for the birth of first indirect methods. Some typical uses of calculus of variations and PMP to derive the first-order necessary conditions for the optimal control problem of complex dynamics and constraints can be seen in the publications of Grigoriev [22].

In the same years some interesting results began to appear, based on the PMP, such as the so-called "primer-vector theory" introduced in 1963 by Lawden [33], which state that, to minimize the performance index, the optimal thrust direction, accordingly to the PMP, must lie along the opposite direction of velocity costate vector.
However, when primer vector theory was first introduced, even with a good initial guess, a single solution required considerable computational times. Nevertheless, in these first years indirect methods received much more attention respect to direct approaches, that have begun to be effectively applied only in later years, exploiting the computational speedups. In fact, to the author's best knowledge, early research efforts to develop trajectory optimization tools based on direct methods date back to the 1980s.

Since this early stages, a lot of efforts and researches had been made in the field of indirect methods, which started to be successfully applied to a wide variety of low-thrust trajectory optimization problems. Kechichian [30] analyzed the minimum-time, rendezvous problem for constant acceleration spacecraft based on non-singular, equinoctial orbital elements. Guelman [23] analyzed the related of power limited, minimum time Earth-to-Moon transfers. He considered both Moon impact and Moon injection scenar-

[1] In the Russian literature, it is called the "Pontryagin Maximum Principle" because of a different sign convention used in defining the variational Hamiltonian

ios within the Circular-Restricted Three-Body Problem (CR3BP). The trajectories were obtained by considering a sequence of Two-Body Problems and subsequently patching together the individual trajectory segments. Nah and Vadali [61] first and Casalino and Colasurdo [11] then, treated the optimization problem for a spacecraft with a variable specific impulse propulsion system. Even if this kind of thrusters are currently under development, the authors analysis resulted in an improvement of the performance comparing to the trajectories obtained with constant-specific-impulse thrusters, and are therefore of great interest for future applications.

Despite the much more accurate results in terms of optimality respect to direct methods, indirect methods suffer from numerical difficulties that arise during the integration of Euler-Lagrange differential equations, due to their discontinuous nature. Therefore the single shooting method, based on a Quasi-Newton solver, can have a very poor convergence radius, making it pretty inefficient for the chosen kind of problems if one tries to apply it directly.
Most of the literatures on indirect methods resorted to a solution approaching the optimal one, including assigning a priori the switching structure [32], using the model of fuel consumption rate proportional to the quadratic of thrust magnitude [61], and reducing the dimension of the problem considered [37].
In this regards, Casalino and Colasurdo [13] have developed an indirect method for the optimization of finite-thrust trajectories. This method is based on the preliminary assumption of the switching structure of the control, i.e., the trajectory is divided into an assigned sequence of thrust and coast arcs which join where state or control jumps. The application of the theory of optimal control is strightforward. The resulting boundary value problem is solved using a shooting procedure based on Newton's method.

Alternatives have been proposed, for instance, Bertrand and Epenoy [5] use smoothing techniques to limit numerical issues, and a shooting technique with a continuation method is used to solve the interplanetary transfer problem accurately. More specifically, the optimization process begins with the solution of a related but easier problem, that, for a fuel optimal problem, is typically constructed with the performance index of integral of quadratic of thrust magnitude and consequently called energy-optimal problem. It implies continuous rather than bang-bang optimal control and thus has relatively large convergence radius. Therefore, it is relatively easy to be solved using single shooting methods. Besides the quadratic term, Bertrand and Epenoy [5] considered perturbing the performance index by logarithmic terms, which even imply differentiable optimal controls. A perturbation parameter within the domain $[0, 1]$ is used to connect the fuel-optimal problem (the parameter is equal to 0) with the energy-optimal problem

(the parameter equals 1). Once the energy-optimal problem has been faced, the fuel-optimal problem can be solved by continuosly decreasing the perturbation parameter from 1 to 0 and taking the solution in the current iteration as an initial guess for that in the next one. This approach is quite robust, as the use of the continuation technique generally increases the radius of convergence of Newton-based algorithms, while the control structure does not need to be known or assumed a priori, since it can be determined automatically. The ways of decreasing the parameter to insure convergence, namely the so-called zero path following, includes the discrete continuation method, the piecewise-linear continuation methods and the predictor-corrector continuation methods [24].

Another problem that rises using indirect methods is the very high sensitivity, making them difficult to initialize. Despite the homotopic approach, initial guess for the costates of the energy-optimal problem are still needed. The problem of finding a suitable initial guess for the adjoint states has attracted much attention. In particular, von Stryk and Bulirsch [62] proposed to use both direct and indirect methods combined in a hybrid scheme to overcome the initial guess problem and applied the method to the reentry problem. Further approaches to calculate the adjoint states based on trajectories obtained from direct methods are proposed e.g. by Martell and Lawton [35] and Seywald and Kumar [54]. However, all these approaches still require the direct method to obtain initial near-optimal guesses for the indirect solution.
A different approach to solve the initialization problem, is presented by Haberkorn [24]: the authors introduce another homotopy, exploiting the idea that when the initial and final conditions are the same, the identically null control is a trivial and unique solution. Introducing the homotopic parameter in the initial conditions, throught a discrete continuation, it is possible to find an initial guess for the costates.
The problem of non-intuitive initial guesses has recently been addressed also by Ranieri [46] at the University of Texas at Austin, who employs an adjoint control transformation to give physical meaning to the initial estimates of the costate vector. The main idea is to replace the velocity costates with angles that describe the direction of the thrust. These new unknowns have actual physical significance; therefore intelligent estimates of their initial guesses can be made.
Finally, Sim et al. [55] exploit genetic algorithms (GA) combined to shooting method to solve optimal control problems: indeed GA are able to overcome the disadvantages of the shooting method, searching for a global optimum, and additionally they do not require initial guesses of the solution.

1.2.2 Low-Thrust in n-Body Models

In general, few works have focused on the design of low-thrust trajectories defined in n-body model. The first work facing the combination of a thrust and a n-body ballistic arc was carried out by Belbruno [4]. A spiral arc was linked to a transit orbit that led to an interior ballistic capture at the Moon.
Other examples, concerning transfers to libration point orbits, can be find in Gomez et al. [20] and Howell [27]. They developed transfer trajectories via the stable manifold with impulsive maneuvers in the Sun-Earth/Moon system. Starchville and Melton [57] used a dynamical systems approach and combined a thrust arc with a naturally convergent coast to a libration point orbit. They computed solution in the Earth-Moon circular restricted and elliptic-restricted problem. The benefits of using the stable invariant manifolds have been indagated also by Mingotti [38], by using a direct approach. Similarly, Ozimek and Howell [43] adopted an hybrid approach to solve the TPBVP related to the transfer from Earth parking orbit to the stable manifold.
Topputo [59] indagated the combination of low-thrust trajectory with the benefits of low-energy transfers, such as the ballistic capture or ejection.
Finally Russell [51] developed an efficient low-thrust trade analisys tool. The resolution approach includes a global search for mass optimal solutions, analytic derivatives and a modified adjoint control transformation; practical examples dealing with transfers in the Jupiter-Europa and Earth-Moon restricted three-body problems are investigated by the author.

1.3 Motivations and Goals

Low-thrust propulsion is considered the best option for future interplanetary transfers and the design of low-thrust optimal trajectories is still an open research field, even if lots of works are available in literature, based on direct and indirect methods. Although the efficiency of both methods, the use of an indirect approach seems to be preferable in practical applications, specially in solving high-dimensional optimal control problems. Indeed, even using a state-of-the-art NLP solver, the computation of high accurate trajectory by means of a direct method, is still very expensive in terms of memory allocation and computational burden.
The major goal of this work is therefore the development of a robust and efficient software for the design of low-thrust transfers using indirect methods and with the capability to deal with different kinds of constraints and trasversality conditions, arising for instance from multiple gravity assists or flybys. Four cases have been considered and

developed: intermediate rendezvous, intermediate flyby, intermediate gravity assist and free intermediate points. The last case has been added for generality: indeed we noted that in many situations the convergence of the algorithm can be difficult to achieve, specially when solving long duration or multiple-revolution trajectories, and the optimization process fails. The introduction of this last case allows us to split a trajectory into multiple segments, thus increasing the robustness of the optimization process by solving legs of reduced sensitivity.

The previous analysis of the state-of-the-art has highlighted however some critical points and problems associated to indirect methods. In fact they are typically characterized by excellent convergence properties, specially when the initial guess is near a solution, whereas the convergence radius gradually reduces as the initial guess moves away from the searched trajectory. Moreover, it has been observed that the single shooting method is not suitable for this kind of problems because of the numerical difficulties arising during the integration of Euler-Lagrange differential equations. In lights of these drawbacks, most approaches use continuation methods to address the problem. Typically this process is based on the introduction of a continuation parameter in the performance index. In this context, a new smoothing techinique is exploited, mainly based on the approximation of the discontinuous behaviour of the optimal control function, while keeping the performance index unchanged. This smoothing approximation, proposed in [2], was already tested for planet-to-planet transfers, but needs further efforts to be rigorously developed and validated also for other kinds of transfers.

An important aspect, is that during the development of the optimal control formulation, we assume the hypothesis that the departure, the arrival and the encounter dates are fixed, in order to avoid additional conditions of optimality and simplify the associated Multi-Point Boundary Value Problem (MPBVP). As better described in chapter 3, the optimization of these variables are restored by embedding the multi-point boundary value problem in a parametric optimization problem, in which these mission parameters form the parameter vector. In this way, the algorithm, besides solving the MPBVP, is also able to provide an optimization of the departure date and transfer times. Bearing this in mind, an evaluation of first guesses of these variables (i.e. departure epoch and times of flight) becomes necessary: for this reason another topic faced in this work is represented by the development of a software interface that allows the interaction between our tool and a global optimization algorithm developed by Carrara [9] at Politecnico di Milano. More specifically the global optimizer is used with the aim to quickly identify the potential dates of encounter, to be used as initial guesses for the local optimization algorithm.

The design of low-thrust transfers in the restricted three body problem is an additional

goal of the thesis: this research field is relatively modern and it is particularly attractive since the exploitation of non-keplerian orbits can sensitively reduce the total amount of propellant necessary to carry out an interplanetary transfer [60]. Therefore, the application of the primer-vector control theory to the restricted three-body dynamics is analyzed in the frame of the present thesis, and a practical software extension for the proposed tool is developed for an efficient design of these trajectories.

1.4 Dissertation Overview

The remainder of the thesis is organized as follows:

In the first part of chapter 2, the two-body dynamics is presented, starting from the basic assumptions used throughout the thesis until the derivation of the state differential equations and the corresponding boundary conditions. In the second part of the chapter the optimal control problem is formulated with a mathematically rigorous formalism. The last part of the chapter illustrates the first order necessary conditions, also known as trasversality conditions that arise from the application of the optimal control theory. Particular emphasis is given to four different tipologies of encounter.

Chapter 3 is completely devoted to the illustration of the main numerical techniques developed for the solution of the optimal control problem. In the first sections, the derivation of a first guess solution, the selection of optimization parameters, the description of a energy-optimal problem and finally, the presentation of a continuation method for the solution of a fuel-optimal solution, are introduced. The chapter terminates with an overview of the complete optimization scheme and its principal steps.

Chapter 4 is dedicated to the rigorous validation of the developed algorithm: an extensive test phase, based on problems of increasing complexity, is performed and the performances of the optimization algorithm are examined. The chapter then moves on with further interesting special test cases concerning multiple revolution trajectories. Finally, the problem of finding an optimal trajectory for a Near-Earth Asteroid rendezvous tour, goal of the 3^{rd} Global Trajectory Optimization Competition held in December 2007 at Politecnico di Torino, is presented.

Finally, in chapter 5 an introduction to the low-thrust trajectories defined in n-body models is given and the equations of the restricted three-body problem are derived. Tracing the pattern already seen for the two-body model, the second part of this chapter is devoted to the application of the optimal control theory. The main differences

between two- and three-body model are highlighted and discussed in details. The chapter ends with some test cases assessed to validate the developed algorithm.

Chapter 6 summarizes the results obtained and suggests an outline of possible future developments.

Chapter 2

The Restricted Two-Body Problem

In this chapter the dynamical models and the control techniques are discussed in detail. In particular, the first part of the chapter is dedicated to the introduction of the dynamical equations for the n-body problem. Special emphasis is given to the two-body model that would be widely used throughout the thesis. This dynamical model is characterized by a certain level of approximation that must be considered to perform the design process and therefore is here outlined. The second part of the chapter is devoted to the optimal control problem and its mathematical formulation. Particular attention is given also to the derivation of the first-order necessary conditions for the boundary value problem.

2.1 Equations of Motion

The motion of n mass particles, moving in the three-dimensional space (x, y, z), takes place according to the universal gravitation law, exposed by Newton [40]

$$m_k \ddot{\boldsymbol{r}}_k = \sum_{\substack{j=1 \\ j \neq k}}^{n} G \frac{m_j m_k}{r_{jk}^3} (\boldsymbol{r}_j - \boldsymbol{r}_k), \qquad k = 1, \ldots, n \tag{2.1}$$

where $r_{jk} = \sqrt{(x_j - x_k)^2 + (y_j - y_k)^2 + (z_j - z_k)^2}$ is the distance between two generic particles and G is the universal gravitational constant. The gravitational force is a conservative force, therefore a potential energy can be defined as

$$U = \sum_{\substack{j=1 \\ j \neq k}}^{n} G \frac{m_j m_k}{r_{jk}}, \tag{2.2}$$

so the equations (2.1) can be rewritten as

$$m_k \ddot{\boldsymbol{r}}_k = \nabla U, \qquad k = 1, \ldots, n \tag{2.3}$$

where ∇ denotes the gradient operator.
Equation (2.3) represents a set of $3n$ second-order differential equations or $6n$ first-order differential equations. If $r_{jk} > 0$, then the real-valued function U is Lipschitz continuous and the standard existence and uniqueness theorems for ordinary differential equations can be applied: given $6n$ initial conditions, the solution of the Cauchy problem exists and is unique [7].
When the motion of a massless particle, such as an asteroid or a spacecraft, is considered, the problem becomes the *restricted* n-body problem, since only the motion of the infinitesimal mass is studied. In the restricted n-body problem, the n-1 primaries, for instance the Sun, the planets etc., are assumed to move under their mutual gravitational interactions, while the n-th body, i.e. the spacecraft, moves in the vector field generated by those primaries and does not influence their motion.
Obviously a n-body model, exploiting the simultaneous gravitational attractions, better represents the real solar system dynamics than the simple and well-known two-body model, but at the expense of a more complicated vector field. Therefore, in preliminary studies the spacecraft orbit is still determined by taking into account only one gravitational attraction at the time. Even in the design of complex multiple gravity assist interplanetary trajectory, different conics - solutions of the two-body problems involved in the transfer - are linked together in order to define the whole trajectory. Such method, also known as patched conics, provides accurate preliminary results, introducing the concept of sphere of influence, that is a region of the space where the motion is assumed to be governed by only one primary.
Throughout this work, a two-body model is considered, and only in chapter 5 the optimal control problem subjected to a more complicated three-body dynamics is treated. Under these assumptions, including the patched conics approximation and subsequent neglection of the time spent inside planets' spheres of influence, the differential equations of motion can be rewritten as

$$\ddot{\boldsymbol{r}} = -\frac{\mu}{r^3}\boldsymbol{r}, \tag{2.4}$$

where $\boldsymbol{r}$ denotes the distance between the spacecraft and the primary and μ is the Sun gravitational constant (μ, 1.32712440018 10^{11} km^3/s^2).
If the spacecraft is subject not only to the Sun gravitational attraction, but also to the

thrust of its own electric propulsion system, a controlled two-body problem arises. In particular, two control variables for spacecraft thrust are considered: the engine thrust ratio $u \in [0, 1]$ and the thrust direction $\boldsymbol{\alpha}$. The resulting ODEs system, expressed in the first-order form and including the differential equation for the spacecraft mass, that is no longer constant, is

$$\begin{cases} \dot{\boldsymbol{r}} & = \boldsymbol{v}, \\ \dot{\boldsymbol{v}} & = \boldsymbol{g}(\boldsymbol{r}) + c_1 \dfrac{u}{m} \boldsymbol{\alpha}, \\ \dot{m} & = -c_2 u, \end{cases} \tag{2.5}$$

where $\boldsymbol{g}(\boldsymbol{r}) = -\dfrac{\mu}{r^3}\boldsymbol{r}$, while constants c_1 and c_2 in Eq.(2.5) are defined as

$$\begin{aligned} c_1 &= T_{max}, \\ c_2 &= \frac{T_{max}}{I_{sp} g_0}, \end{aligned}$$

where T_{max} is the maximal thrust magnitude, I_{sp} is the thruster specific impulse and g_0 is the standard acceleration of gravity at sea level (9.80665 m/s^2). For computing convenience, the variables are adimensionalized by astronomycal unit (AU, 149597870.66 km) and spacecraft initial mass (m_0). Through the definition of the reference velocity as $v_{rcf} = \sqrt{\mu/AU}$, the reference time is given by the ratio $t_{rcf} = v_{rcf}/l_{rcf}$.

2.2 Boundary Conditions

Suitable boundary conditions must be imposed at the trajectory extremities. The integration starts (label 0) when the spacecraft leaves the sphere of influence of the departure body, typically the Earth. Thus the spacecraft position coincides with the Earth's position

$$\boldsymbol{r}(t_0) - \boldsymbol{r}_p(t_0) = 0, \tag{2.6}$$

whereas the spacecraft velocity $\boldsymbol{v}(t_0)$ is in general expressed as

$$\boldsymbol{v}(t_0) = \boldsymbol{v}_p(t_0) + v_\infty^0 \boldsymbol{u}_{\alpha,\delta}^0. \tag{2.7}$$

A spherical formulation is introduced by letting $\boldsymbol{u}_{\alpha,\delta}^0$ be the unit vector of polar angles α and δ in the reference frame. The value v_∞^0 represents the maximum velocity amplitude available at the sphere of influence of the departure body ($C_3 = (v_\infty^0)^2$), that should be

specified by the user or alternatively can be retrieved from the global solution. Equation (2.7) involves the fact that the available initial excess velocity will be completely used: this condition, however, occurs in most practical cases, and it can be assumed without a significant loss of generality. Finally, the initial mass coincides with the nominal mass of the spacecraft m_0, thus

$$m(t_0) - m_0 = 0. \tag{2.8}$$

Summarizing, the initial boundary conditions are

$$\boldsymbol{\psi}^0(\boldsymbol{x}(t_0), t_0) = \begin{bmatrix} \boldsymbol{r}(t_0) - \boldsymbol{r}_p(t_0) \\ \boldsymbol{v}(t_0) - \boldsymbol{v}_p(t_0) - v_\infty^0 \boldsymbol{u}_{\alpha,\delta}^0 \\ m(t_0) - m_0 \end{bmatrix} = 0. \tag{2.9}$$

At the final point (label f), boundary conditions are

$$\boldsymbol{\psi}^f(\boldsymbol{x}(t_f), t_f) = \begin{bmatrix} \boldsymbol{r}(t_f) - \boldsymbol{r}_p(t_f) \\ \boldsymbol{v}(t_f) - \boldsymbol{v}_p(t_f) - v_\infty^f \boldsymbol{u}_{\alpha,\delta}^f \end{bmatrix} = 0, \tag{2.10}$$

which can express, a rendezvous ($v_\infty^f = 0$) or a flyby of the arrival celestial body ($v_\infty^f \neq 0$). Obviously, there are no constraints on final mass since it is the performance index that must be maximazed.

2.2.1 Intermediate Constraints

The problem with only initial and arrival constraints defines the so-called planet-to-planet transfer. More complex transfers, which include intermediate gravity assist, flyby or rendezvous, are frequently encountered in the design of interplanetary missions. Each of these intermediate events is characterized by different conditions that need to be taken into account during the optimization process.

Intermediate Flyby

Let us consider first an intermediate flyby, sketched in Figure 2.1. The spacecraft positions just before and after the flyby are both required to be equal to the target body position, and the spacecraft velocity vector just before and after flyby is continuous. This is due to the fact that the encountered body, such as asteroid, comet or small planet, is not able to introduce gravitational effects. Also the mass must be continuous

astride the flyby, because no impulsive maneuvers of the thruster are considered.

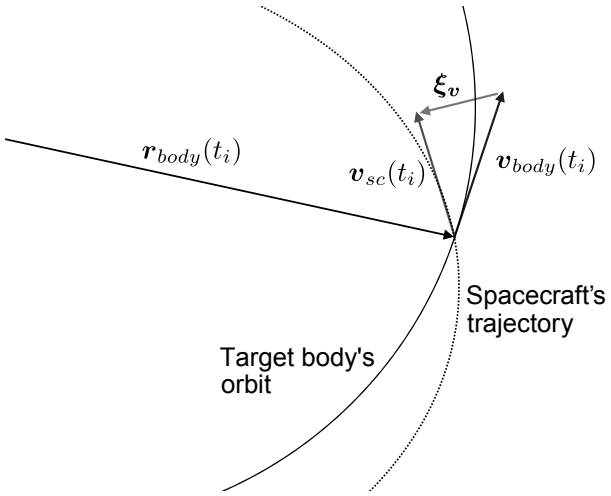

Figure 2.1: Illustration of a flyby maneuver. The vector $\boldsymbol{\xi_v}$ indicates that spacecraft and target body velocity are different.

The complete set of constraints is

$$\boldsymbol{\psi}_i^{flyby}(\boldsymbol{x}(t_i), t_i) = \begin{bmatrix} \boldsymbol{r}(t_i^-) - \boldsymbol{r}_p^i(t_i) \\ \boldsymbol{r}(t_i^+) - \boldsymbol{r}(t_i^-) \\ \boldsymbol{v}(t_i^+) - \boldsymbol{v}(t_i^-) \\ m(t_i^+) - m(t_i^-) \end{bmatrix} = 0, \tag{2.11}$$

where $\boldsymbol{x} = [\boldsymbol{r}, \boldsymbol{v}, m]$ and superscripts $+$ and $-$ denote, respectively, the state immediately before and after the flyby at time t_i. These constraints impose the continuity of the state of the spacecraft, and are in general the simplest among all intermediate conditions.

Intermediate Rendezvous

Rendezvous is a maneuver which takes a spacecraft and another orbital body, that could be an asteroid, a planet but also another spacecraft, originally moving on different orbits, to the same final reference orbit, matching their positions and velocities, see Figure 2.2. Therefore, during an intermediate rendezvous, the conditions are very similar to those already seen for intermediate flyby: in particular, the spacecraft positions just before and after the flyby are still required to be equal to the target body position, but in this case also the velocity of the spacecraft is constrained to match the velocity of the target object. The mass is required to be continuous astride the maneuver.

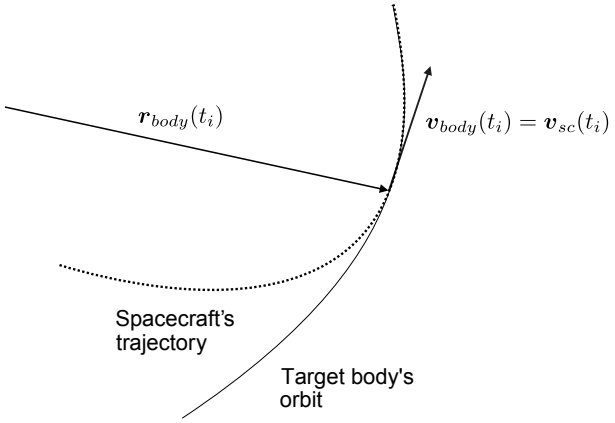

Figure 2.2: Illustration of a rendezvous maneuver.

The complete set of constraints is given by

$$\boldsymbol{\psi}_i^{rdv}(\boldsymbol{x}(t_i), t_i) = \begin{bmatrix} \boldsymbol{r}(t_i^-) - \boldsymbol{r}_p^i(t_i) \\ \boldsymbol{r}(t_i^+) - \boldsymbol{r}(t_i^-) \\ \boldsymbol{v}(t_i^-) - \boldsymbol{v}_p^i(t_i) \\ \boldsymbol{v}(t_i^+) - \boldsymbol{v}(t_i^-) \\ m(t_i^+) - m(t_i^-) \end{bmatrix} = 0. \tag{2.12}$$

Intermediate Gravity Assist

Let us consider now the gravity assist maneuver: in particular, the unpowered gravity assist model is used. As already stated in previous cases, the spacecraft positions just before and after the maneuver must be continuous and equal to the planet position. The spacecraft velocity relative to the planet, when spacecraft is far from the planet, is called the hyperbolic excess velocity, denoted by $\boldsymbol{v}_\infty$. Its magnitude must be unaltered, if unpowered gravity assists are considered, while there are no constraints on the absolute velocity $\boldsymbol{v}$. Mass is continuous astride the gravity assist, as in the previous cases.
Using the patched conics approximation, the time spent inside the planetary sphere of influence is neglected, while two subsequent heliocentric ellipses must be matched together. The pericenter radius of the hyperbolic planetocentric trajectory r_{ph} linking the two heliocentric arcs must therefore be evaluated. Starting from the turn angle δ_{ga}, that indicates the rotation of $\boldsymbol{v}_\infty$ during the gravity assist

$$\delta_{ga} = \frac{1}{2} \arccos\left(\frac{\boldsymbol{v}_\infty^- \cdot \boldsymbol{v}_\infty^+}{|\boldsymbol{v}_\infty^-||\boldsymbol{v}_\infty^+|} \right), \tag{2.13}$$

the eccentricity can be derived

$$e = \frac{1}{\sin \delta_{GA}} \tag{2.14}$$

and finally

$$r_{ph} = \frac{\mu_p}{v_\infty^2}(e-1). \tag{2.15}$$

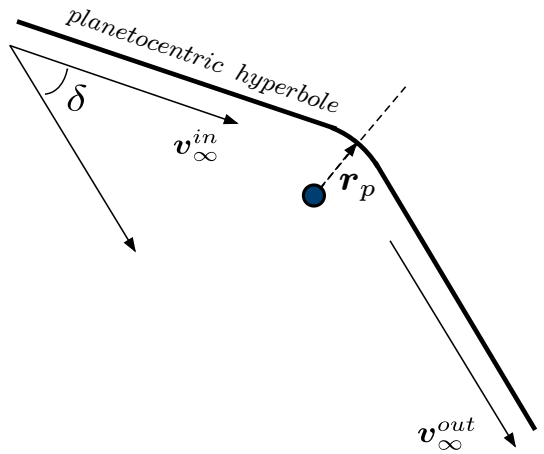

Figure 2.3: Illustration of an unpowered gravity assist maneuver.

However, the minimum gravity assist altitude is conservatively limited to 200 km at each terrestrial planet and Pluto, while altitudes as low as 5 Jovian radii at Jupiter (in order to avoid radiation), 2 planetary radii at Saturn and one planetary radius at Uranus and Neptune (to avoid rings) are permitted. The resulting values of the minimum pericenter radii considered for the gravity assists are given in Table 2.1.

Table 2.1: Minimum pericenter radii.

	M	V	E	M	J	S	U	N	P
$r_{ph_{min}}$ $[km]$	2640	6252	6578	3596	357450	120540	51120	49520	1395

Summarizing, the constraints for gravity assist maneuvers are formulated as

$$\boldsymbol{\psi}_i^{ga}(\boldsymbol{x}(t_i), t_i) = \begin{bmatrix} \boldsymbol{r}(t_i^-) - \boldsymbol{r}_p^i(t_i) \\ \boldsymbol{r}(t_i^+) - \boldsymbol{r}(t_i^-) \\ v_\infty(t_i^+) - v_\infty(t_i^-) \\ m(t_i^+) - m(t_i^-) \end{bmatrix} = 0 \tag{2.16}$$

and the inequality constraints on the pericenter radius

$$r_{ph_{min}} - r_{ph} \leq 0. \tag{2.17}$$

Free Intermediate Points

This last case has been added for generality and it is quite different respect to the previous ones, because it does not involve necessarily an encounter with an orbital body. As already pointed out, it is one of splitting the trajectory into multiple segments and is particularly useful when solving long duration, multirevolution or very sensitive trajectories. The conditions arising from this case are very similar to the intermediate flyby and rendezvous ones, but with the difference that the position $\boldsymbol{r}(t_i)$ is never imposed: in fact the spacecraft position vector, as well as the velocity vector and mass, are only required to be continuous just before and after the intermediate points.
Therefore constraints can be summarized as

$$\boldsymbol{\psi}_i^{fip}(\boldsymbol{x}(t_i), t_i) = \begin{bmatrix} \boldsymbol{r}(t_i^+) - \boldsymbol{r}(t_i^-) \\ \boldsymbol{v}(t_i^+) - \boldsymbol{v}(t_i^-) \\ m(t_i^+) - m(t_i^-) \end{bmatrix} = 0. \tag{2.18}$$

2.3 Optimal Control Problem

In this section we recollect some notions of the optimal control theory and develop step by step the problem for the trajectory optimization, starting from the simple problem with fixed terminal time and no path constraints.
The goal of the optimal control problem is to find the optimal control input $\boldsymbol{u}$ for a generally nonlinear system such that the associated performance index

$$\mathcal{J} = \int_{t_0}^{t_f} \mathcal{L}(\boldsymbol{x}, \boldsymbol{u}, t) dt \tag{2.19}$$

is minimized, and such that the constraints at final time t_f

$$\boldsymbol{\psi}^f(\boldsymbol{x}(t_f), t_f) = 0 \quad \text{q equations}, \tag{2.20}$$

is satisfied. In equations (2.19) and (2.20) $\boldsymbol{x}$ is the n-dimensional state vector, $\boldsymbol{u}$ is the m-dimensional control vector and $\mathcal{L}$ is the accumulated cost. Instead of solving a

constrained optimization problem, it is advantageous to consider the corresponding unconstrained optimization problem, defined by adjoining the system differential equations and the terminal constraints to the performance index through the Lagrange multiplier functions $\boldsymbol{\lambda}(t)$, and through a multiplier vector $\boldsymbol{\nu}$ (a q-vector of constant scalar values), respectively:

$$\mathcal{J} = \boldsymbol{\nu}^T \boldsymbol{\psi}^f(\boldsymbol{x}(t_f), t_f) + \int_{t_0}^{t_f} \left\{ \mathcal{L}(\boldsymbol{x}, \boldsymbol{u}, t) + \boldsymbol{\lambda}^T (\boldsymbol{f}(\boldsymbol{x}, \boldsymbol{u}, t) - \dot{\boldsymbol{x}}) \right\} dt. \tag{2.21}$$

We define the Hamiltonian function $\mathcal{H}$ as

$$\mathcal{H} = \mathcal{L} + \boldsymbol{\lambda}^T \boldsymbol{f}. \tag{2.22}$$

If the generally nonlinear system represents the motion of a spacecraft produced by a two body gravitational interaction and thrust acceleration, Eq. (2.5), the Hamiltonian becomes

$$\mathcal{H} = \boldsymbol{\lambda_r} \cdot \boldsymbol{v} + \boldsymbol{\lambda_v} \cdot \left(-\frac{\mu}{r^3} \boldsymbol{r} + c_1 \frac{u}{m} \boldsymbol{\alpha} \right) - \lambda_m c_2 u + c_2 u, \tag{2.23}$$

being $\mathcal{L} = c_2 u$ (in minimum-fuel consumption problem).

We can now rewrite (2.21) as

$$\mathcal{J} = \boldsymbol{\nu}^T \boldsymbol{\psi}^f(\boldsymbol{x}(t_f), t_f) + \int_{t_0}^{t_f} \left\{ \mathcal{H} - \boldsymbol{\lambda}^T \dot{\boldsymbol{x}} \right\} dt. \tag{2.24}$$

In order to obtain the necessary optimality conditions we follow the analysis of Pontryagin et al. [45] and consider the variation in the augmented performance index due to variations in the control vector $\boldsymbol{u}(t)$ for fixed times t_0 and t_f,

$$\delta \mathcal{J} = \boldsymbol{\nu}^T \boldsymbol{\psi}_x^f \delta \boldsymbol{x} \big|_{t_f} + \delta \boldsymbol{\nu}^T \boldsymbol{\psi}^f + \\ + \int_{t_0}^{t_f} \left\{ \mathcal{H}_x^T \delta \boldsymbol{x} + \mathcal{H}_u^T \delta \boldsymbol{u} - \boldsymbol{\lambda}^T \delta \dot{\boldsymbol{x}} + \delta \boldsymbol{\lambda}^T [\mathcal{H}_\lambda - \dot{\boldsymbol{x}}] \right\} dt. \tag{2.25}$$

Integrating by parts, we obtain

$$\int_{t_0}^{t_f} \boldsymbol{\lambda}^T \delta \dot{\boldsymbol{x}} dt = \boldsymbol{\lambda}^T \delta \boldsymbol{x} \big|_{t_0}^{t_f} - \int_{t_0}^{t_f} \dot{\boldsymbol{\lambda}}^T \delta \boldsymbol{x} dt, \tag{2.26}$$

and then

$$\delta\mathcal{J} = \left[\boldsymbol{\nu}^T\boldsymbol{\psi}_x^f - \boldsymbol{\lambda}^T\right]\delta\boldsymbol{x}\Big|_{t_f} + \boldsymbol{\lambda}^T\delta\boldsymbol{x}\Big|_{t_0} + \delta\boldsymbol{\nu}^T\boldsymbol{\psi}^f + \\ + \int_{t_0}^{t_f}\left\{\left(\mathcal{H}_x + \dot{\boldsymbol{\lambda}}\right)^T\delta\boldsymbol{x} + \mathcal{H}_u^T\delta\boldsymbol{u} + \left(\mathcal{H}_\lambda - \dot{\boldsymbol{x}}\right)^T\delta\boldsymbol{\lambda}\right\}dt. \quad (2.27)$$

The necessary condition for the augmented performance index to be minimized is that the first variation of $\mathcal{J}$ equals zero, $\delta\mathcal{J} = 0$. This condition is satisfied by setting to zero the coefficient of arbitrary increments $\delta\boldsymbol{x}$, $\delta\boldsymbol{u}$, $\delta\boldsymbol{\lambda}$ and $\delta\boldsymbol{\nu}$. Thus, from eq. (2.27) we derive the well-known Euler-Lagrange equations and the associated boundary conditions known as trasversality conditions

$$\begin{aligned}
\dot{\boldsymbol{x}} &= \mathcal{H}_\lambda, && (2.28)\\
\dot{\boldsymbol{\lambda}} &= -\mathcal{H}_x, && (2.29)\\
\mathcal{H}_u &= 0, && (2.30)\\
\boldsymbol{\psi}^f &= 0, && (2.31)\\
\boldsymbol{\lambda}^T(t_f) &= \boldsymbol{\nu}^T\boldsymbol{\psi}_x^f. && (2.32)
\end{aligned}$$

Note that $\boldsymbol{x}(t_0)$ is assumed to be known (or fixed), therefore its variation is equal to zero.

Optimal control law follows directly from Eq. (2.30), that is an application of Pontryagin maximum principle: a more general expression is in fact

$$\boldsymbol{u} = \arg\min_{\boldsymbol{u}\in U} H(\boldsymbol{x}, \boldsymbol{\lambda}, \boldsymbol{u}, t), \quad (2.33)$$

where U defines the domain of feasible controls.

Equation (2.29) represents the costate differential equations, that in the specific case of spacecraft trajectory yields

$$\dot{\boldsymbol{\lambda}} = -\mathcal{H}_x = \begin{cases} \dot{\boldsymbol{\lambda}}_r = \dfrac{\mu}{r^3}\boldsymbol{\lambda}_v - \dfrac{3\mu\boldsymbol{r}\cdot\boldsymbol{\lambda}_v}{r^5}\boldsymbol{r}, \\ \dot{\boldsymbol{\lambda}}_v = -\boldsymbol{\lambda}_r, \\ \dot{\lambda}_m = -c_1\dfrac{u}{m^2}\lambda_v. \end{cases} \quad (2.34)$$

Even if they are of secondary interest from practical point of view, costate equations must be integrated simultaneously with state equations since the optimal control law is function of both. Boundary conditions are splitted between state and costate variables

as can be seen from eqs. (2.31) and (2.32). In particular, if the problem is characterized also by constraints at initial time t_0, eq. (2.24) becomes

$$\mathcal{J} = \boldsymbol{\nu}_0^T \boldsymbol{\psi}^0(\boldsymbol{x}(t_0), t_0) + \boldsymbol{\nu}_f^T \boldsymbol{\psi}^f(\boldsymbol{x}(t_f), t_f) + \int_{t_0}^{t_f} \{\mathcal{H} - \boldsymbol{\lambda}^T \dot{\boldsymbol{x}}\} dt. \tag{2.35}$$

Integrating by parts and differentiating as seen before, the following boundary conditions are derived in addition to (2.28)-(2.30)

$$\begin{aligned} \boldsymbol{\psi}^0 &= 0, & (2.36)\\ \boldsymbol{\lambda}^T(t_0) &= -\boldsymbol{\nu}_0^T \boldsymbol{\psi}_x^0, & (2.37)\\ \boldsymbol{\psi}^f &= 0, & (2.38)\\ \boldsymbol{\lambda}^T(t_f) &= \boldsymbol{\nu}_f^T \boldsymbol{\psi}_x^f. & (2.39) \end{aligned}$$

Substituting equation (2.9) into (2.37) we obtain

$$\boldsymbol{\lambda}_{\boldsymbol{r}_0}^T = -\boldsymbol{\nu}_{01}^T \frac{\partial(\boldsymbol{r}(t_0) - \boldsymbol{r}_p(t_0))}{\partial \boldsymbol{r}(t_0)}, \tag{2.40}$$

$$\boldsymbol{\lambda}_{\boldsymbol{v}_0}^T = -\boldsymbol{\nu}_{02}^T \frac{\partial(\boldsymbol{v}(t_0) - \boldsymbol{v}_p(t_0) - v_\infty^0 \boldsymbol{u}_{\alpha,\delta})}{\partial \boldsymbol{v}(t_0)}, \tag{2.41}$$

$$\lambda_{m_0} = -\nu_{03} \frac{\partial(m(t_0) - m_0))}{\partial m(t_0)}, \tag{2.42}$$

where

$$\boldsymbol{\nu}_0 = [\boldsymbol{\nu}_{01}^T, \boldsymbol{\nu}_{02}^T, \nu_{03}]^T. \tag{2.43}$$

Equation (2.40) tells that the position Lagrange multipliers $\boldsymbol{\lambda}_r(t_0)$ are free, as we expected, since the spacecraft initial position vector is fixed. Similarly, from (2.42), the mass multiplier is free, indeed the initial mass is fixed and equal to m_0. Regarding equation (2.41) some other considerations are necessary: indeed, if $v_\infty^0 = 0$, it becomes

$$\boldsymbol{\lambda}_{\boldsymbol{v}_0}^T = -\boldsymbol{\nu}_{02}^T \frac{\partial(\boldsymbol{v}(t_0) - \boldsymbol{v}_p(t_0))}{\partial \boldsymbol{v}(t_0)}, \tag{2.44}$$

which in turn, means the initial velocity $\boldsymbol{v}(t_0)$ is known and fixed, and the corresponding multipliers are free, as seen for the position and mass ones. If, instead, $v_\infty^0 \neq 0$, equation (2.7) is still in force, but, with a more careful analysis it can be inferred that it is in reality a scalar constraint on the magnitude of initial velocity, i.e

$$\|\boldsymbol{v}(t_0) - \boldsymbol{v}_p(t_0)\| - v_\infty^0 = 0. \tag{2.45}$$

Thus, the relation (2.41) leads to a transversality constraint on the velocity multipliers:

$$\boldsymbol{\lambda_v}(t_0) = \nu_{02}\frac{\boldsymbol{v}(t_0) - \boldsymbol{v}_p(t_0)}{\sqrt{(\boldsymbol{v}(t_0) - \boldsymbol{v}_p(t_0))^2}} = \nu_{02}v_\infty^0\boldsymbol{u}_{\alpha,\delta}, \tag{2.46}$$

which states the initial velocity costate vector must be parallel to the departure excess velocity vector, while the velocity vector $\boldsymbol{v}(t_0)$ is free.
At terminal time, spacecraft position is always fixed and equal to the target body, so that $\boldsymbol{\lambda_r}(t_f)$ vector is free. Pertaining the terminal spacecraft velocity, two possibilities are available: if the final maneuver is a rendezvous with the arrival body, then $\boldsymbol{v}(t_f)$ is fixed and equal to the arrival body velocity, while the corresponding Lagrange multipliers are free. If on the contrary a flyby of the arrival body has to be performed, then $v_\infty^f \neq 0$: the velocity vector $\boldsymbol{v}(t_f)$ is free while velocity costate must satisfy

$$\boldsymbol{\lambda_v}(t_f) = -\nu_{f2}\frac{\boldsymbol{v}(t_f) - \boldsymbol{v}_p(t_f)}{\sqrt{(\boldsymbol{v}(t_f) - \boldsymbol{v}_p(t_f))^2}} = \nu_{f2}v_\infty^f\boldsymbol{u}_{\alpha,\delta}^f, \tag{2.47}$$

where ν_{f2} refers to the second component of vector $\boldsymbol{\nu}_f$, as already seen for the initial boundary conditions (eq. (2.43)). In both cases, final mass is free since it is the optimization index. The corresponding costate is

$$\lambda_m(t_f) = 0. \tag{2.48}$$

In summary, state (2.5) and costate equations (2.34) combined with a set of boundary conditions yield a Two-Point-Boundary-Value-Problem (TPBVP).

2.3.1 Inequality constraints on the control variables

If the optimal problem is also subjected to equality/inequality constraints on the control variables, additional considerations are necessary. Suppose, for example, the following general inequality constraint on the control variables

$$\boldsymbol{C}(\boldsymbol{u}, t) \leq 0, \tag{2.49}$$

where $\boldsymbol{C} = \{C_1, C_2, \ldots, C_q\}$, can be imposed. Following procedures identical to those explained for terminal constraints, we adjoin (2.49) to the performance index, but since the constraint apply over the whole trajectory, it is included inside the integral

$$\mathcal{J} = \boldsymbol{\nu}^T\boldsymbol{\psi}(\boldsymbol{x}(t_f), t_f) + \int_{t_0}^{t_f}\left\{\mathcal{L}(\boldsymbol{x}, \boldsymbol{u}, t) + \boldsymbol{\lambda}^T(\boldsymbol{f}(\boldsymbol{x}, \boldsymbol{u}, t) - \dot{\boldsymbol{x}}) + \boldsymbol{\mu}^T\boldsymbol{C}(\boldsymbol{u}, t)\right\}dt. \tag{2.50}$$

Defining the Hamiltonian function $\mathcal{H}$ as

$$\mathcal{H} = \mathcal{L} + \boldsymbol{\lambda}^T \boldsymbol{f} + \boldsymbol{\mu}^T \boldsymbol{C}(\boldsymbol{u}, t), \tag{2.51}$$

we obtain a change in the optimality condition due to the additional term

$$0 = \mathcal{H}_u = \boldsymbol{\lambda}^T \boldsymbol{f}_u + \mathcal{L}_u + \boldsymbol{\mu}^T \boldsymbol{C}_u. \tag{2.52}$$

All other equations remain unchanged. In low-thrust trajectory optimization problems, this kind of constraint frequently appears as a result of the propulsion system technology, that imposes limits on the control. As we have already seen in section 2.1, the control variable $\boldsymbol{u}$ consists of the unit vector of thrust direction $\boldsymbol{\alpha}$ and the thrust ratio u

$$\boldsymbol{u} = u\boldsymbol{\alpha}. \tag{2.53}$$

In this case the limits on the control are therefore

$$u \leq 1, \tag{2.54}$$

$$\boldsymbol{\alpha} \cdot \boldsymbol{\alpha} - 1 = 0. \tag{2.55}$$

The Hamiltonian can be expressed as

$$\mathcal{H} = \mathcal{L} + \boldsymbol{\lambda}^T \boldsymbol{f} + \mu_1 C_1(\boldsymbol{\alpha}) + \mu_2 C_2(u), \tag{2.56}$$

where

$$\mu_2 \begin{cases} \geq 0, & C_2(u) = 0, \\ = 0, & C_2(u) < 0. \end{cases} \tag{2.57}$$

The optimality condition (2.52) is

$$\mathcal{H}_u = 0 \Rightarrow \begin{cases} \dfrac{\partial \mathcal{H}}{\partial \boldsymbol{\alpha}} = 0, \\ \dfrac{\partial \mathcal{H}}{\partial u} = 0. \end{cases} \tag{2.58}$$

The first one leads to

$$\frac{\partial \mathcal{H}}{\partial \boldsymbol{\alpha}} = \boldsymbol{\lambda}_v \frac{c_1 u}{m} - 2\mu_1 \boldsymbol{\alpha} = 0 \tag{2.59}$$

and indicates that either $\boldsymbol{\lambda}_v$ is parallel to $\boldsymbol{\alpha}$ or u and μ_1 are zero or $\boldsymbol{\lambda}_v$ and μ_1 are zero. Because the latter two are not true in general, we conclude that $\boldsymbol{\alpha} = \boldsymbol{\lambda}_v / \lambda_v$ or

$\boldsymbol{\alpha} = -\boldsymbol{\lambda}_v/\lambda_v$. To chose the direction, we rely on the Pontryagin's maximum principle that states the necessary condition for a minimum requires that the admissible controls are chosen such that the Hamiltonian $\mathcal{H}$ is minimized at all points along the path. From eq.(2.56), $\mathcal{H}$ is clearly minimized when

$$\boldsymbol{\alpha} = -\boldsymbol{\lambda}_v/\lambda_v, \tag{2.60}$$

that means the optimal thrust is always directed as the velocity costate $\boldsymbol{\lambda}_v$.
Substituting $\boldsymbol{\alpha}$ from $\mathcal{H}$

$$\mathcal{H} = \boldsymbol{\lambda_r} \cdot \boldsymbol{v} + \boldsymbol{\lambda_v} \cdot \boldsymbol{g}(\boldsymbol{r}) - c_1 \frac{u}{m} \lambda_v - \lambda_m c_2 u + c_2 u + \mu_2 C_2(u). \tag{2.61}$$

Defining the switching function as

$$\rho = 1 - \frac{c_1}{c_2 m} \lambda_v - \lambda_m, \tag{2.62}$$

then

$$\mathcal{H} = \boldsymbol{\lambda_r} \cdot \boldsymbol{v} + \boldsymbol{\lambda_v} \cdot \boldsymbol{g}(\boldsymbol{r}) + (c_2 u)\rho + \mu_2 C_2(u). \tag{2.63}$$

and therefore, applying the minimum principle, we find that $\mathcal{H}$ is minimized if $u = 1$ when $\rho < 0$ and $u = 0$ when $\rho > 0$. When $\rho = 0$, then $0 \leq u \leq 1$. These results lead to the Lawden's well-known primer vector control law, summarized in eq. (2.64)

$$\boldsymbol{u} = -\frac{\boldsymbol{\lambda}_v}{\lambda_v}, \qquad u = \begin{cases} 0 & \text{if} \quad \rho > 0 \\ 1 & \text{if} \quad \rho < 0 \\ 0 \leq u \leq 1 & \text{if} \quad \rho = 0. \end{cases} \tag{2.64}$$

2.3.2 Interior-point constraints

By introducing interior-point constraints we obtain a more general type of boundary value problem, termed as Multi-Point-Boundary-Value-Problem (MPBVP). In optimal control theory, interior-point constraints are treated similarly to final constraints, indeed having for example

$$\boldsymbol{\psi}_i = \boldsymbol{\chi}(\boldsymbol{x}(t_i), t_i) = 0 \tag{2.65}$$

in an intermediate point t_i in time interval, we simply adjoin Eq.(2.65) to the performance index

$$\mathcal{J} = \boldsymbol{\nu}^T \boldsymbol{\psi}(\boldsymbol{x}(t_f), t_f) + \boldsymbol{\pi}^T \boldsymbol{\chi}(\boldsymbol{x}(t_i), t_i) + \int_{t_0}^{t_f} \{\mathcal{H} - \boldsymbol{\lambda}^T \dot{\boldsymbol{x}}\} dt, \tag{2.66}$$

where $\boldsymbol{\pi}$ are the adjoint multipliers associated with the interior-point constraints. The first variation is, then,

$$\delta\mathcal{J} = \delta\big(\boldsymbol{\nu}^T \boldsymbol{\psi}(\boldsymbol{x}(t_f), t_f) + \boldsymbol{\pi}^T \boldsymbol{\chi}(\boldsymbol{x}(t_i), t_i)\big) + \delta \int_{t_0}^{t_f} \{\mathcal{H} - \boldsymbol{\lambda}^T \dot{\boldsymbol{x}}\} dt. \tag{2.67}$$

Splitting the integral into $\int_{t_0}^{t_i^-} + \int_{t_i^+}^{t_f}$, integrating by parts, and regrouping terms, we obtain

$$\begin{aligned}\delta\mathcal{J} = \big[\boldsymbol{\nu}^T \boldsymbol{\psi}_x - \boldsymbol{\lambda}^T\big]\delta\boldsymbol{x}\big|_{t_f} + \big[\boldsymbol{\pi}^T \boldsymbol{\chi}_{x^-} - \boldsymbol{\lambda}^T\big]\delta\boldsymbol{x}\big|_{t_i^-} + \\ + \big[\boldsymbol{\pi}^T \boldsymbol{\chi}_{x^+} + \boldsymbol{\lambda}^T\big]\delta\boldsymbol{x}\big|_{t_i^+} + \boldsymbol{\lambda}^T\delta\boldsymbol{x}\big|_{t_0} + \\ + \int_{t_0}^{t_f} \big\{\big(\mathcal{H}_x + \dot{\boldsymbol{\lambda}}\big)^T \delta\boldsymbol{x} + \mathcal{H}_u^T \delta\boldsymbol{u} + \big(\mathcal{H}_\lambda - \dot{\boldsymbol{x}}\big)^T \delta\boldsymbol{\lambda}\big\} dt,\end{aligned} \tag{2.68}$$

where t_i^+ and t_i^- denote respectively the instant just before and after the intermediate point t_i, and consequently

$$\begin{aligned}\boldsymbol{\chi}_{x^-} &= \frac{\partial \boldsymbol{\chi}}{\partial \boldsymbol{x}(t_i^-)} \\ \boldsymbol{\chi}_{x^+} &= \frac{\partial \boldsymbol{\chi}}{\partial \boldsymbol{x}(t_i^+)}.\end{aligned}$$

Therefore, in addition to (2.28)-(2.32), we have two new trasversality conditions expressed by

$$\big[\boldsymbol{\pi}^T \boldsymbol{\chi}_{x^-} - \boldsymbol{\lambda}^T\big]\delta\boldsymbol{x}\big|_{t_i^-} = 0, \tag{2.69}$$

$$\big[\boldsymbol{\pi}^T \boldsymbol{\chi}_{x^+} + \boldsymbol{\lambda}^T\big]\delta\boldsymbol{x}\big|_{t_i^+} = 0. \tag{2.70}$$

The application of these relations to the different intermediate maneuvers already presented in section 2.2.1, leads to different conditions that are carefully illustrated in the next subsections.

Intermediate Flyby

Consider again an intermediate flyby and remember the corresponding constraints given in Eq. (2.11). Substituting this relation into Eqs. (2.69)-(2.70), yields

- just before the flyby

$$\begin{cases} \boldsymbol{r}_i^- \rightarrow \text{fixed} \\ \boldsymbol{v}_i^- \rightarrow \text{free} \\ m_i^- \rightarrow \text{free} \end{cases} \Rightarrow \begin{cases} \boldsymbol{\lambda}_{\boldsymbol{r}_i}^- \rightarrow \text{free} \\ \boldsymbol{\lambda}_{\boldsymbol{v}_i}^- = \boldsymbol{\pi}_1 \\ \lambda_{m_i}^- = \pi_2 \end{cases} \tag{2.71}$$

- just after the flyby

$$\begin{cases} \boldsymbol{r}_i^+ \rightarrow \text{fixed} \\ \boldsymbol{v}_i^+ \rightarrow \text{free} \\ m_i^+ \rightarrow \text{free} \end{cases} \Rightarrow \begin{cases} \boldsymbol{\lambda}_{\boldsymbol{r}_i}^+ \rightarrow \text{free} \\ \boldsymbol{\lambda}_{\boldsymbol{v}_i}^+ = \boldsymbol{\pi}_1 \\ \lambda_{m_i}^+ = \pi_2. \end{cases} \tag{2.72}$$

Therefore, $\boldsymbol{\lambda}_{\boldsymbol{v}}$ and λ_m are the same just before and after the flyby, while the position multiplier vector $\boldsymbol{\lambda}_{\boldsymbol{r}}$ presents a free discontinuity. Under these considerations, and remembering that also the mass m is the same before and after the flyby, the shooting function ρ results to be continuous astride the encounter.
In Table 2.2 the constraints and the conditions for the flyby maneuver are summarized.

Table 2.2: Summary of constraints and conditions for intermediate flyby.

Constraints $\boldsymbol{\Psi}_i$	$\boldsymbol{r}(t_i) - \boldsymbol{r}_p(t_i) = 0$ $\boldsymbol{v}(t_i^+) - \boldsymbol{v}(t_i^-) = 0$ $m(t_i^+) - m(t_i^-) = 0$
Trasversality conditions	$\boldsymbol{\lambda}_{\boldsymbol{v}_i}^- - \boldsymbol{\lambda}_{\boldsymbol{v}_i}^+ = 0$ $\lambda_{m_i}^- - \lambda_{m_i}^+ = 0$
Free variables	$\boldsymbol{v}(t_i)$, $m(t_i)$, $\boldsymbol{\lambda}_{\boldsymbol{r}}(t_i)$, $\boldsymbol{\lambda}_{\boldsymbol{v}}(t_i)$, $\lambda_m(t_i)$

Intermediate Rendezvous

For the intermediate rendezvous, the conditions are slightly different to those obtained for the intermediate flyby. In fact remembering equation (2.12), the velocity is also constrained, so the conditions just before the rendezvous are

- just before the rendezvous

$$\begin{cases} \boldsymbol{r}_i^- \rightarrow \text{fixed} \\ \boldsymbol{v}_i^- \rightarrow \text{fixed} \\ m_i^- \rightarrow \text{free} \end{cases} \Rightarrow \begin{cases} \boldsymbol{\lambda}_{\boldsymbol{r}_i}^- \rightarrow \text{free} \\ \boldsymbol{\lambda}_{\boldsymbol{v}_i}^- \rightarrow \text{free} \\ \lambda_{m_i}^- = \pi_1 \end{cases} \tag{2.73}$$

- just after the rendezvous

$$\begin{cases} \boldsymbol{r}_i^+ \rightarrow \text{fixed} \\ \boldsymbol{v}_i^+ \rightarrow \text{fixed} \\ m_i^+ \rightarrow \text{free} \end{cases} \Rightarrow \begin{cases} \boldsymbol{\lambda}_{\boldsymbol{r}_i}^+ \rightarrow \text{free} \\ \boldsymbol{\lambda}_{\boldsymbol{v}_i}^+ \rightarrow \text{free} \\ \lambda_{m_i}^+ = \pi_1. \end{cases} \tag{2.74}$$

This time only the mass multiplier λ_m is the same before and after the encounter, while in general $\boldsymbol{\lambda}_r$ and $\boldsymbol{\lambda}_v$ could present free discontinuities.
In Table 2.3 the constraints and the conditions for the rendezvous maneuver are summarized.

Table 2.3: Summary of constraints and conditions for intermediate rendezvous.

Constraints $\boldsymbol{\Psi}_i$	$\boldsymbol{r}(t_i) - \boldsymbol{r}_p(t_i) = 0$ $\boldsymbol{v}(t_i) - \boldsymbol{v}_p(t_i) = 0$ $m(t_i^+) - m(t_i^-) = 0$
Trasversality conditions	$\lambda_{m_i}^- - \lambda_{m_i}^+ = 0$
Free variables	$m(t_i)$, $\boldsymbol{\lambda}_{\boldsymbol{r}}(t_i)$, $\boldsymbol{\lambda}_{\boldsymbol{v}}(t_i)$, $\lambda_m(t_i)$

Intermediate Gravity Assist

Consider now an intermediate gravity assist: the constraints in this case are expressed in Eq. (2.16). Applying the trasversality conditions (2.69)-(2.70), we have

- just before the gravity assist

$$\begin{cases} \boldsymbol{r}_i^- \rightarrow \text{fixed} \\ \boldsymbol{v}_i^- \rightarrow \text{free} \\ m_i^- \rightarrow \text{free} \end{cases} \Rightarrow \begin{cases} \boldsymbol{\lambda}_{\boldsymbol{r}_i}^- \rightarrow \text{free} \\ \boldsymbol{\lambda}_{\boldsymbol{v}_i}^- = 2\pi_1 \boldsymbol{v}_\infty^- \\ \lambda_{m_i}^- = \pi_2 \end{cases} \tag{2.75}$$

- just after the gravity assist

$$\begin{cases} \boldsymbol{r}_i^+ \rightarrow \text{fixed} \\ \boldsymbol{v}_i^+ \rightarrow \text{free} \\ m_i^+ \rightarrow \text{free} \end{cases} \Rightarrow \begin{cases} \boldsymbol{\lambda}_{\boldsymbol{r}_i}^+ \rightarrow \text{free} \\ \boldsymbol{\lambda}_{\boldsymbol{v}_i}^+ = 2\pi_1 \boldsymbol{v}_\infty^+ \\ \lambda_{m_i}^+ = \pi_2. \end{cases} \tag{2.76}$$

As listed in previous section, for an intermediate gravity assist maneuver there is also a 1-D inequality constraint (2.17) that must be satisfied. Theoretically it should be added to the performance index

$$\mathcal{J} = \boldsymbol{\nu}^T \boldsymbol{\psi}(\boldsymbol{x}(t_f), t_f) + \boldsymbol{\pi}^T \boldsymbol{\chi}(\boldsymbol{x}(t_i), t_i) + \kappa\sigma(\boldsymbol{x}(t_i), t_i) + \int_{t_0}^{t_f} \{\mathcal{H} - \boldsymbol{\lambda}^T \dot{\boldsymbol{x}}\} dt, \tag{2.77}$$

thus leading to a more general expression of Eqs. (2.69)-(2.69):

$$\left[\boldsymbol{\pi}^T \boldsymbol{\chi}_{x^-} + \kappa\sigma_{x^-} - \boldsymbol{\lambda}^T\right] \delta\boldsymbol{x}\big|_{t_i^-} = 0, \tag{2.78}$$

$$\left[\boldsymbol{\pi}^T \boldsymbol{\chi}_{x^+} + \kappa\sigma_{x^+} + \boldsymbol{\lambda}^T\right] \delta\boldsymbol{x}\big|_{t_i^+} = 0. \tag{2.79}$$

This means that the derivatives of r_{ph} with respect to the state variables must be evaluated. These quantities are not immediately available, thus some additional considerations about the gravity assist maneuver must be pointed out. At this purpose, the formulation presented in [29] could be used as guideline. Obtaining these quantities however remains rather complicated, so we decide to treat the maneuver as a free-high gravity assist, so that no inequalities constraints arise during the analytic formulation. This eliminates the necessity of deriving and implementing new transversality conditions (2.78)-(2.79), but (2.69)-(2.70) can still be used as constraint conditions associated

with the optimal control problem.
In section 3.4.1 a possible artifice to restore, at least numerically, the constraint on r_{ph} will be shown: more specifically, r_{ph} is added to the parameter vector and determined by means of a parameter optimization problem.
In Table 2.4 the constraints and the conditions for the gravity assist maneuver are summarized.

Table 2.4: Summary of constraints and conditions for intermediate gravity assist.

Constraints $\boldsymbol{\Psi}_i$	$\boldsymbol{r}(t_i) - \boldsymbol{r}_p(t_i) = 0$
	$v_\infty^- - v_\infty^+ = 0$
	$m(t_i^+) - m(t_i^-) = 0$
Trasversality conditions	$\boldsymbol{\lambda}_{\boldsymbol{v}_i}^- - 2\pi_1 \boldsymbol{v}_\infty^- = 0$
	$\boldsymbol{\lambda}_{\boldsymbol{v}_i}^+ - 2\pi_1 \boldsymbol{v}_\infty^+ = 0$
	$\lambda_{m_i}^- - \lambda_{m_i}^+ = 0$
Free variables	$\boldsymbol{v}(t_i)$, $m(t_i)$,
	$\boldsymbol{\lambda}_{\boldsymbol{r}}(t_i)$, $\boldsymbol{\lambda}_{\boldsymbol{v}}(t_i)$, $\lambda_m(t_i)$
	π_1

From the conditions reported above can be inferred that the primer vector must be parallel to the hyperbolic excess velocity just before and after the gravity assist, and its magnitude is continuos. Therefore, since λ_v, λ_m and m are the same just before and after the gravity assist, the shooting function ρ must be continuos as already seen for the flyby case.

Free Intermediate Points

Finally from equations (2.18), we obtain the trasversality conditions for the general case of intermediate points:

- just before the auxiliary point

$$\begin{cases} \boldsymbol{r}_i^- \rightarrow \text{free} \\ \boldsymbol{v}_i^- \rightarrow \text{free} \\ m_i^- \rightarrow \text{free} \end{cases} \Rightarrow \begin{cases} \boldsymbol{\lambda}_{\boldsymbol{r}_i}^- = \boldsymbol{\pi}_1 \\ \boldsymbol{\lambda}_{\boldsymbol{v}_i}^- = \boldsymbol{\pi}_2 \\ \lambda_{m_i}^- = \pi_3 \end{cases} \tag{2.80}$$

- just after the auxiliary point

$$\begin{cases} \boldsymbol{r}_i^+ \rightarrow \text{free} \\ \boldsymbol{v}_i^+ \rightarrow \text{free} \\ m_i^+ \rightarrow \text{free} \end{cases} \Rightarrow \begin{cases} \boldsymbol{\lambda}_{\boldsymbol{r}_i}^+ = \boldsymbol{\pi}_1 \\ \boldsymbol{\lambda}_{\boldsymbol{v}_i}^+ = \boldsymbol{\pi}_2 \\ \lambda_{m_i}^+ = \pi_3. \end{cases} \tag{2.81}$$

that is the costate, as well as the state, must be fully continuous. This means that the switching function ρ is continuous also in this case.
In Table 2.5 the constraints and the conditions for the multiple shooting case are summarized.

Table 2.5: Summary of constraints and conditions for the multiple shooting.

Constraints	$\boldsymbol{r}(t_i^+) - \boldsymbol{r}(t_i^-) = 0$
$\boldsymbol{\Psi}_i$	$\boldsymbol{v}(t_i^+) - \boldsymbol{v}(t_i^-) = 0$
	$\boldsymbol{m}(t_i^+) - \boldsymbol{m}(t_i^-) = 0$
Trasversality	$\boldsymbol{\lambda}_{\boldsymbol{r}_i}^- - \boldsymbol{\lambda}_{\boldsymbol{r}_i}^+ = 0$
conditions	$\boldsymbol{\lambda}_{\boldsymbol{v}_i}^- - \boldsymbol{\lambda}_{\boldsymbol{v}_i}^+ = 0$
	$\lambda_{m_i}^- - \lambda_{m_i}^+ = 0$
Free	$\boldsymbol{r}(t_i)$,$\boldsymbol{v}(t_i)$, $m(t_i)$,
variables	$\boldsymbol{\lambda}_{\boldsymbol{r}}(t_i)$, $\boldsymbol{\lambda}_{\boldsymbol{v}}(t_i)$, $\lambda_m(t_i)$

2.4 Free time variables

In the previous sections, we assumed the hypothesis of fixed times, i.e. the variables t_0, t_i and t_f have not been considered in the variation of the performance index δJ. If these variables are changed in free parameters, additional optimality conditions arise. In particular, considering a TPBVP with free initial and final times (it is likewise for free intermediate times t_i), the first variation of the performance index reads

$$\begin{aligned} \delta\mathcal{J} = \left[\boldsymbol{\nu}_0^T \boldsymbol{\psi}_x^0 + \boldsymbol{\lambda}^T\right]\delta\boldsymbol{x}\Big|_{t_0} + \left[\boldsymbol{\nu}_f^T \boldsymbol{\psi}_x^f - \boldsymbol{\lambda}^T\right]\delta\boldsymbol{x}\Big|_{t_f} + \\ + \int_{t_0}^{t_f} \left\{\left(\mathcal{H}_x + \dot{\boldsymbol{\lambda}}\right)^T \delta\boldsymbol{x} + \mathcal{H}_u^T \delta\boldsymbol{u} + \left(\mathcal{H}_\lambda - \dot{\boldsymbol{x}}\right)^T \delta\boldsymbol{\lambda}\right\} dt + \\ + \left[-\mathcal{H}_0 + \boldsymbol{\nu}_0^T \boldsymbol{\psi}_{t_0}^0\right]\delta t_0 + \left[\mathcal{H}_f + \boldsymbol{\nu}_f^T \boldsymbol{\psi}_{t_f}^f\right]\delta t_f, \end{aligned} \tag{2.82}$$

thus, additional transversality conditions come out

$$\mathcal{H}_0 = \boldsymbol{\nu}_0^T \boldsymbol{\psi}_{t_0}^0, \tag{2.83}$$

$$\mathcal{H}_f = -\boldsymbol{\nu}_f^T \boldsymbol{\psi}_{t_f}^f. \tag{2.84}$$

As can be seen, they require the computation of the derivative of constraints functions $\boldsymbol{\psi}^0$ and $\boldsymbol{\psi}^f$ with respect to initial and final time: this operation requires careful attention since times derivatives are not immediately available and their derivation can be quite tricky.

Chapter 3

Numerical Techniques

This chapter is devoted to the accurate description of the main numerical techniques developed for the solution of the optimal control problem and the corresponding multipoint boundary value problem.
In particular, the chapter opens with an overview of the complete optimal control problem (section 3.1) along with its main characteristics and resolution difficulties. Successive sections (3.2-3.5) are dedicated to the presentation of the main numerical techniques adopted to counteract these issues: the decription follows therefore a functional scheme rather than a chronological one, so that it should be clear the purpose for which each of this technique has been introduced.
Finally, in section 3.6, a brief overview of the overall optimization process and its architecture is reported, along with the fundamental steps required to solve optimal problems in a standard way, regardless of their complexity.

3.1 Introduction

The calculus of variations, introduced in the previous chapter, converts the optimal control problem in a multi-point boundary value problem. It involves indeed a set of differential equations for the state $\boldsymbol{x}$ and the costate variables $\boldsymbol{\lambda}$, given by

$$\dot{\boldsymbol{x}} = \mathcal{H}_{\lambda} \qquad n \text{ differential equations,} \tag{3.1}$$

$$\dot{\boldsymbol{\lambda}} = -\mathcal{H}_{x} \qquad n \text{ differential equations.} \tag{3.2}$$

The m-vector $\boldsymbol{u}(t)$ is determined by the optimality condition

$$\mathcal{H}_u = 0 \qquad\qquad m \text{ algebraic equations,} \tag{3.3}$$

that plays the role of algebraic constraint. System of equations (3.1)-(3.2) is coupled with initial and final boundary conditions, splitted between state and costate variables

$$\boldsymbol{\psi}^0 = 0, \qquad\qquad \boldsymbol{\lambda}^T(t_0) = -\boldsymbol{\nu}_0^T \boldsymbol{\psi}_x^0, \tag{3.4}$$

$$\boldsymbol{\psi}^f = 0, \qquad\qquad \boldsymbol{\lambda}^T(t_f) = \boldsymbol{\nu}_f^T \boldsymbol{\psi}_x^f, \tag{3.5}$$

and the intermediate boundary constraints

$$\boldsymbol{\psi}^i = 0, \qquad \boldsymbol{\lambda}^T(t_i^-) = \boldsymbol{\pi}^T \boldsymbol{\psi}_x^i, \qquad \boldsymbol{\lambda}^T(t_i^+) = -\boldsymbol{\pi}^T \boldsymbol{\psi}_x^i. \tag{3.6}$$

Moreover, the problem is characterized by stationarity conditions related to free initial and final times

$$H_0 = \boldsymbol{\nu}_0^T \boldsymbol{\psi}_{t_0}^0, \tag{3.7}$$

$$H_f = -\boldsymbol{\nu}_f^T \boldsymbol{\psi}_{t_f}^f, \tag{3.8}$$

and finally, if even intermediate times are considered as free parameters, the associated additional conditions

$$H_i^- = -\boldsymbol{\nu}_i^T \boldsymbol{\psi}_{t_i^-}^i, \qquad\qquad H_i^+ = \boldsymbol{\nu}_i^T \boldsymbol{\psi}_{t_i^+}^i. \tag{3.9}$$

Needless to say, this problem is not very easy to solve. However, in the previous chapter, we have seen that as the number of variables increases, the multi-point boundary value problem becomes more complex and additional conditions arise. This fact suggests that by limiting the number of variables, considered within the optimal control formulation, the problem complexity can be significantly reduced.
For instance, considering a fixed-time transfer problem, in which the variables t_0, t_i and t_f are known, the optimal control problem can be simplified by removing additional conditions (3.7)-(3.9). If a solution to the MPBVP is obtained, this represents the optimal trajectory for those particular boundary conditions. However, the solution found cannot be considered the globally optimal one, since some variables and conditions are neglected. To counteract this issue, the MPBVP are embedded in a parametric

optimization problem, including these unknown values in the design vector.

$$\boldsymbol{\Upsilon} = [\xi_t^0, \xi_{ToF}^0, \ldots, \xi_{ToF}^{n-1}]. \tag{3.10}$$

This approach indeed, allows us to not only solve the MPBVP, but also to provide an optimization for those variables that have not been considered within the optimal control problem. The trasversality conditions associated with these variables are not used, but we can presume that they are implicity driven to zero by the optimization process.

Departure date and transfer times are not the only variables that have been removed from the optimal control formulation. In fact, in order to simplify the trasversality conditions, also the polar angles α^0, δ^0, α^f and δ^f for the direction of the departure and arrival excess velocity, are considered fixed within the optimal control problem, and are optimized via the parametric optimization. Moreover, as introduced in section 2.3.2, the issue regarding the perycenter radius during intermediate gravity assist, can be avoided by following the same phylosophy and considering a parametric optimization for the r_{ph}.

Summarizing, within the optimal control formulation, some variables can be considered fixed in order to reduce its complexity. Despite this, their value is optimized by including them in the parametric optimization problem, in which the MPBVP is nested. Bearing this in mind, an initial evaluation of these variables becomes necessary.

3.2 Global Optimum Solution

To obtain initial guesses for those variables included in the parametric problem, there are different options, including the possibility to use insight into the problem to select reasonable values. However, as highlighted in the review of the state-of-the-art, indirect methods are extremely sensitive and demand for a good initial guess to obtain convergence to the optimal solution.

More accurate initial values can be achieved by using global optimization techniques combined with heuristical shape-based methods [44] or impulsive maneuver approximations [56]. At this purpose, an already existing software, developed at Politecnico di Milano by Carrara [9], is exploited. This tool is characterized by two distinct phases: the first implements a genetic algorithm to quickly identify the potential dates of encounter, and to provide a first estimate of the ΔV budget using a succession of Lambert's arcs. This allows us to search for a global optimum without the need of initial guesses. The second phase, is a local optimization based on the Sims and Flanagan direct method

[56]. Figure 3.1 illustrates the structure of the trajectory used in this method. As shown, the trajectory is divided into legs that begin and end at body nodes.

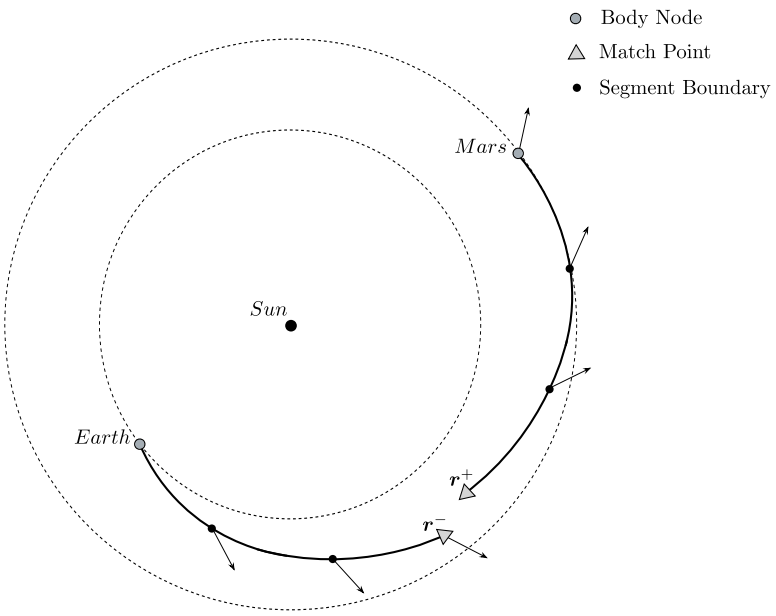

Figure 3.1: Trajectory structure of the Carrara optimization tool.

On each leg is a match point, and the trajectory is propagated forwards from the previous body node and backwards from the subsequent body node to the match point, in order to reduce the integration errors. Each leg is also subdivided into segments containing an impulsive ΔV_i at the end of each segment, in order to approximate a continuous thrust problem.

The propagation of the trajectory assumes the two-body dynamical model, and gravity assists are assumed to cause an instantaneous change in the direction of the $\boldsymbol{v}_\infty$ vector. The trajectory structure leads to a constrained, nonlinear optimization problem characterized by a large number of optimization variables. At the beginning and ending body nodes, indeed, the optimization variables include the velocity of the spacecraft relative to the body, the mass of the spacecraft, and the corresponding epoch. At an intermediate body, there are two sets of variables, one at arrival and one at departure, to account, for example, for changes in velocity for a gravity assist, changes in mass, or changes in time for a rendezvous. All of these independent variables have associated upper and lower bounds.

The primary optimization constraints are that the position, velocity, and mass of the spacecraft must be continuous at the match points. Other constraints can include, for instance, the maximum allowable value of the thrust magnitude on each segment etc.

The problem is finally solved using Matlab's optimization toolbox function fmincon, which implements a sequential quadratic programming scheme.

The solution obtained is therefore exploited for the initialization of optimization parameters listed before (launch date, transfer times etc). In particular, a graphical interface has been developed to allows the user to select suitable intermediate points directly from the plotted trajectory. It is worth observing that starting from the global solution, even initial and final values for the excess velocities can be derived. In fact, even if these quantities, unlike other variables, remain fixed and are not considered in the parametric optimization (section 2.2), they should anyway be specified by the user.

3.3 Minimum Energy Solution

At this point, let us focus our attention on the optimal control problem embedded in the parametric optimization problem. We have already seen how, by assuming a fixed-time formulation, it could be simplified respect to the original one. However, because of the discontinuous nature of the bang-bang control law, numerical difficulties in the integration of Euler-Lagrange differential equations arise. Thus, the convergence of the algorithm to the optimal solution could still be difficult to obtain, specially when a single shooting method, based on gradient information, is used. Moreover, shooting methods require good initial guesses that lie within the domain of convergence. This requirement is specially difficult to satisfy because it involves the Lagrange multipliers, whose physical meaning is non-intuitive. To this aim the global optimal solution could not be used, since it does not include the dynamics of the costates. Therefore, in order to counteract these issues we consider first an easier MPBVP, in which the control is expressed in terms of acceleration

$$\begin{cases} \dot{\boldsymbol{r}} &= \boldsymbol{v}, \\ \dot{\boldsymbol{v}} &= -\dfrac{\mu}{r^3}\boldsymbol{r} + \boldsymbol{u}, \\ \dot{m} &= \dfrac{c_2 m u}{c_1}. \end{cases} \tag{3.11}$$

Also the performance index has a slightly different structure, that is

$$\mathcal{J} = \frac{1}{2}\int_{t_0}^{t_f} \boldsymbol{u}^T \boldsymbol{u} dt, \tag{3.12}$$

justifying the name of energy-optimal problem by which it is usually identified. The Hamiltonian related to this problem changes consequently

$$\mathcal{H} = \frac{1}{2}\boldsymbol{u}^T\boldsymbol{u} + \boldsymbol{\lambda_r}\cdot\boldsymbol{v} + \boldsymbol{\lambda_v}\cdot\left(-\frac{\mu}{\|\boldsymbol{r}\|^3}\boldsymbol{r} + \boldsymbol{u}\right), \tag{3.13}$$

and substituting in equation 2.51, we obtain the optimal control law

$$\boldsymbol{u} = -\boldsymbol{\lambda_v}, \tag{3.14}$$

that means the primer vector has the same magnitude and the opposite direction of the velocity costate vector. By applying eq.(2.29), the costates differential equations are derived

$$\dot{\boldsymbol{\lambda}} = -\mathcal{H}_x = \begin{cases} \dot{\boldsymbol{\lambda}}_r = \dfrac{\mu}{r^3}\boldsymbol{\lambda}_v - \dfrac{3\mu\boldsymbol{r}\cdot\boldsymbol{\lambda}_v}{r^5}\boldsymbol{r} \\ \dot{\boldsymbol{\lambda}}_v = -\boldsymbol{\lambda}_r, \end{cases} \tag{3.15}$$

where the equation for mass multiplier λ_m has intentionally been neglected in this first phase, because it does not affect others equations and it is unnecessary for control parametrization.

The main advantage of such a formulation is that the problem is characterized by continuous rather than bang-bang optimal control and thus has relatively large convergence radius. In addition, there are no upper or lower boundaries on acceleration variable, thus enhancing the possibilities to easily find a solution using single shooting methods. Before proceeding, some further considerations on the absence of boundaries for the acceleration must be reported: this fact indeed, leads sometimes to dummy solutions, i.e. the energy-optimal solutions found are characterized by accelerations such that the thrust required is out of defined boundaries. This fact remains completely hidden at this stage of the optimization process, but could lead to infeasible starting solution for the successive steps (fuel-optimal problem). In order to discard this type of solutions, a constraint on the level of achievable accelerations is introduced. At this purpose, a rather obvious and simple way, is to evaluate at each point along the trajectory the thrust corresponding to the required acceleration and eventually compute the violation of the allowable value. However, this implementation is rather onerous from the computational point of view, as well as unnecessary, because we require a general limitation of the level of acceleration, not point by point. Thus, for instance, a possibility is to compute the average value of the required acceleration and evaluate, after converting to the corresponding thrust level, the constraint violation. In this way the computational cost decreases and it is sufficient to avoid possible dummy solutions. If the average

required thrust is over the allowable threshold, the energy-optimal solution can not be used as first guess, the optimization process fails and the mission scenario is assumed to be infeasible.

In summary, the energy-optimal trajectory is computed by solving the system of differential equations (3.11)-(3.15): practical test cases have demonstrated that, with the assumption of $\boldsymbol{\lambda}_r$, $\boldsymbol{\lambda}_v = 0$ as first guess (i.e. $\boldsymbol{u} = 0$), the convergence is always obtained with simple shooting methods.
This approach allows us to provide a first estimate, specially for the Lagrange multipliers, to be used as first guess in the successive steps, thus representing a fundamental phase in the resolution process.

3.3.1 Multiple Shooting Technique

Once the energy-optimal problem has been formulated, an efficient method for the resolution of the related MPBVP, is needed. At this purpose, a number of techniques have been proposed [6]. However, one rather obvious approach is to divide the trajectory in multiple segments that are solved as independent TPBVPs, using a shooting method. This approach is often referred to as indirect multiple shooting and it is particularly interesting because of the possibility of a parallel implementation, in which all phases are computed and propagated in parallel for the constraints evaluation. This characteristic however has not been further investigated, but it is surely an interesting aspect that can be developed in future works.
It should be noted that the use of a shooting techniques, in order to solve the energy-optimal problem, doesn't involve any numerical difficulty, as the control law in this case is characterized by a continuous profile.
In general any trajectory can be decomposed into many phases, typically as much as the intermediate encounters plus one. However, more generally speaking, those points, at which the trajectory is divided, not necessarily coincide with real celestial bodies encounters, indeed fictitious points can be considered. For this reason, from now on, we will talk about those points as nodes. At this point, it is sufficient to know that each of these nodes is characterized by a set of optimization variables $\boldsymbol{\xi^i}$, a set of initial conditions $\boldsymbol{C}_i$ and a set of constraints $\boldsymbol{\Psi}_i$, that will be described in detail in section 3.4.
The resolution procedure can be summarize in the following steps:

1. For each trajectory leg, integrate the differential equations (3.11)-(3.15), starting from 0 to ToF^i with given initial conditions $\boldsymbol{C}_i$. A Adams-Bashforth-Moulton variable step variable order scheme, using an absolute and relative tolerance of

$1e^{-10}$ is applied.

2. In general at the final boundary, i.e. the $i+1$-th node, there will be discrepancies from the desired values that means there is a constraints violation $\delta\boldsymbol{\Psi}_{i+1}$. At this point a multidimensional root finding problem arise.

3. By employing a gradient search method, for instance a Newton-based solver, it is possible to find the adjustement of the initial boundary variables, $\boldsymbol{\xi^i}$, to reduce the constraint's violations at the final boundary to zero $\delta\boldsymbol{\Psi}_{i+1} = 0$.

Figure 3.2 illustrates the resolution strategy described above. As a matter of fact, the multiple shooting technique reduces the optimal control problem to the solution of a set of nonlinear equations. The solution of this problem is embedded in the parametric optimization, by simply including the values of variables at each initial boundary to the optimization vector $\boldsymbol{\Upsilon}$, already defined in eq.(3.10). The new optimization variables vector is

$$\boldsymbol{\xi} = \left[\boldsymbol{\Upsilon}, \boldsymbol{\xi^0}, \boldsymbol{\xi^1}, ..., \boldsymbol{\xi^f}\right]^T, \tag{3.16}$$

where $\boldsymbol{\xi^i}$ represents the set of unknown variables at the i-th node.

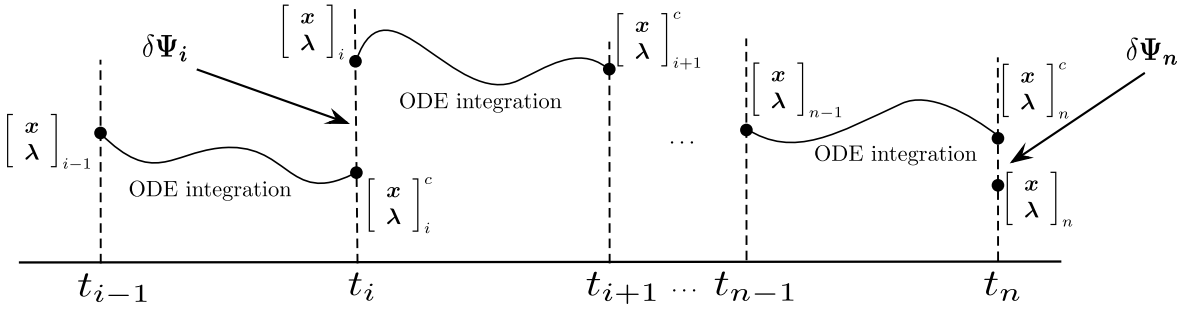

Figure 3.2: Illustration of the indirect multiple shooting method. The superscript "c" stands for "calculated", i.e. the state and costate obtained from the integration of the equations of motion.

3.4 Parameters Selection

As explained in previous sections, the original problem is formulated as a parametric optimization problem. Therefore the definition of an overall variable vector $\boldsymbol{\xi}$, i.e. a vector that comprises all the optimization variables for the specific problem, is required. Some of these variables, such as the departure date and transfer times, can be easily taken into account since their number is known and equal to the number of trajectory

legs plus one. The number of other variables depends instead on the type of the intermediate encounter. Hence the need to identify some basic entities that will be used as building block for all trajectories. Two possible choices arise: the first, adopted for instance by Ocampo [41], considers each segment as a building block of the entire trajectory: combining different type of segments is possible to generate any kind of trajectory. The second option, adopted for the proposed algorithm, considers the nodes themselves as basic entities, while the trajectory segments are view as the arcs connecting two subsequent points. The selection of the design variables is performed mainly by following the guidelines given by Olympio [42].

3.4.1 Interior nodes

As explained in section 2.3.2, each node is characterized by its own set of free variables, along with constraints and conditions, necessary to integrate the Euler-Lagrange equations and depending on the type of encounter they represent. Then we can associate each node to a variable vector $\boldsymbol{\xi}^i$, typically defined as

$$\boldsymbol{\xi^i} = [\boldsymbol{\xi_r^i}, \boldsymbol{\xi_v^i}, \xi_m^i, \boldsymbol{\xi_{\lambda_r}^i}, \boldsymbol{\xi_{\lambda_v}^i}, \xi_{\lambda_m}^i]^T, \tag{3.17}$$

where ξ_p is the counterpart of physical variables p, so that, for instance, $\boldsymbol{\xi_v^i}$ stands for the decision variables corresponding to the physical parameter $\boldsymbol{v}(t_i)$. The superscript "i" denotes the encounter number, so that $i = 1, \dots, n$.
Let us consider the case in which the i-th node corresponds to an intermediate flyby. As already indicated in the Table 2.2, the free variables are

$$\boldsymbol{v}(t_i), m(t_i), \boldsymbol{\lambda_r}(t_i), \boldsymbol{\lambda_v}(t_i), \lambda_m(t_i), \tag{3.18}$$

thus the corresponding decision vector will be composed by

$$\boldsymbol{\xi^i} = [\boldsymbol{\xi_v^i}, \xi_m^i, \boldsymbol{\xi_{\lambda_r}^i}, \boldsymbol{\xi_{\lambda_v}^i}, \xi_{\lambda_m}^i]^T. \tag{3.19}$$

Now, being the i-th node an interior point, it represents either the initial boundary for the i-th segment as well as the final boundary for the $i-1$-th trajectory leg. In the first case, the only explicit constraint is

$$\boldsymbol{r}(t_i^+) = \boldsymbol{r}_p(t_i), \tag{3.20}$$

whereas the velocity vector, the mass and all the Lagrange multipliers are free variables

$$\begin{aligned} \boldsymbol{v}(t_i^+) &= \boldsymbol{\xi}_{\boldsymbol{v}}^{\boldsymbol{i}}, && (3.21)\\ m(t_i^+) &= \xi_m^i, && (3.22)\\ \boldsymbol{\lambda_r}(t_i^+) &= \boldsymbol{\xi}_{\boldsymbol{\lambda_r}}^{\boldsymbol{i}}, && (3.23)\\ \boldsymbol{\lambda_v}(t_i^+) &= \boldsymbol{\xi}_{\boldsymbol{\lambda_v}}^{\boldsymbol{i}}, && (3.24)\\ \lambda_m(t_i^+) &= \xi_{\lambda_m}^i, && (3.25) \end{aligned}$$

In the second case, instead, we have

$$\boldsymbol{r}(t_i^-) - \boldsymbol{r}_p(t_i) = 0, \tag{3.26}$$

while for the velocity, mass and their corresponding costates we can impose

$$\begin{aligned} \boldsymbol{v}(t_i^-) &- \boldsymbol{\xi}_{\boldsymbol{v}}^{\boldsymbol{i}} = 0, && (3.27)\\ m(t_i^-) &- \xi_m^i = 0, && (3.28)\\ \boldsymbol{\lambda_v}(t_i^-) &- \boldsymbol{\xi}_{\boldsymbol{\lambda_v}}^{\boldsymbol{i}} = 0, && (3.29)\\ \lambda_m(t_i^-) &- \xi_{\lambda_m}^i = 0, && (3.30) \end{aligned}$$

thus restoring the continuity of these variables astride the node. Note that no relation has been imposed on the position multiplier vector $\boldsymbol{\lambda_r}(t_i^-)$ since it can assume different values before and after the flyby. Different notations have been used for initial and final conditions. In fact, relations (3.20)-(3.25) are treated as initial conditions, then imposed a priori, before the integration of ODE system; in this way they are implicitly satisfied, and expressed as $a = b$. Relations (3.26)-(3.30), instead, represent a set of constraints that must be satisfied after the ODE integration, thus expressed in the form $a - b = 0$.

The same strategy can be adopted also for all other cases. Table 3.1 reports a complete overview of all possible constraints, conditions and decision variables for each encounter case.

A particular point that should be noted is that for each node, the constraint vector and the decision vector have the same dimension, because the optimality conditions, stated in terms of the adjoint differential equations, the maximum principle, and associated boundary (transversality) conditions, uniquely define the values of the optimization variables.

Table 3.1: Implemented constraints, implemented conditions and decision variables for each intermediate case.

	Decision variables $\boldsymbol{\xi^i}$	Implemented constraints $\boldsymbol{\Psi_i}$	Implemented conditions $\boldsymbol{C_i}$
Intermediate flyby	$\boldsymbol{\xi^i_v}$, ξ^i_m $\boldsymbol{\xi^i_{\lambda_r}}$, $\boldsymbol{\xi^i_{\lambda_v}}$, $\xi^i_{\lambda_m}$	$\boldsymbol{r}(t_i^-) - \boldsymbol{r}_P(t_i) = 0$ $\boldsymbol{v}(t_i^-) - \boldsymbol{\xi^i_v} = 0$ $m(t_i^-) - \xi^i_m = 0$ $\boldsymbol{\lambda_v}(t_i^-) - \boldsymbol{\xi^i_{\lambda_v}} = 0$ $\lambda_m(t_i^-) - \xi^i_{\lambda_m} = 0$	$\boldsymbol{r}(t_i^+) = \boldsymbol{r}_P(t_i)$ $\boldsymbol{v}(t_i^+) = \boldsymbol{\xi^i_v}$ $m(t_i^+) = \xi^i_m$ $\boldsymbol{\lambda_r}(t_i^+) = \boldsymbol{\xi^i_{\lambda_r}}$ $\boldsymbol{\lambda_v}(t_i^+) = \boldsymbol{\xi^i_{\lambda_v}}$ $\lambda_m(t_i^+) = \xi^i_{\lambda_m}$
Intermediate rendezvous	ξ^i_m $\boldsymbol{\xi^i_{\lambda_r}}$, $\boldsymbol{\xi^i_{\lambda_v}}$, $\xi^i_{\lambda_m}$	$\boldsymbol{r}(t_i^-) - \boldsymbol{r}_P(t_i) = 0$ $\boldsymbol{v}(t_i^-) - \boldsymbol{v}_P(t_i) = 0$ $m(t_i^-) - \xi^i_m = 0$ $\lambda_m(t_i^-) - \xi^i_{\lambda_m} = 0$	$\boldsymbol{r}(t_i^+) = \boldsymbol{r}_P(t_i)$ $\boldsymbol{v}(t_i^+) = \boldsymbol{v}_P(t_i)$ $m(t_i^+) = \xi^i_m$ $\boldsymbol{\lambda_r}(t_i^+) = \boldsymbol{\xi^i_{\lambda_r}}$ $\boldsymbol{\lambda_v}(t_i^+) = \boldsymbol{\xi^i_{\lambda_v}}$ $\lambda_m(t_i^+) = \xi^i_{\lambda_m}$
Intermediate gravity assist	$\boldsymbol{\xi^i_v}$, ξ^i_m $\boldsymbol{\xi^i_{\lambda_r}}$, $\boldsymbol{\xi^i_{\lambda_v}}$, $\xi^i_{\lambda_m}$ ξ^i_ν, $\xi^i_{r_{ph}}$	$\boldsymbol{r}(t_i^-) - \boldsymbol{r}_P(t_i) = 0$ $v_\infty^- - v_\infty^+ = 0$ $m(t_i^-) - \xi^i_m = 0$ $\boldsymbol{\lambda_v}(t_i^-) - 2\xi^i_\nu \boldsymbol{v}_\infty^- = 0$ $2\xi^i_\nu \boldsymbol{v}_\infty^+ - \boldsymbol{\xi^i_{\lambda_v}} = 0$ $\lambda_m(t_i^-) - \xi^i_{\lambda_m} = 0$ $r^i_{ph} - \xi^i_{r_{ph}} = 0$	$\boldsymbol{r}(t_i^+) = \boldsymbol{r}_P(t_i)$ $\boldsymbol{v}(t_i^+) = \boldsymbol{\xi^i_v}$ $m(t_i^+) = \xi^i_m$ $\boldsymbol{\lambda_r}(t_i^+) = \boldsymbol{\xi^i_{\lambda_r}}$ $\boldsymbol{\lambda_v}(t_i^+) = \boldsymbol{\xi^i_{\lambda_v}}$ $\lambda_m(t_i^+) = \xi^i_{\lambda_m}$
Free intermediate points	$\boldsymbol{\xi^i_r}$, $\boldsymbol{\xi^i_v}$, ξ^i_m $\boldsymbol{\xi^i_{\lambda_r}}$, $\boldsymbol{\xi^i_{\lambda_v}}$, $\xi^i_{\lambda_m}$	$\boldsymbol{r}(t_i^-) - \boldsymbol{\xi^i_r} = 0$ $\boldsymbol{v}(t_i^-) - \boldsymbol{\xi^i_v} = 0$ $m(t_i^-) - \xi^i_m = 0$ $\boldsymbol{\lambda_r}(t_i^-) - \boldsymbol{\xi^i_{\lambda_r}} = 0$ $\boldsymbol{\lambda_v}(t_i^-) - \boldsymbol{\xi^i_{\lambda_v}} = 0$ $\lambda_m(t_i^-) - \xi^i_{\lambda_m} = 0$	$\boldsymbol{r}(t_i^+) = \boldsymbol{\xi^i_r}$ $\boldsymbol{v}(t_i^+) = \boldsymbol{\xi^i_v}$ $m(t_i^+) = \xi^i_m$ $\boldsymbol{\lambda_r}(t_i^+) = \boldsymbol{\xi^i_{\lambda_r}}$ $\boldsymbol{\lambda_v}(t_i^+) = \boldsymbol{\xi^i_{\lambda_v}}$ $\lambda_m(t_i^+) = \xi^i_{\lambda_m}$

The second column of the table reports the terminal constraints of each trajectory segment, while, in the last column, the initial conditions for the subsequent phases are listed. As can be seen, either the former and the latter are indipendent from the next phase, but depend solely on the current value of the decision vector.

On the gravity assist problem

As can be seen, in Table 3.1, for the intermediate gravity assist maneuver, an additional decision variable $\xi_{r_{ph}}$ and a correspondent new constraint

$$r_{ph} - \xi_{r_{ph}} = 0 \tag{3.31}$$

have been added, in order to numerically restore the condition on the minimum pericenter radius, and therefore obtain feasible solutions. More specifically, each time a gravity assist is performed, the r_{ph} calculated from equation (2.15) must satisfy also equation (3.31). Limiting the allowable range in which $\xi_{r_{ph}}$ is sought, typically the interval $[r^i_{ph_{min}}, \infty]$, automatically leads to satisfy the constraint on the minimum pericenter radius.

3.4.2 Initial and final nodes

To this point, only intermediate nodes have been considered and described in detail. However also the initial and the arrival node have to be included for the correct evaluation of the optimization vector. In this regard, the initial conditions corresponding to the first node are

$$C_0(\boldsymbol{x}(t_0)) = \begin{bmatrix} \boldsymbol{r}(t_0) = \boldsymbol{r}_p(t_0) \\ \boldsymbol{v}(t_0) = \boldsymbol{v}_p(t_0) + v^0_\infty \boldsymbol{u}^0_{\alpha,\delta} \\ m(t_0) = m_0 \\ \boldsymbol{\lambda_r}(t_0) = \boldsymbol{\xi^0_{\lambda_r}} \\ \boldsymbol{\lambda_v}(t_0) = \boldsymbol{\xi^0_{\lambda_v}} \\ \lambda_m(t_0) = \xi^0_{\lambda_m} \end{bmatrix} \tag{3.32}$$

where the spherical formulation of the unknowns vector $\boldsymbol{v_0}$, already presented in section 2.2, is used. Moreover, the initial trasversality condition (2.46) must be added if $v^0_\infty \neq 0$

$$\Psi_0(\boldsymbol{x}(t_0)) = \left[\boldsymbol{\lambda_v}(t_0) - \nu_0 v^0_\infty \boldsymbol{u}^0_{\alpha,\delta}\right]. \tag{3.33}$$

The decision variables are then

$$\boldsymbol{\xi^0} = [\boldsymbol{\xi^0_{\lambda_r}}, \boldsymbol{\xi^0_{\lambda_v}}, \xi^0_{\lambda_m}, \xi^0_\alpha, \xi^0_\delta, \xi^0_\nu]. \tag{3.34}$$

For the final node instead, the corresponding terminal constraints are given by

$$\Psi_n(\boldsymbol{x}(t_f)) = \begin{bmatrix} \boldsymbol{r}(t_f^-) - \boldsymbol{r}_p(t_f) = 0 \\ \boldsymbol{v}(t_f^-) - (\boldsymbol{v}_p(t_f) + v_\infty^f \boldsymbol{u}_{\alpha,\delta}^f) = 0 \\ m(t_f^-) - \xi_m^f = 0 \\ \lambda_m(t_f^-) = 0 \end{bmatrix}. \tag{3.35}$$

The trasversality condition (2.47)

$$\boldsymbol{\lambda_v}(t_f^-) - \nu_f v_\infty^f \boldsymbol{u}_{\alpha,\delta}^f = 0 \tag{3.36}$$

must be added, if $v_\infty^f \neq 0$. Finally, the decision variables involved are

$$\boldsymbol{\xi^f} = [\xi_m^f, \xi_\alpha^f, \xi_\delta^f, \xi_\nu^f]. \tag{3.37}$$

It is worth remembering that the values of v_∞^0 and v_∞^f are specified by the user, or alternatively can be retrieved from the global solution.
Figure 3.3 shows the multiphase problem decomposition: the two diamonds symbols are, respectively, the departure and the arrival bodies. The circle symbols are the intermediate bodies while the double-circled symbol represents a free intermediate point.

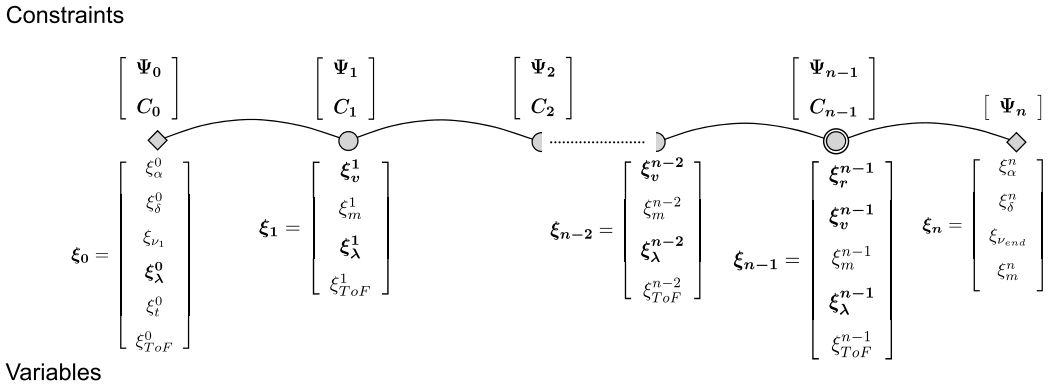

Figure 3.3: Sketch of the multiphase problem decomposition.

Returning at the energy-optimal problem, it should be noted that, since the simplified dynamics adopted at this stage does not include the equations for mass multipliers, the decision variables $\xi_{\lambda_m}^i$, as well as the implemented conditions and constraints relating to this variable, presented in Table 3.1, should be neglected in this first phase. For instance at the i-th node

$$\boldsymbol{\xi^i} = [\boldsymbol{\xi_r^i}, \boldsymbol{\xi_v^i}, \xi_m^i, \boldsymbol{\xi_{\lambda_r}^i}, \boldsymbol{\xi_{\lambda_v}^i}]^T. \tag{3.38}$$

3.5 Minimum Fuel Solution

Once a solution of the energy-optimal problem is found, the original fuel-optimal problem can be solved, using the current energy solution as first guess for the unknows. This time, however, a complete dynamical model is considered, thus initial guesses for the mass costates at each node should be provided, having been neglected during the previous phase. Since there are no informations about these quantities, we chose to generate them randomly. However two conditions can be conveniently used to reduce the search space for these parameters: the first can be obtained recalling eq. (2.34), which indicates that the derivative of λ_m with respect to time is nonpositive; the second is given by eq. (2.48), which says the final value of λ_m is zero. Combining these two conditions, yields that

$$\lambda_m(t_0) \geq 0, \tag{3.39}$$

therefore initial values for $\lambda_m(t_0)$ must be sought in the positive interval. Moreover, from the analyzes carried out, we notice that rarely initial values are outside the $[0, 1]$ interval, thus the search space for these parameters can be further restricted. Therefore we have at the generic node i

$$\boldsymbol{\xi^i} = \begin{bmatrix} \boldsymbol{\Xi^i_{energy}} \\ rand(0,1) \end{bmatrix}, \tag{3.40}$$

where $\boldsymbol{\Xi^i_{energy}}$ indicates the optimized decision vector at the i-th node, output of the energy-optimal problem.
Nevertheless, the solution of the discontinuous problem is still difficult to obtain because of the numerical difficulties arising during the integration of Euler-Lagrange differential equations. Then, in order to increase the radius of convergence of the solver, a smoothing approximation on the control is introduced. The resolution occurs through a continuation method, that is, by solving a series of problems gradually closer to the original one. This approach aims to overcome the numerical obstacles, without the need of an a priori knowledge of the control structure.

3.5.1 Continuation Method

Roughly speaking, the method of continuation augments the capabilities of conventional numerical techniques, by softening the requirements on the quality of the initial guess and iteratively solving a sequence of problems. Continuation method in fact, embeds a problem in the family of neighboring MPBVPs, which depends continuously on the

so-called continuation parameter p, defined in an appropriate partition of the interval $p \in [p_0, p_N]$, i.e.

$$p \rightarrow p_0, p_1, \ldots, p_N. \tag{3.41}$$

The problem family is built in such a way that, for instance, for the lowest values of p the family degenerates to a problem with a relatively easily obtainable solution, while increasing p reduces to the problem whose solution is desired.
A number of techniques exist to built a continuation method: for instance it can be obtained, by introducing the continuation parameter directly in the performance index

$$I_\epsilon = \int_{t_0}^{t_f} [u(t) - \epsilon F(u(t))] dt, \tag{3.42}$$

where F is a continuous function satisfying

$$F(w) \geq 0 \qquad \forall w \in [0, 1]. \tag{3.43}$$

For a list of possible suitable functions F, see Bertrand and Epenoy [5]. For example using a quadratic penalty function, the performance index becomes

$$I_\epsilon = \int_{t_0}^{t_f} [u(t) - \epsilon u(t)(1 - u(t))] dt. \tag{3.44}$$

The optimal control direction holds the same form as (2.60), while the magnitude becomes

$$\begin{cases} u = 0 & \text{if} \quad \rho > \epsilon, \\ u = 1 & \text{if} \quad \rho < -\epsilon, \\ u = \frac{1}{2} - \frac{\rho}{2\epsilon} & \text{if} \quad |\rho| \leq \epsilon, \end{cases} \tag{3.45}$$

with $\epsilon \rightarrow 0$, the problem is more and more discontinuous and finally reduces to the original one.
Another technique to build a smoothing-continuation method, is to approximate the discontinuous behaviour of the optimal control magnitude, defining it as a function of both the switching funtion ρ and the continuation parameter p. This approach is particularly interesting because, unlike the other methods, it keeps the performance index unchanged, thus its value can be costantly monitorated, during all the continuation phase. In this regard, two possibilities, proposed in [2], have been adopted: the first

uses exponential as approximating function, so the optimal thrust magnitude becomes

$$u = \frac{1}{1 + \exp(2p\rho)}. \tag{3.46}$$

The second is obtained choosing the arctangent function

$$u = \frac{1}{2} + \frac{1}{\pi} \arctan(-p\rho). \tag{3.47}$$

Both smoothing approximations are illustrated in Figure 3.4. As can be seen, they quickly tend to approximate a discontinuous profile as the value of continuation parameter p increases. In particular, from the experience gained during the extensive test phase, an initial p value equal to $p = 1$ can be chosen. Then, at each successive iteration, the value of p can be increased by a factor of two. In this way the discontinuous profile will be approximated within few iterations, keeping at the same time a gradual smoothness.

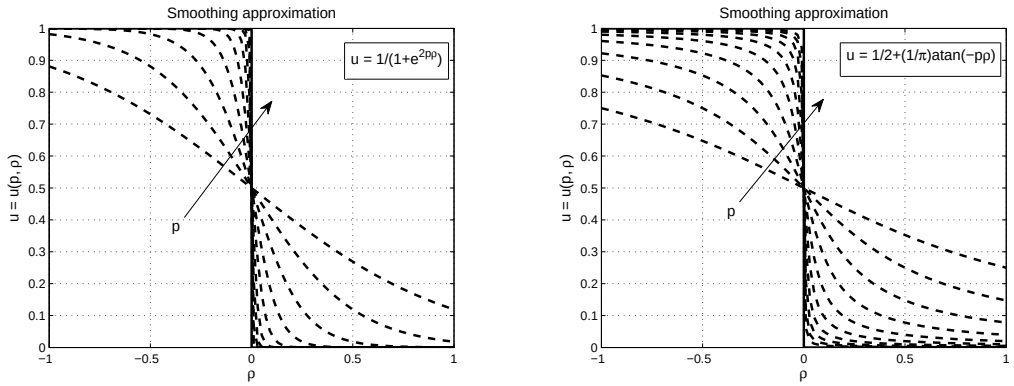

(a) (b)

Figure 3.4: Smoothing approximation: (a) exponential approximation; (b) arctangent approximation.

The problem is solved using the indirect multiple shooting method already presented in section 3.3.1, with the difference that this time the system of differential equations to be integrated is the one composed by (2.5) and (2.34), here reported for the sake of

completeness

$$\begin{cases} \dot{\boldsymbol{r}} &= \boldsymbol{v}, \\ \dot{\boldsymbol{v}} &= \boldsymbol{g}(\boldsymbol{r}) - c_1 \frac{u}{m} \frac{\boldsymbol{\lambda_v}}{\lambda_v}, \\ \dot{m} &= -c_2 u, \\ \dot{\boldsymbol{\lambda}}_r &= \frac{\mu}{r^3} \boldsymbol{\lambda}_v - \frac{3\mu \boldsymbol{r} \cdot \boldsymbol{\lambda}_v}{r^5} \boldsymbol{r}, \\ \dot{\boldsymbol{\lambda}}_v &= -\boldsymbol{\lambda}_r, \\ \dot{\lambda}_m &= -c_1 \frac{u}{m^2} \lambda_v. \end{cases} \tag{3.48}$$

The solution found is used as first guess for the next iteration and the continuation parameter p is continuosly increased at each iteration. For the generic node i

$$\boldsymbol{\xi_k^i} = \left[\begin{array}{c} \boldsymbol{\Xi_{k-1}^i} \end{array} \right], \tag{3.49}$$

where $\boldsymbol{\Xi_{k-1}^i}$ indicates the optimized decision vector at the i-th node, output of the fuel-optimal problem solved using the k-1-th value of p for the smoothing approximation. The continuation stops when p reach a user defined limit p_{max}.
During continuation method, the optimization process is executed multiple times, and even if the last iterations usually demand less computational efforts respect to the first ones, the overall computational time could significantly increase. For this reason it is suggested to limit the maximum number of iterations allowable: a reasonably low value should be selected, so that the optimization is still carried out, but with a lower computational time. The users should not be worried in case the convergence is not achieved at the k-th iteration of the continuation method, since the successive optimizations allow the solver to still find a feasible solution. In case this does not happen, an increase of the number of iterations is recommended.

3.5.2 The Discontinuous Problem

The last solution obtained from the continuation method resembles a "bang-bang" control: however this depends on the final value of p, and it is much more true as the higher the final value of p. Nevertheless it is not really discontinuous, thus a final optimization is performed in which a really discontinuous control law, (2.64), is considered. Choosing a final value of p high enough, this last step does not cause any major difficulties and the solver is usually able to reach the convergence in few iterations.

3.6 Optimization Process

At this point, an overview of the optimization process seems necessary, in order to summarize its fundamental steps and give also an insight of the architecture of the algorithm.

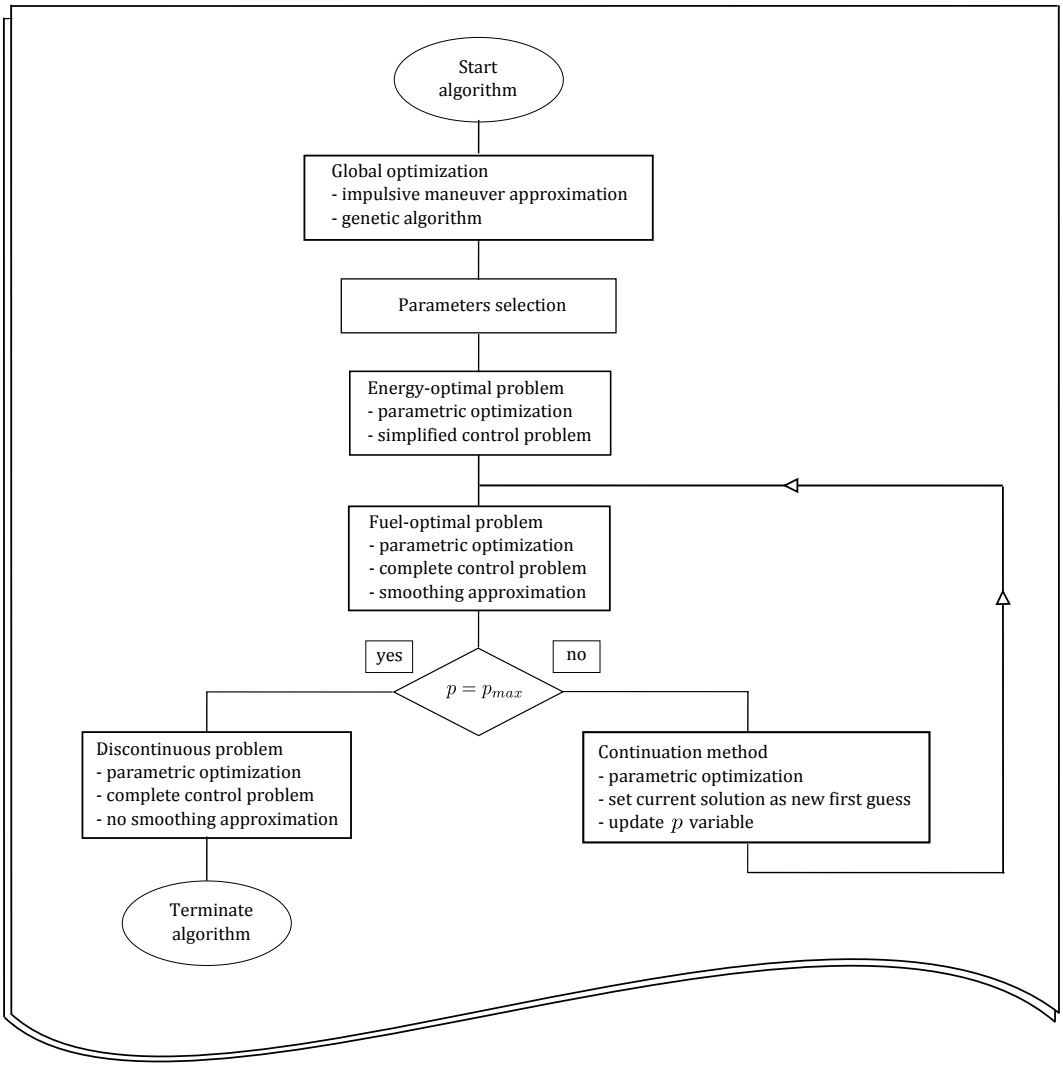

Figure 3.5: Optimization architecture.

As can be seen in Figure 3.5, the process starts with the use of global optimization techniques for the generation of a first guess solution and the inizialization of optimization parameters not included within the optimal control problem, as seen in section 3.2.
The second step mainly regards the definition of the entire optimization variables vector,

throught the selection of parameters as described in section 3.4:

$$\boldsymbol{\xi} = \left[\boldsymbol{\Upsilon}, \boldsymbol{\xi^0}, \boldsymbol{\xi^1}, ..., \boldsymbol{\xi^f}\right]^T, \tag{3.50}$$

in which for a generic node i, $\boldsymbol{\xi^i}$ is given by

$$\boldsymbol{\xi^i} = [\boldsymbol{\xi_r^i}, \boldsymbol{\xi_v^i}, \xi_m^i, \boldsymbol{\xi_{\lambda_r}^i}, \boldsymbol{\xi_{\lambda_v}^i}, \xi_{\lambda_m}^i, \xi_\nu^i]^T. \tag{3.51}$$

Note that this step includes also the initialization of the optimization variables $\boldsymbol{\xi^i}$, achieved by setting to zero the adjoint multipliers ξ_ν^i and the costate variables $\boldsymbol{\xi_\lambda^i}$, whereas the state variables can be obtained from the global solution previously calculated. The procedure continues with the resolution of the energy-optimal problem by means of a parameter optimization technique, as explained in 3.3.1.

The solution obtained from the energy-optimal problem is used as first guess for the fuel-optimal problem, which in turn is always solved through a parametric optimization, this time however, it is also embedded in a continuation method, based on a smoothing approximation.

Finally, when the continuation parameter reaches the values of p_{max}, a real discontinuous problem is solved.

Chapter 4

Results and Validations

In order to validate the optimization algorithm and assess its performances, an extensive test phase has been carried out. Significant test cases have been considered and are reported in this chapter, ordered by increasing complexity. In particular, in section 4.1 a relatively simple planet-to-planet transfer is considered and described in detail, in order to highlight step by step the intermediate solutions obtained during the optimization process. The validation procedure continues in section 4.2, where intermediate flybys are introduced, and follows in section 4.3 with MGA transfers, involving an increasing number of planets. Some interesting results concerning multiple revolution trajectories are outlined in section 4.4, while section 4.5 is devoted to a Near-Earth Asteroid rendezvous tour, proposed during the 3^{rd} Global Trajectory Optimization Competition.

4.1 Planet-to-Planet Transfers: Earth-Mars

Let us consider as first test case the relatively simple transfer from Earth to Mars. This example will be used to remark the overall optimization process, already presented in chapter 3, with the description and the illustration of the intermediate solutions obtained at each step.

In particular, we consider the case in which the spacecraft starts from Earth's position, with a $v_\infty^0 = 0.2$ km/s with respect to Earth's velocity, and arrives at Mars, with the same heliocentric velocity of this planet. As already explained in section 2.2, this value of v_∞^0 is considered fixed, defined by the user or alternatively obtained from the global solution.

The initial mass of the spacecraft is 1500 kg, while the propulsion system is able to provide a maximum thrust of 0.33 N with a $I_{sp} = 3800$ s.

The search space for departure epoch and transfer times is $[4000, 4300]$ MJD2000, and $[200, 500]$ days respectively. The other unknowns, $\boldsymbol{\xi}^i_{\boldsymbol{r}}$, $\boldsymbol{\xi}^i_{\boldsymbol{v}}$, $\boldsymbol{\xi}^i_{\boldsymbol{\lambda_r}}$ or $\boldsymbol{\xi}^i_{\boldsymbol{\lambda_v}}$ are sought in the interval $[-\infty, \infty]$. As already explained in section 3.5, the search space for the mass multipliers $\xi^i_{\lambda_m}$ is set to $[0, 1]$. These assumptions hold for all the following test cases, except where otherwise specified. Finally, for this particular case, the final mass is sought in the interval $[500, 1500]$ kg.

Referring to section 3.4 the optimization variables for this problem are: the launch date ξ^0_t, the time of flight ξ^0_{ToF}, the angles ξ^0_α, ξ^0_δ for the identification of the direction of the initial launch velocity, the initial costates $\boldsymbol{\xi}^0_{\boldsymbol{\lambda_r}}$, $\boldsymbol{\xi}^0_{\boldsymbol{\lambda_v}}$ and $\xi^0_{\lambda_m}$, the adjoint multiplier ξ_{ν^0}, the arrival velocity direction angles ξ^f_α, ξ^f_δ, the adjoint multiplier ξ^f_ν and the final mass ξ^f_m. Complessively we have 16 unknown variables, that will be initialized during the first step of the optimization process. However, as explained in section 3.4.2, the fact that in this specific case the final velocity is equal to the one of the target body, allows us to neglect the trasversality condition (3.36). Therefore, the design variables ξ^f_α, ξ^f_δ and ξ^f_ν, will not be necessary for the solution, since the only unknown parameter is ξ^f_m. Nevertheless, the algorithm still considers these variables in the optimization vector, even when $v^f_\infty = 0$, and initializes them automatically, but they are not used during the optimization process.

The energy optimal solution obtained is reported in Figure 4.1

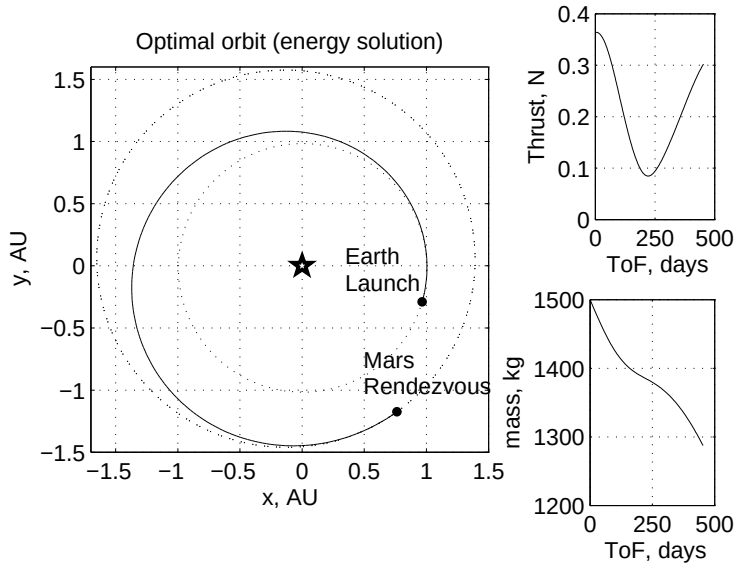

Figure 4.1: Energy-optimal solution for the Earth-Mars tranfer.

As can be seen, the thrust profile overcomes the maximum allowable range of thrust

at the beginning of the transfer. This behaviour is due to the fact that, in the energy-optimal problem, the maximum thrust constraint is not active as the control is given in terms of acceleration. However, as explained in section 3.3, the average value of thrust lies in the allowable range and, therefore, this solution can still be considered a good first guess for the fuel-optimal problem. It is worth reporting the value of final mass in order to make a comparison between this solution and the fuel-optimal one: in this case we have $m_f = 1287$ kg.

The optimization process proceeds with the continuation method (step 2), that is carried out for values of the parameter p ranging from 1 to 1024. At each iteration the value of p is doubled, but this choice is purely based on the experience gained during the extensive test phases, and can be modified by the user. From Figure 4.2 we can notice how the discontinuous behaviour, typical of a bang-bang control law, is progressively obtained thanks to the smoothing approximation on the control amplitude and consequently on the mass consumption.

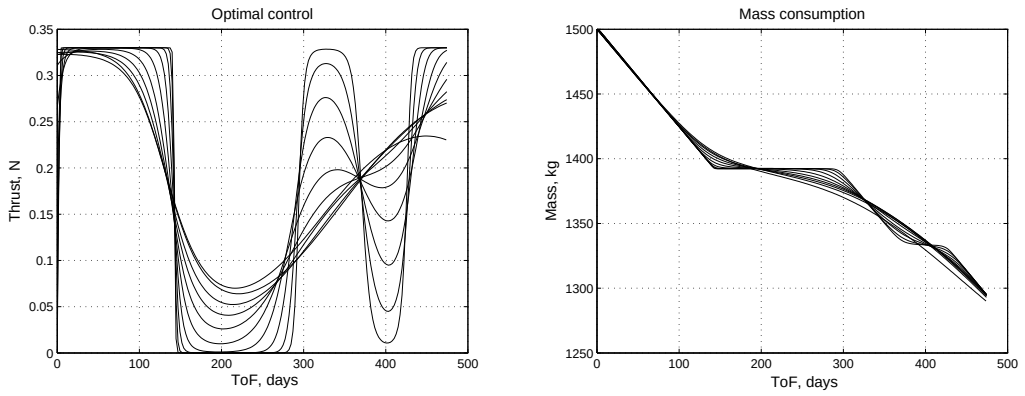

(a) (b)

Figure 4.2: Smoothing approximation for the EM transfer: (a) Thrust magnitude profile; (b) Mass consumption profile.

The last step is solving the discontinuous fuel-optimal problem. Figure 4.3 illustrates the final trajectory and the optimal control amplitude obtained. Bold arcs refer to thrust arcs.

It is interesting to note how the final trajectory fully respect the contraints on the maximum admissible thrust, even if the optimization process has begun with a non rigorously feasible solution. The final value for the mass is $m_f = 1295.04$ kg, that means the fuel-optimal solution has a lower consumption with respect to the energy-optimal one: the reasons of this behavior are strictly related with the change in the optimal control law (see eq.(2.64) and eq.(3.14)), and the resulting change in the dynamics

equations. Moreover, the thrust values of the energy-optimal solution are often outside the admissible range and this fact is reflected in a higher propellant consumption. Table 4.1 reports the identified optimal values for the unknown parameters, while the corresponding trajectory is plotted in Figure 4.3.

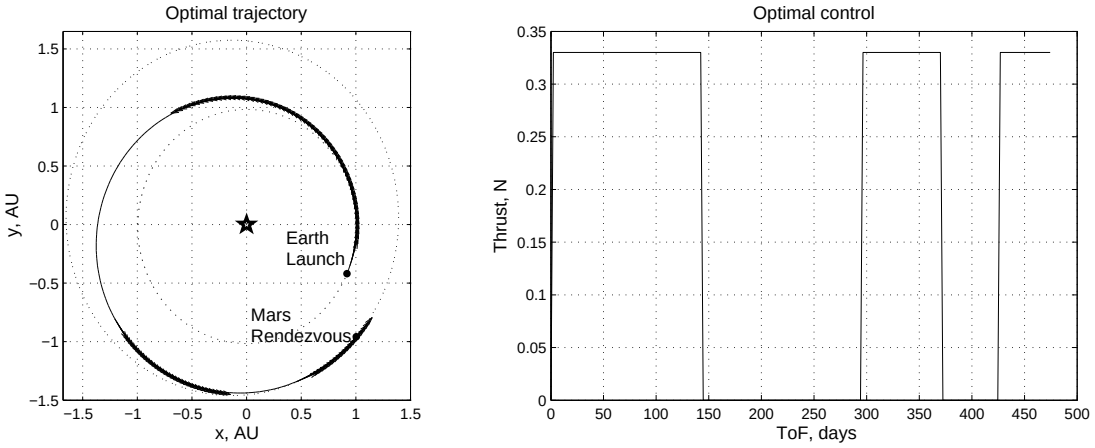

Figure 4.3: Transfer trajectory and optimal control amplitude for the Earth-Mars transfer.

Table 4.1: Solution for Earth-Mars transfer.

Parameter	Value
Launch epoch, MJD2000	4260.62
TOF, days	474.43
$\boldsymbol{\lambda}_{\boldsymbol{r}}^0$	$[-0.611; 0.258; 0.1325]^T$
$\boldsymbol{\lambda}_{\boldsymbol{v}}^0$	$[-0.227; -0.642; -0.088]^T$
λ_m^0	0.139
α^0, rad	1.230
δ^0, rad	0.128
ν^0	-3.432
m_f, kg	1295.04

4.2 One Intermediate Flyby: E-Apophis-E

A simple single-encounter trajectory is presented here. More specifically, a spacecraft with a low-thrust propulsion system performs a flyby of the asteroid Apophis and then

returns to Earth. This mission scenario is presented by Olympio in [42].
The spacecraft is assumed to be equipped with a thruster that provides a T_{max} of 0.3 N with $I_{sp} = 2500$ s. The launch velocity is fixed to $v_\infty^0 = 2500$ m/s, and the initial mass is $m_0 = 1500$ kg.
The overall number of unknowns of this problem is 28: the launch date ξ_t^0, the times of flight ξ_{ToF}^0, ξ_{ToF}^1, the initial launch velocity direction $\xi_\alpha^0, \xi_\delta^0$, the initial costates $\boldsymbol{\xi}_{\boldsymbol{\lambda_r}}^0$, $\boldsymbol{\xi}_{\boldsymbol{\lambda_v}}^0$ and $\xi_{\lambda_m}^0$, the adjoint multiplier ξ_ν^0, the intermediate costates $\boldsymbol{\xi}_{\boldsymbol{\lambda_r}}^i$, $\boldsymbol{\xi}_{\boldsymbol{\lambda_v}}^i$ and $\xi_{\lambda_m}^i$, the intermediate velocity vector $\boldsymbol{\xi}_{\boldsymbol{v}}^i$, the intermediate mass ξ_m^i, the final mass ξ_m^f, the arrival velocity direction ξ_α^f, ξ_δ^f and the adjoint multipier ξ_ν^f.
Table 4.2 defines the search space for departure epoch and transfer times, that in this case are bounded with very narrow margins, which essentially constraints them to be nearly fixed. This is done in order to replicate the reference solution. Other unknowns like $\boldsymbol{\xi}_{\boldsymbol{r}}^i$, $\boldsymbol{\xi}_{\boldsymbol{v}}^i$ or $\boldsymbol{\xi}_{\boldsymbol{\lambda}}^i$ are again sought in the interval $[-\infty, \infty]$. The allowable ranges for intermediate and final mass are instead $[500, 1500]$ kg and $[750, 1500]$ kg, respectively.

Table 4.2: Search space for E-Apophis-E transfer.

	departure epoch [MJD2000]	t_{EA} [days]	t_{AE} [days]
upper	4718	210	440
lower	4718	200	410

The optimal solution obtained is described in Table 4.3. Again the value of m_f is higher than the one obtained for the energy-optimal solution equal to $m_f = 1095.8$ kg.

Table 4.3: Solution parameters.

Parameter	Value
Launch date, MJD2000	4718
TOF_1, days	200
mass at Apophis, kg	1325
Flyby date, MJD2000	4918
TOF_2, days	440
Final mass, kg	1137
Arrival date, MJD2000	5358

Figure 4.4 shows the optimal trajectory and thrust profile, which are in agreement with those presented in [42]. The vertical dotted line represents the date of intermediate encounter.

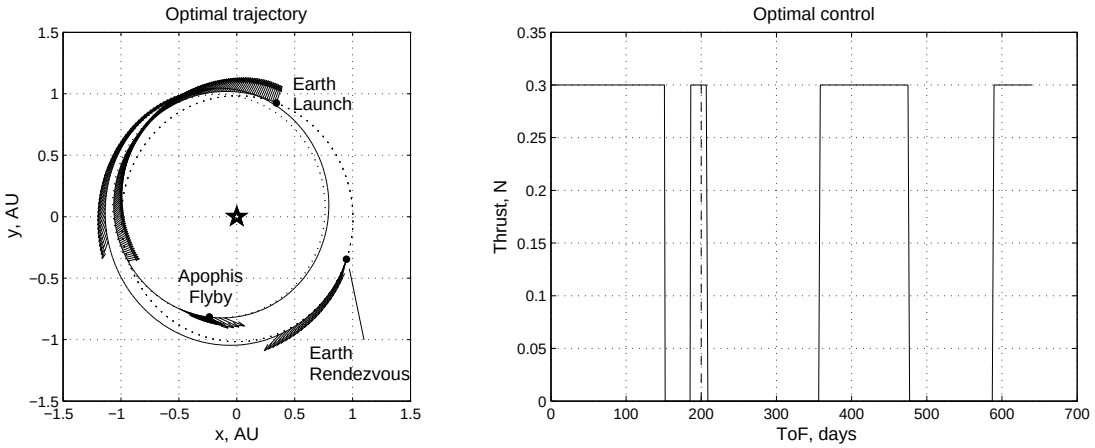

Figure 4.4: Transfer trajectory and optimal control amplitude for an Earth-Apophis-Earth mission.

The convergence is generally good and the solver is able to satisfy the constraints easily, as can be seen in Figure 4.5, which shows the continuity of the switching function at the flyby.

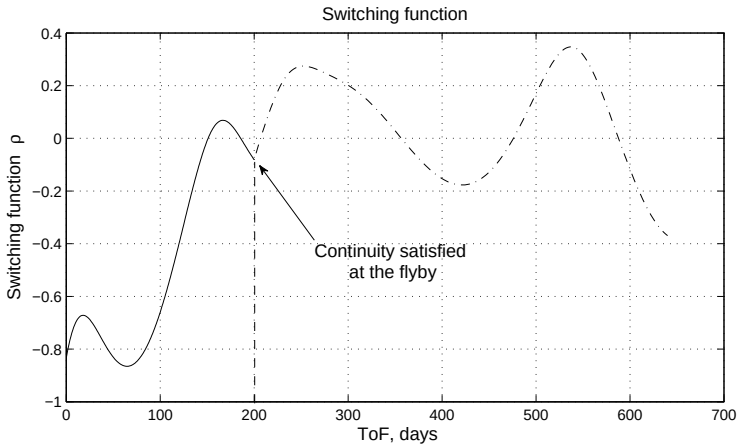

Figure 4.5: Switching function for an Earth-Apophis-Earth mission.

It is worth investigating what happens if the upper and lower bounds on the departure epoch and on transfer times are extended, while keeping the bounds for all the remaining variables unchanged.

The solution is represented in Figure 4.6 and is characterized by an highter value of the final mass, $m_f = 0.9552$, thus supplying a better solution to the problem. It is interesting to note also that the new departure epoch is scheduled only about 46 days before the launch date of the reference solution seen before, whereas the transfer times

are comparable with the values obtained previously (see Tables 4.3-4.5).
Table 4.4 summarizes the updated bounds for this test case.

Table 4.4: Search space for E-Apophis-E transfer (extended bounds).

	departure epoch [MJD2000]	t_{EA} [days]	t_{AE} [days]
upper	4518	100	400
lower	5018	300	440

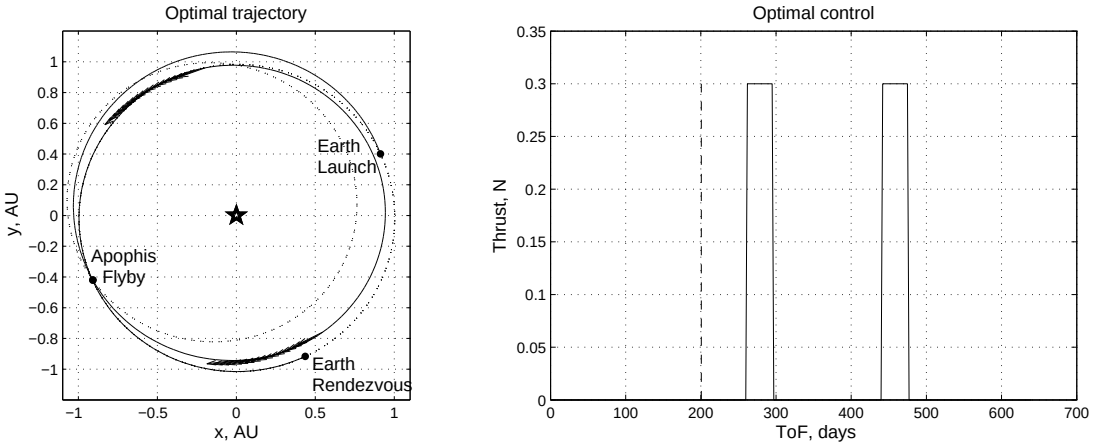

Figure 4.6: Transfer trajectory and optimal control amplitude for an Earth-Apophis-Earth mission (extended bounds).

Table 4.5: Solution parameters (extended bounds).

Parameter	Value
Launch date, MJD2000	4672.19
TOF_1, days	200.58
mass at Apophis, kg	1500
Flyby date, MJD2000	4872.77
TOF_2, days	438.68
Final mass, kg	1432.76
Arrival date, MJD2000	5311.4536

4.3 Multiple Gravity-Assist Trajectories

4.3.1 Earth-Venus-2001HY7

Multiple gravity assist trajectories are addressed in this section. The first test case is a simple trajectory with a single gravity assist at Venus and a final rendezvous with asteroid 2001 HY7.
The assumed upper and lower bounds for departure epoch and times of flight are reported in Table 4.6. The characteristics of the spacecraft and the search space for all the other optimization variables are the same as for the Earth-Mars test case.

Table 4.6: Search space for the Earth-Venus-2001 HY7 transfer.

	departure epoch [MJD2000]	t_{EV} [days]	t_{V-HY7} [days]
upper	8036	400	400
lower	4383	70	70

Referring to section 3.4 and Table 3.1, the unknown variables are complessively 30:

$$\boldsymbol{\xi} = [\xi_t^0,\, \xi_{ToF}^0,\, \boldsymbol{\xi}_{\boldsymbol{\lambda}}^0,\, \xi_\alpha^0,\, \xi_\delta^0,\, \xi_\nu^0,\, \xi_{ToF}^1,\, \boldsymbol{\xi}_{\boldsymbol{v}}^1,\, \xi_m^1,\, \boldsymbol{\xi}_{\boldsymbol{\lambda}}^1,\, \xi_\nu^1,\, \xi_{r_{ph}}^1,\, \xi_\alpha^f,\, \xi_\delta^f,\, \xi_\nu^f,\, \xi_m^f].$$

The optimal trajectory and the optimal control amplitude vs. time are depicted in Fig. 4.7.

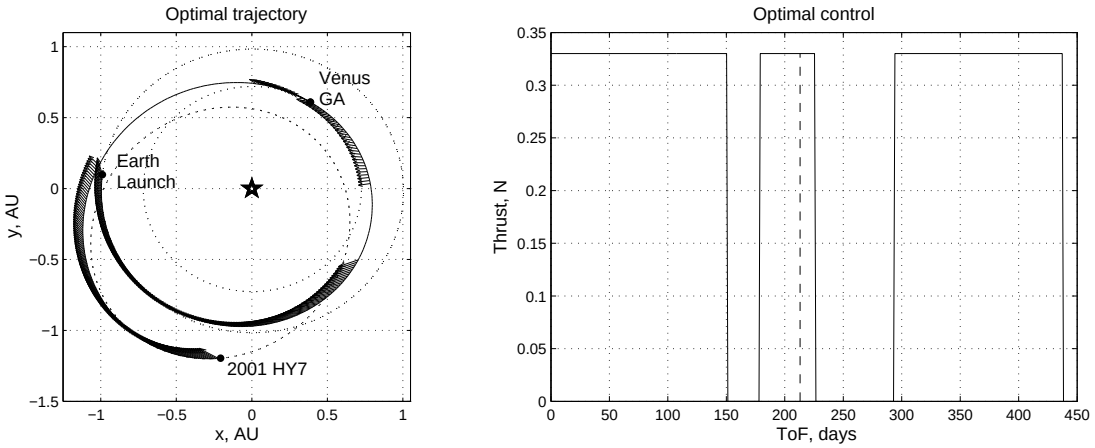

Figure 4.7: Earth-Venus-2001 HY7 trajectory and optimal control amplitude.

Figure 4.8 reports instead the switching function ρ for this problem. As can be seen, it

is continuous at the gravity assist, meaning that the conditions on the costate variables, presented in section 2.3.2, are completely satisfied.
Moreover, we find again that the value of m_f achieved in the energy-optimal solution (equal to 1084 kg) is lower than the one obtained for the fuel-optimal, $m_f = 1237.95$.

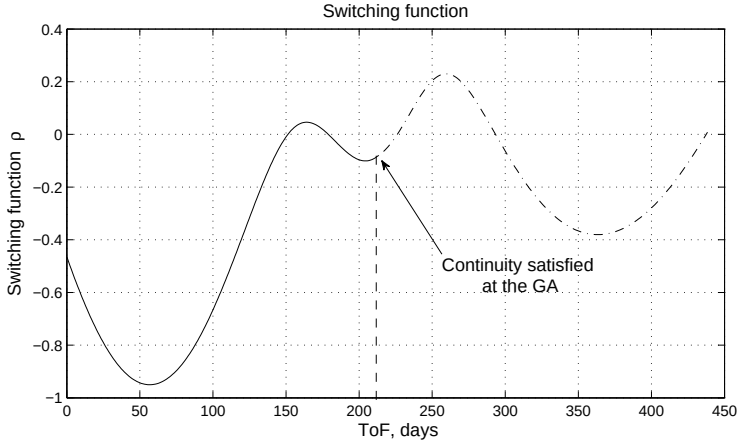

Figure 4.8: Switching function for the Earth-Venus-2001 HY7 transfer.

Finally, Table 4.7 summarizes the trajectory main characteristics.

Table 4.7: Earth-Venus-2001 HY7 rendezvous trajectory.

Parameter	Value
Launch date	5551.77
Launch V_∞, km/s	0.2
Venus GA date	5764.84
Venus GA altitude, km	29898.9
Venus GA V_∞, km/s	4.81
2001 HY7 arrival date	5990.125
Total TOF, years	1.2
Final mass, kg	1237.95

4.3.2 Earth-Venus-Earth-Mars

Two gravity assists are here introduced for an Earth-Venus-Earth-Mars transfer. The mission starts with $v_\infty^0 = 0.5$ km/s, while the relative velocity with respect to the arrival planet is set to $v_\infty^f = 2$ km/s. Lower and upper bounds for launch date and transfer times are listed in Table 4.8, whereas the main characteristics of the spacecraft and the

search space for the other optimization variables are the same as for the Earth-Mars problem.

Table 4.8: Search space for the EVEM transfer.

	departure epoch [MJD2000]	t_{EV} [days]	t_{VE} [days]	t_{EM} [days]
upper	9132	400	400	400
lower	4383	50	50	50

The total number of optimization variables obviously increases to 44:

$$\boldsymbol{\xi} = [\xi_t^0,\, \xi_{ToF}^0,\, \boldsymbol{\xi}_{\boldsymbol{\lambda}}^0,\, \xi_\alpha^0,\, \xi_\delta^0,\, \xi_\nu^0,\, \xi_{ToF}^1,\, \boldsymbol{\xi}_{\boldsymbol{v}}^1,\, \xi_m^1,\, \boldsymbol{\xi}_{\boldsymbol{\lambda}}^1,\, \xi_\nu^1,\, \xi_{r_{ph}}^1,$$
$$\xi_{ToF}^2,\, \boldsymbol{\xi}_{\boldsymbol{v}}^2,\, \xi_m^2,\, \boldsymbol{\xi}_{\boldsymbol{\lambda}}^2,\, \xi_\nu^2,\, \xi_{r_{ph}}^2,\, \xi_\alpha^f,\, \xi_\delta^f,\, \xi_\nu^f,\, \xi_m^f].$$

Figure 4.9 illustrates the optimal trajectory and the corresponding control magnitude history.

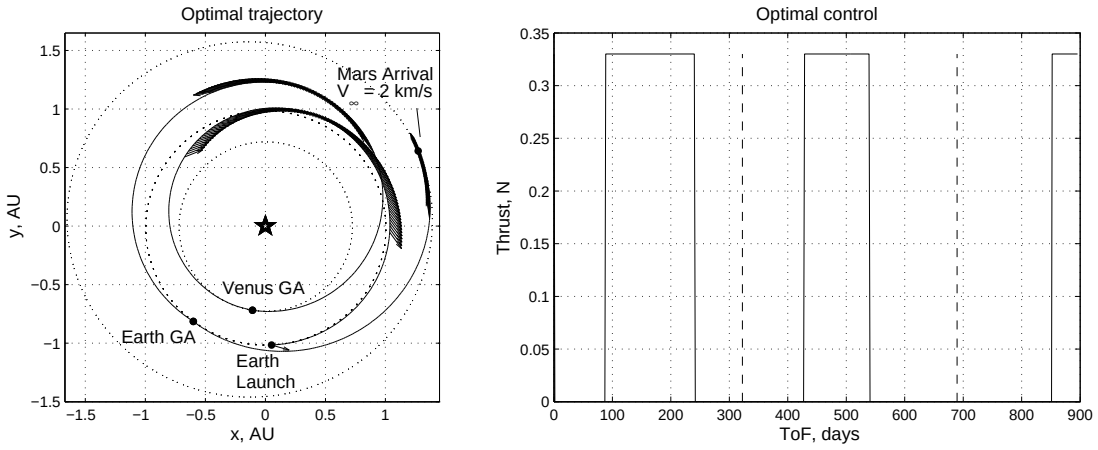

Figure 4.9: Earth-Venus-Earth-Mars trajectory and optimal control amplitude.

It is interesting to note how the continuity condition of the switching function is respected in both gravity assist meneuvers, as highlighted in Figure 4.10. For the sake of completeness, the main results for the optimal trajectory are listed in Table 4.9. Even in this test case, the fuel-optimal solution turns out to be more conservative in terms of mass consumption with respect to the energy-optimal solution where the final value of the spacecraft mass is $m_f = 1023.1$ kg.

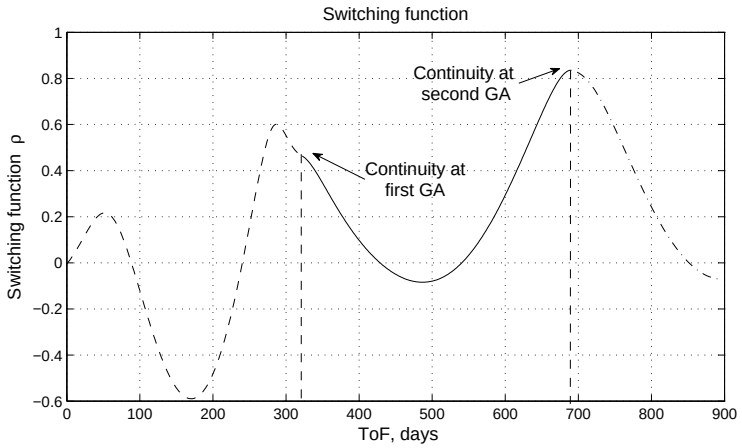

Figure 4.10: Switching function for the Earth-Venus-Earth-Mars transfer.

Table 4.9: EVEM transfer trajectory.

Parameter	Value
Launch date, MJD2000	6018.47
Launch V_∞, km/s	0.5
Venus flyby date, MJD2000	6340.739
Venus flyby altitude, km	31924.237
Venus flyby V_∞, km/s	4.36
Earth flyby date, MJD2000	6707.94
Earth flyby altitude, km	28260.00
Earth flyby V_∞, km/s	2.815
Mars arrival date, MJD2000	6913.98
Total TOF, years	2.453
Final mass, kg	1263.43

4.3.3 Earth-Venus-Earth-Jupiter

As next study case, we consider an Earth-Venus-Earth-Jupiter rendezvous mission, with a v_∞^0 at launch of 2.19 km/s. The initial mass is 18333 kg and the chosen thruster parameters are $T_{max} = 2.26$ N and $I_{sp} = 6000$ s. This mission scenario is presented also in [63], where a preliminary study of nuclear-electric propulsion missions is assessed. Moreover, it represents a good validation test as it involves multiple gravity assists and allows us to test the algorithm for missions towards outer planet, where trajectories could be very sensitive and the convergence more tricky.

At this point, it should be clear that the transfer is automatically split into different phases by the algorithm in the first steps of the optimization process, and typically the

nodes correspond to the encountered bodies. In this particular example we have three different arcs in which the first one goes from launch to the gravity assist at Venus, the second refers to the trajectory leg between the first and the second gravity assist maneuver and the last goes from the gravity assist at Earth to the Jupiter rendezvous. Unfortunately, this decomposition turns out to be insufficient since the convergence for the last trajectory leg is quite difficult due to its long duration. Thus, in order to increase the robustness of the algorithm, the Earth-Jupiter arc is split in two addictional segments, for a total of four trajectory legs for the entire transfer. As explained in section 3.2, the intermediate point is manually taken from the trajectory calculated with the global optimizer and the corresponding values of position and velocity are used as a good initial guess for the local optimization. The number of optimization variables obviously increases, since all the state and costate variables at the intermediate point must be identified. However, convergence improves and the computational time is reduced. In this particular case, with two gravity assists and one intermediate point, there are 59 unknown variables:

$$\begin{aligned}\boldsymbol{\xi} = [&\xi_t^0,\, \xi_{ToF}^0,\, \boldsymbol{\xi}_{\boldsymbol{\lambda}}^0,\, \xi_\alpha^0,\, \xi_\delta^0,\, \xi_\nu^0,\\ &\xi_{ToF}^1,\, \boldsymbol{\xi}_{\boldsymbol{v}}^1,\, \xi_m^1,\, \boldsymbol{\xi}_{\boldsymbol{\lambda}}^1,\, \xi_\nu^1,\, \xi_{r_{ph}}^1,\, \xi_{ToF}^2,\, \boldsymbol{\xi}_{\boldsymbol{v}}^2,\, \xi_m^2,\, \boldsymbol{\xi}_{\boldsymbol{\lambda}}^2,\, \xi_\nu^2,\, \xi_{r_{ph}}^2,\\ &\xi_{ToF}^3,\, \boldsymbol{\xi}_{\boldsymbol{r}}^3,\, \boldsymbol{\xi}_{\boldsymbol{v}}^3,\, \xi_m^3,\, \boldsymbol{\xi}_{\boldsymbol{\lambda}}^3,\, \xi_\alpha^f,\, \xi_\delta^f,\, \xi_\nu^f,\, \xi_m^f].\end{aligned}$$

In general, intermediate points are identified in chronological order by a cardinal number. In this case we have only one intermediate point between Earth gravity assist and Jupiter rendezvous, indicated as point 1.
The search space for departure epoch and transfer times is defined in Table 4.10.

Table 4.10: Search space for EVEJ transfer.

	departure epoch [MJD2000]	t_{EV} [days]	t_{VE} [days]	t_{E1} [days]	t_{1J} [days]
upper	6820	200	370	250	955
lower	6800	170	340	163	788

As in the previous cases, the final mass for the fuel-optimal solution (equal to 15307 kg), is greater than the value of 12612.13 kg provided by the solution of the energy-optimal problem.
The results are listed in Table 4.11 and the obtained trajectory is depicted in Fig. 4.11. Despite some minor differences, there is a good agreement between our solution and the

reference one [63], obtained by the optimization program GALLOP, which implements a direct method.

Table 4.11: EVEJ rendezvous trajectory.

Parameter	Value
Launch date, MJD2000	6806.01
Launch V_∞, km/s	2.19
Venus flyby date, MJD2000	6982.86
Venus flyby altitude, km	217
Venus flyby V_∞, km/s	5.46
Earth flyby date, MJD2000	7329.86
Earth flyby altitude, km	200
Earth flyby V_∞, km/s	10.19
Jupiter arrival date, MJD2000	8469.974
Total TOF, years	4.56
Final mass, kg	15307

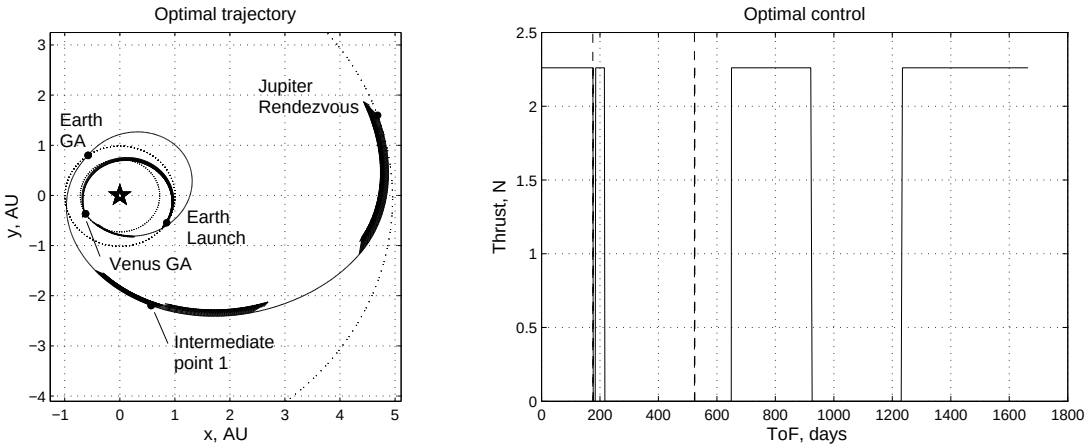

Figure 4.11: Earth-Venus-Earth-Jupiter trajectory and optimal control amplitude.

Additional considerations regard the altitudes of the hyperbolic passages. With respect to the previous multiple gravity assist trajectories, the solution for this test case requires larger velocity changes and consequently lower hyperbolic pericenter radii. The constraint on the minimum admissible radius eq. (2.17) becomes very critical. However, the numerical formulation adopted in section 3.4.1, fits for the purpose, allowing the algorithm to obtain a feasible solution even in this case.

4.4 Multiple Revolution Transfers

4.4.1 Earth-Mars

We have already discussed about the insertion of an intermediate point and the subsequent split of the trajectory into multiple phases: it is very useful, specially for trajectory arcs with long transfer times as it improves the robustness of the method. Similarly, this section shows how intermediate points can be used to design transfers involving multiple revolution trajectories. Let us consider an ipotetical mission to Mars, with a transfer time that can vary between 500 and 800 days and a minimum of one complete revolution. A 2000 kg spacecraft is supposed to be equipped with a cluster of electric engines delivering a maximum of 0.33 N of thrust at an $I_{sp} = 3000$ s. Despite its semplicity, this example is aimed at understanding how the algorithm can operate. If no intermediate points are considered, the energy-optimal solution obtained could be like the one reported in Fig. 4.12.

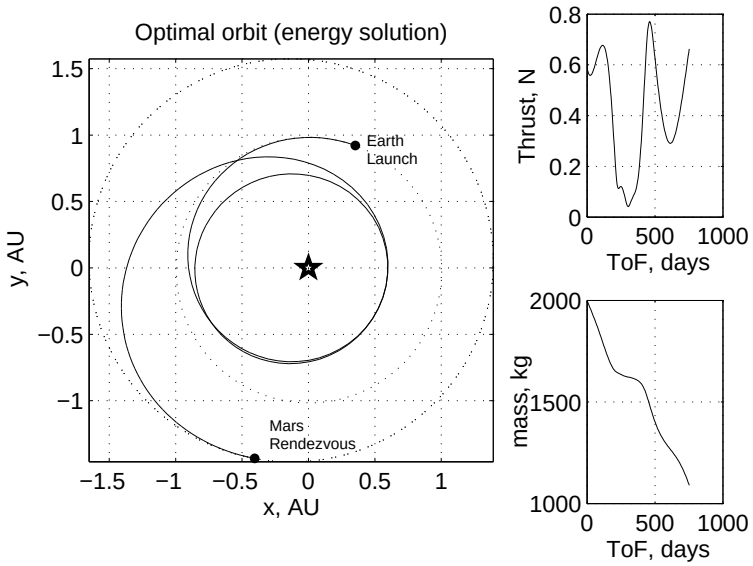

Figure 4.12: Earth-Mars multiple revolution tranfer without intermediate points (energy-optimal solution).

As can be seen, the algorithm forces the thrust to values out of its admissible range: in section 4.1, we have already encountered such a situation and we have already stated that this happens because in the energy-optimal problem the maximum thrust constraint is not active as the control is given in terms of acceleration. This time however, unlike the previous case, the energy-optimal solution is not suitable to be used as first

guess for the successive steps, since the violation of the maximum thrust constraint is very large. The corresponding trajectory is too much distant from the solution and typically involves a failure in the optimization process.
The introduction of an intermediate point helps to find a feasible solution for this kind of problems, by solving legs of reduced sensitivity. The bounds on the departure epoch from Earth and on the transfer time from Earth to Mars are the same. However the energy-optimal solution obtained in this way and reported in Figure 4.13, is better than the previous one, as it requires values of thrust which fall within the admissible range.

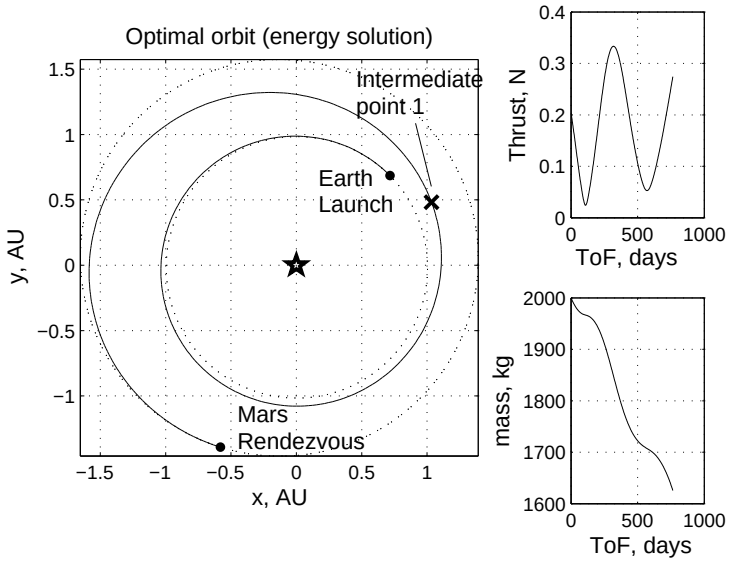

Figure 4.13: Earth-Mars multiple revolution transfer with intermediate points (energy-optimal solution).

When this solution is used as first-guess for the continuation process to compute the fuel-optimal solution, the optimization procedure has no convergence problems. The optimal trajectory and the corresponding thrust magnitude profile are depicted in Figure 4.14. For the sake of completeness, the main results are also reported in Table 4.12.

4.4.2 Earth-Venus

Following the same approach presented in section 4.4.1, a further planet-to-planet multiple revolution transfer is investigated in this section: a rendezvous problem from Earth to Venus. This example is taken from [5], and is also analyzed by Jiang et al. in [29]. The algorithm tends to have some troubles with this kind of trajectories, because of

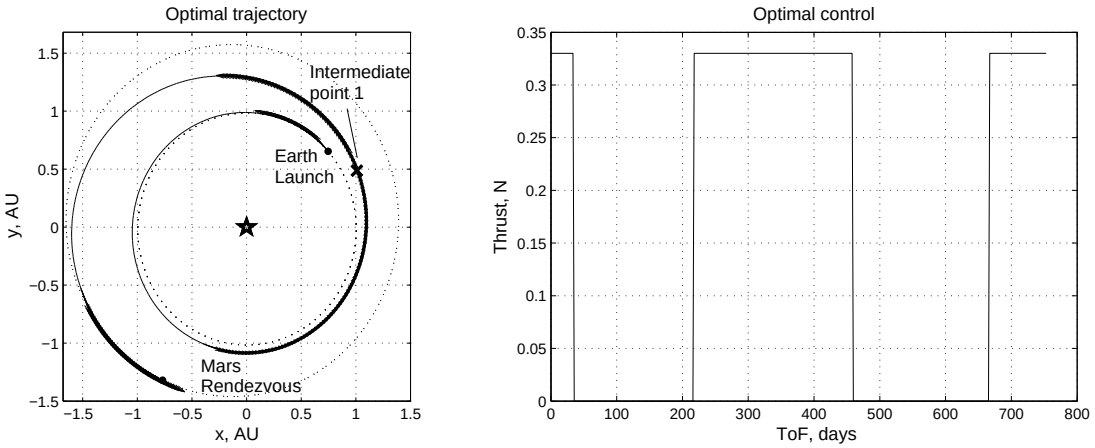

Figure 4.14: Earth-Mars multiple revolution tranfer trajectory and optimal control amplitude.

Table 4.12: Earth-Mars rendezvous trajectory.

Parameter	Value
Launch date, MJD2000	7976.91
Launch V_∞, km/s	0
Mars arrival date, MJD2000	8729.8
Mars arrival V_∞, km	0
Total TOF, years	2.06
Initial mass, kg	2000
Thrust amplitude, N	0.33
Specific impulse, s	3000
Final mass, kg	1650

their long duration and sensitivity. Splitting the trajectory into different legs, using intermediate points can bring great benefits to the tool, as already shown in the previous case. To this aim, we split the trajectory into 5 different legs by introducing 4 intermediate points, identified in chronological order as point 1, point 2, point 3 and point 4. It is worth recalling that these points are manually taken from the trajectory calculated with the global optimizer and the corresponding values of position and velocity represent only first-guesses that are optimized by the algorithm. Thus, it is not necessary to select specific points: the user should rather select them based on experience. In general there are no bounds on the position and velocity of these points, as they are sough in the interval $[-\infty, \infty]$. In this case however, the search space for the position is set to $[\boldsymbol{r}_i - 10\%, \boldsymbol{r}_i + 10\%]$, due to the fact that the presence of subsequent intermediate

points may cause the overlap of different trajectory legs. $\boldsymbol{r}_i$ represents the first guess position obtained by the user from the global solution, whereas the 10% value is purely based on the experience gained during the extensive test phases. The search space for the departure epoch and transfer times is defined in Table 4.13.

Table 4.13: EV rendezvous search space.

	departure epoch [MJD2000]	t_{E1} $[days]$	t_{12} $[days]$	t_{23} $[days]$	t_{34} $[days]$	t_{4V} $[days]$	n^o revolutions
upper	2110	380	190	100	200	300	3
lower	2000	280	130	30	110	250	3

In the previous table, the minimum and maximum number of revolutions are reported, in particular they are both equal to 3, as we want to reproduce the solution obtained by Bertrand [5]. Nevertheless, it is worth specifying that these parameters are used only in the global optimization phase.
The resulting optimal trajectory is presented in Figure 4.15 and described in Table 4.14 together with some characteristics on the spacecraft.

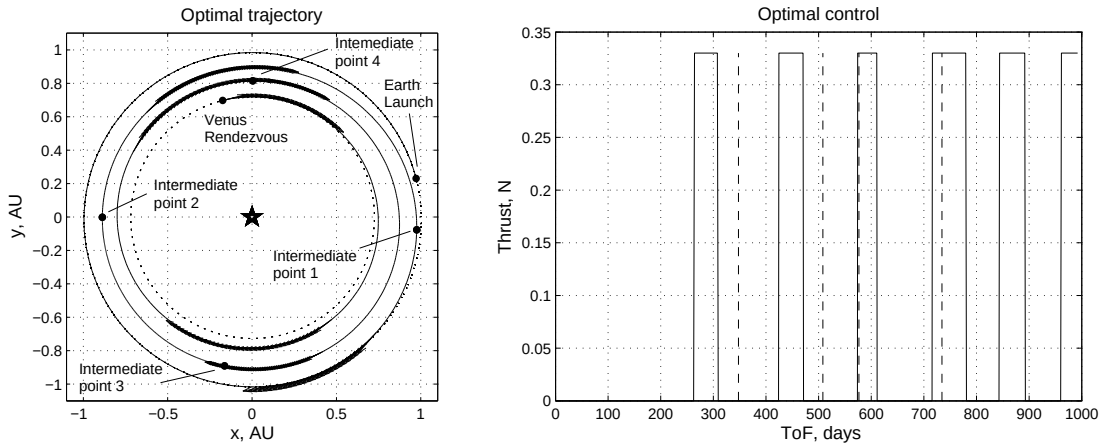

Figure 4.15: Earth-Venus multiple revolution tranfer trajectory and optimal control magnitude. Vertical dashed line refers to the intermediate points.

Again the fuel-optimal solution shows less propellant consumption and the value of $m_f = 1290.3$ kg is higher than the one obtained from the solution of the energy-optimal problem (equal to 1285.4 kg).

Table 4.14: Multiple-revolution Earth-Venus rendezvous trajectory.

Parameter	Value
Launch date, MJD2000	2105
Launch V_∞, km/s	0
Venus arrival date, MJD2000	3097.3
Venus arrival V_∞, km	0
Total TOF, years	2.72
Initial mass, kg	1500
Thrust amplitude, N	0.33
Specific impulse, s	3800
Final mass, kg	1290.3

4.5 3^{rd} Global Trajectory Optimization Competition

GTOC (Global Trajectory Optimization Competition) is a yearly competition among universities and research centers that aims at advancing the automation of the trajectory design process. The 3^{rd} edition, held in December 2007 at Politecnico di Torino, introduces the problem of finding an optimal trajectory for a Near-Earth Asteroid rendezvous tour: it is required to rendezvous with at least three asteroids and visit each asteroid for at least sixty days; in addition, the spacecraft must return to Earth and the tour must last at most ten years. The transfers could include one or more gravity assists on Earth.
The characteristics of the probe were imposed and are reported in Table 4.15.

Table 4.15: GTOC mission parameters.

Mass	2000 kg
I_{sp}	3000 s
T_{max}	150 mN
$v^0_{\infty_{max}}$	0.5 km/s
$v^f_{\infty_{max}}$	0 km/s

This kind of mission is gaining increasing interest not only for the study of asteroid's conformation and characteristics, that could provide information on the origin of the solar system and life on Earth, but also for the challenge that they represents in terms of trajectory optimization, due to the long duration of the mission (10 years) and the

limited controllability of the ion engine. The solution is very complex and expensive, representing a good convergence test for the algorithm.
The traditional first step in designing multiple asteroid tour missions is to identify a reduced list of potential target among asteroids database. This could be achieved throught different kind of techniques and using different selection criteria like the asteroids' orbital elements, dimensions and so on [39]. The second step is to quickly identify the potential dates of encounter and to estimate ΔV budgets throught global optimization methods, using for example shape-based model or impulsive maneuver approximations [44, 56]. The last step is to optimize the choosen asteroid sequences with fairly accurate methods (i.e., local optimization methods), that is the step on which we focus in this dissertation.
Bearing this in mind, we decided to use the asteroid sequence submitted by the team TAC (The Aerospace Corporation), which exploits the sequence E-88-E-96-49-E, where 88, 96 and 49 are the asteroids as cataloged in the list provided by the organizers [15]. This sequence has been used in Carrara's tool to obtain a global first guess solution for the local optimization.
Despite the complexity of this kind of trajectory, the presence of multiple encounters leads to a succession of relatively short and non particularly critical legs. The introduction of intermediate points is therefore unnecessary.
The total number of unknowns for this problem is 84. Table 4.16 defines the search space for departure epoch and transfer times, while other unknowns like $\boldsymbol{\xi}_{\boldsymbol{r}}^i$, $\boldsymbol{\xi}_{\boldsymbol{v}}^i$ or $\boldsymbol{\xi}_{\boldsymbol{\lambda}}^i$ are again sought in the interval $[-\infty, \infty]$.

Table 4.16: GTOC mission limits.

	Dep. Epoch	E-88	88-88	88-E	E-96	96-96	96-49	49-49	49-E
Upper	6824	587	443	836	587	552	572	513	894
Lower	6024	187	60	436	187	152	372	113	494

The results obtained are slightly different from the solution provided by team TAC. In fact the two solutions are characterized by quite different values for the departure epoch and transfer times, that inevitably affect the performance index, as reported in Table 4.17. However such a difference is already present in the global solution used as first guess, where the value of final adimensionalized mass is 0.7829. This may be due to the fact that the original performance index used in GTOC is slightly different from

the one used in our simulations:

$$\mathcal{J} = \frac{m_f}{m_0} + K\frac{\min_{j=1,3}(\tau_j)}{\tau_{max}}, \tag{4.1}$$

where m_0 and m_f are the spacecraft initial and final mass, respectively; τ_j, with $j = 1, 3$, represents the stay-time at the j-th asteroid in the rendezvous sequence and $\min_{j=1,3}(\tau_j)$ is the shortest asteroid stay-time; $\tau_{max} = 10$ years is the maximum trip time, and $K = 0.2$.

Table 4.17: GTOC mission results.

Analysis Author	Departure Epoch [MJD2000]	ToF [days]	m_f/m_0
TAC	6194	$\begin{pmatrix} 377 \\ 267 \\ 627 \\ 362 \\ 425 \\ 492 \\ 353 \\ 676 \end{pmatrix}$	0.8235
Rasotto	6566.43	$\begin{pmatrix} 580 \\ 88 \\ 641 \\ 441 \\ 320 \\ 567 \\ 295 \\ 682 \end{pmatrix}$	0.7956

All the boundary constraints on state variables and the optimality conditions on costates are fully respected, with a maximum constraint violation of the order of 10^{-7}.
Figure 4.16 reports the solution obtained for the fuel-optimal problem. The corresponding thrust magnitude profile is depicted in Figure 4.17(a), whereas the mass consumption is plotted in Figure 4.17(b). Vertical dashed lines represent dates of intermediate

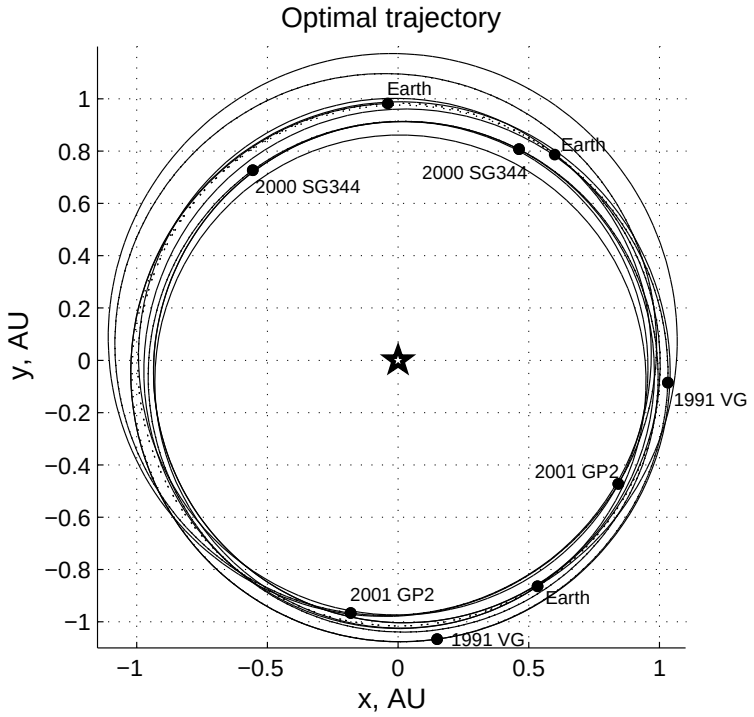

Figure 4.16: Optimal trajectory for GTOC sequence (mass solution).

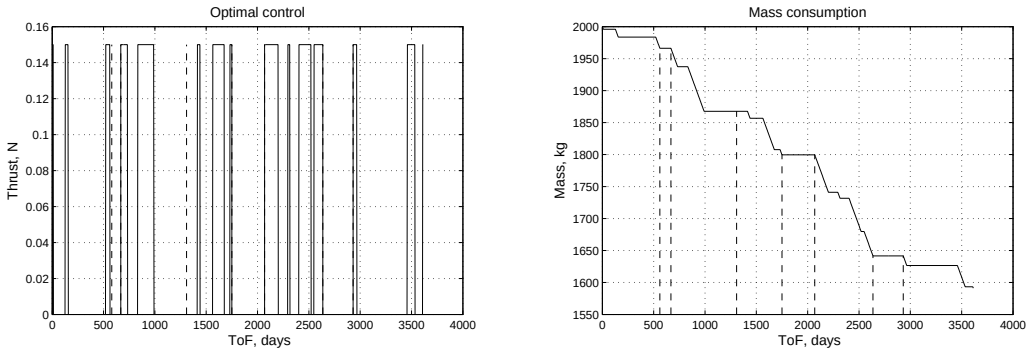

(a) (b)

Figure 4.17: GTOC problem: (a) Thrust magnitude vs time; (b) Mass consumption.

encounters, i.e. arrival and departure from asteroids and the Earth gravity assist. During rendezvous with asteroids, thrust is turned off for all the duration of the transfer and there is no mass consumption: indeed we don't have any change in orbit and the spacecraft moves along with the orbital body. The final mass is about 79.56% of the initial spacecraft mass m_0, i.e. about 1591 kg. By comparing the value obtained for

the energy-optimal solution, equal to 1544.7 kg, we find that it is slightly higher, which means the final solution has lower consumption. Also the time of flight is slightly higher: the mass-optimal solution last complessively 3613 days, 108 days more than the energy-optimal solution. This is not surprising since both departure epoch and transfer times are changed in the last optimization procedure in order to satisfy all the constraints. Figure 4.18 illustrates the phases of the problem and the distance to Sun over time.

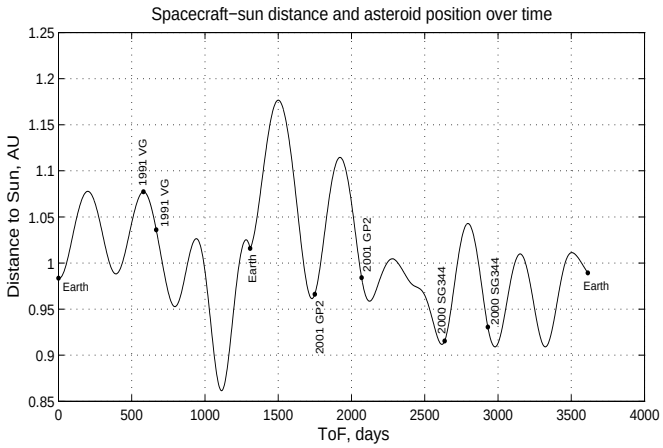

Figure 4.18: Spacecraft-sun distance and asteroid position over time.

For the sake of a clearer illustration, in Figures 4.19-4.25 the final trajectory has been divided and plotted into its different phases. For each section we report the transfer trajectories and the corresponding control histories. The plots on the left show the transfer trajectories and the thrust vector (indicated by the arrows). Time histories of thrust magnitude and direction are shown in the plots on the right.

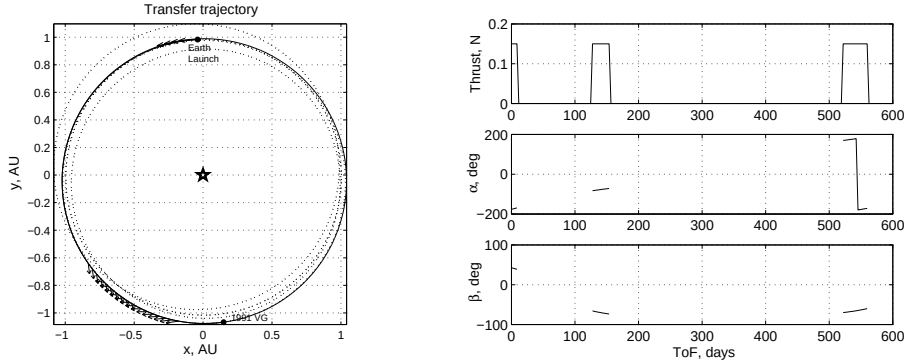

Figure 4.19: Transfer Earth-1991 VG: thrust magnitude and direction.

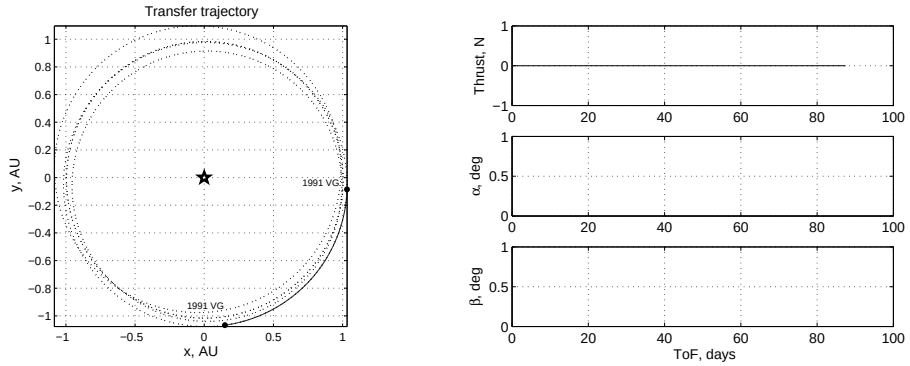

Figure 4.20: Transfer 1991 VG-1991 VG: thrust magnitude and direction.

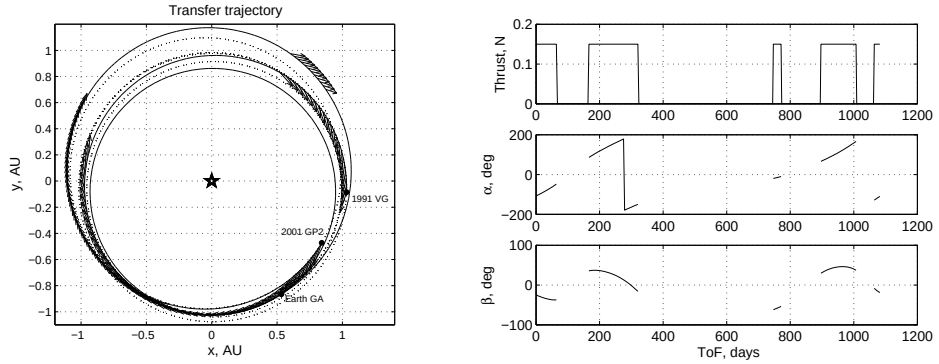

Figure 4.21: Transfer 1991 VG-Earth-2001 GP2: thrust magnitude and direction.

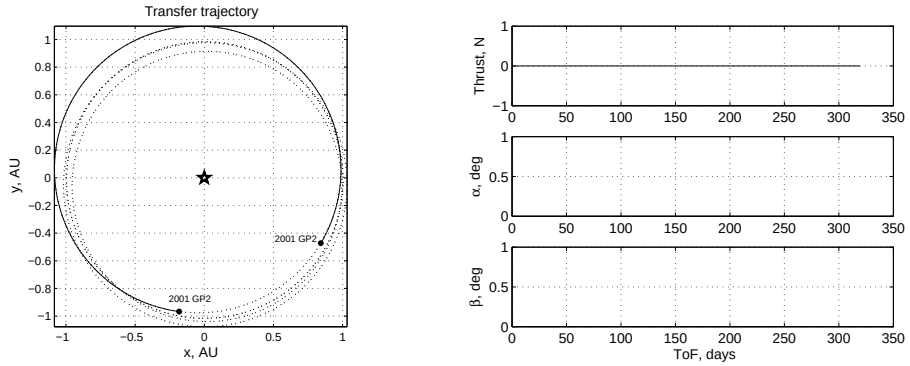

Figure 4.22: Transfer Earth-2001 GP2-Earth-2001 GP2: thrust magnitude and direction.

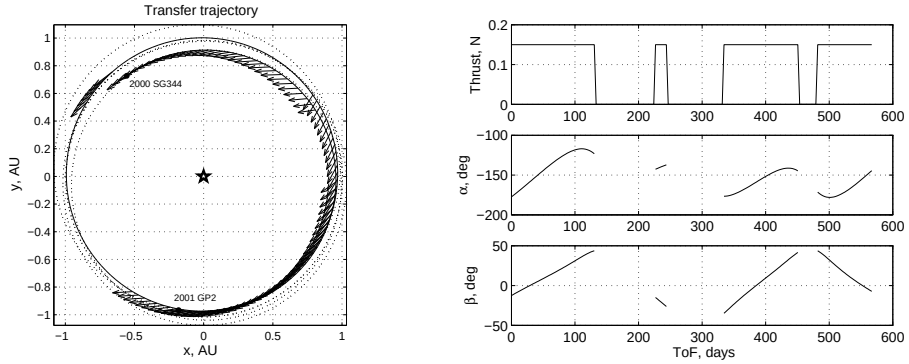

Figure 4.23: Transfer 2001 GP2-2000 SG344: thrust magnitude and direction.

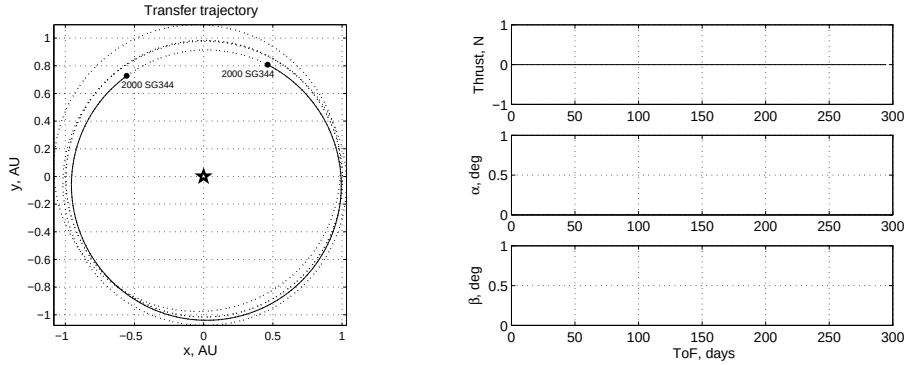

Figure 4.24: Transfer 2000 SG344-2000 SG344: thrust magnitude and direction.

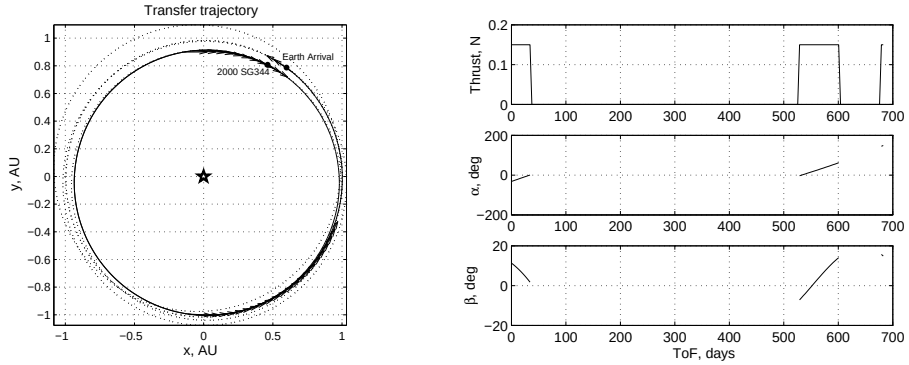

Figure 4.25: Transfer 2000 SG344-Earth: thrust magnitude and direction.

Chapter 5

The Restricted Three-Body Problem

In many instances, keplerian motion and the related trajectory design methods such as the patched two-body approximation, presented in chapter 2 and used throughout the thesis, are inadequate to support new mission concepts. While standard approaches remain valuable for some missions, new trajectory design tools, that exploit multi-body dynamics become necessary in such cases. To this purpose, the two-body model is here replaced by three-body dynamics. The first part of the chapter is dedicated to the review of the most important notions and the derivation of the equations of motion. Then, in the second part, the optimal control problem is derived and solved within this new dynamical model. The last part of the chapter presents the numerical techniques used to solve it, along with the results obtained for low-thrust transfer trajectories from some sample Earth orbits to halo orbits.

5.1 Equations of Motion

Recalling equations (2.1) for $k = 1, 2, 3$, the equations of motion for the general three-body problem read

$$\ddot{\boldsymbol{R}}_1 = -Gm_2\frac{\boldsymbol{R}_1 - \boldsymbol{R}_2}{R_{21}^3} - Gm_3\frac{\boldsymbol{R}_1 - \boldsymbol{R}_3}{R_{31}^3}, \tag{5.1}$$

$$\ddot{\boldsymbol{R}}_2 = -Gm_1\frac{\boldsymbol{R}_2 - \boldsymbol{R}_1}{R_{12}^3} - Gm_3\frac{\boldsymbol{R}_2 - \boldsymbol{R}_3}{R_{32}^3}, \tag{5.2}$$

$$\ddot{\boldsymbol{R}}_3 = -Gm_1\frac{\boldsymbol{R}_3 - \boldsymbol{R}_1}{R_{13}^3} - Gm_2\frac{\boldsymbol{R}_3 - \boldsymbol{R}_2}{R_{23}^3}, \tag{5.3}$$

where $\boldsymbol{R}_i$, $i = 1, 2, 3$ are the position vectors expressed in an inertial reference frame. Suppose now that the two masses m_1 and m_2 represent the primaries, whereas m_3 the spacecraft mass: the restricted three-body problem is obtained by neglecting the effect of the spacecraft's gravitational attraction on the primaries. Thus, the equations read

$$\ddot{\boldsymbol{R}}_1 = -Gm_2\frac{\boldsymbol{R}_1 - \boldsymbol{R}_2}{R_{21}^3}, \tag{5.4}$$

$$\ddot{\boldsymbol{R}}_2 = -Gm_1\frac{\boldsymbol{R}_2 - \boldsymbol{R}_1}{R_{12}^3}, \tag{5.5}$$

$$\ddot{\boldsymbol{R}}_3 = -Gm_1\frac{\boldsymbol{R}_3 - \boldsymbol{R}_1}{R_{13}^3} - Gm_2\frac{\boldsymbol{R}_3 - \boldsymbol{R}_2}{R_{23}^3}. \tag{5.6}$$

The primaries are assumed to move under their mutual gravitational interaction described by the equations (5.4)-(5.5). Among all the conics, solutions of the corresponding Kepler problem, the primaries are assumed to move on circular orbits around their common center of mass: this defines the circular restricted three-body problem (CRTBP). The equations (5.4)-(5.6) can be rewritten in an inertial frame with the origin located at the barycenter of the two primaries:

$$\ddot{\boldsymbol{R}} = -Gm_1\frac{\boldsymbol{R} - \boldsymbol{R}_1}{R_1^3} - Gm_2\frac{\boldsymbol{R} - \boldsymbol{R}_2}{R_2^3}, \tag{5.7}$$

where $\boldsymbol{R}$, R_1 and R_2 denote the spacecraft's position and its distance from the primaries respectively. The equations of the CRTBP written in an inertial reference frame are time-dependent because $\boldsymbol{R}_1$ and $\boldsymbol{R}_2$ in equation (5.7) have explicit dependence on time. Thus, to make the equations autonomous, it is convenient to rewrite the dynamics in a rotating frame, where the primaries are at rest. The synodic system is used: it is centered at the barycenter of the primaries and rotates uniformly with them. The primaries are fixed on the x-axis, the y-axis is in their plane of motion, and the z-axis is bi-normal to x and y.

Eq. (5.7) can be rewritten in the synodic reference frame as

$$\frac{d^2\boldsymbol{r}}{dt^2} + 2\boldsymbol{\omega} \times \frac{d\boldsymbol{r}}{dt} + \boldsymbol{\omega} \times (\boldsymbol{\omega} \times \boldsymbol{r}) = -Gm_1\frac{\boldsymbol{r} - \boldsymbol{r_1}}{r_1^3} - Gm_2\frac{\boldsymbol{r} - \boldsymbol{r_2}}{r_2^3}, \tag{5.8}$$

where $\boldsymbol{r} = [x, y, z]^T$ denotes the spacecraft's position in the synodic reference frame, $\boldsymbol{r}_1 = [x_1, 0, 0]^T$ and $\boldsymbol{r}_2 = [x_2, 0, 0]^T$ denote the two fixed position of m_1 and m_2, with respect to the barycenter of the synodic reference frame, whereas r_1 and r_2 are the spacecraft's distance from the primaries.

The left hand side of equations (5.8) contains the centrifugal and Coriolis terms due to

the rotation of the reference frame, and $\boldsymbol{\omega} = [0, 0, n]^T$ is the uniform angular velocity of the primaries around their center of mass.
Equation (5.8) can be written as

$$\begin{aligned}
\ddot{x} - 2n\dot{y} - n^2 x = -Gm_1\frac{x - x_1}{r_1^3} - Gm_2\frac{x - x_2}{r_2^3} &= \frac{\partial}{\partial x}\left(\frac{Gm_1}{r_1} + \frac{Gm_2}{r_2}\right), \\
\ddot{y} - 2n\dot{x} - n^2 y = -Gm_1\frac{y}{r_1^3} - Gm_2\frac{y}{r_2^3} &= \frac{\partial}{\partial y}\left(\frac{Gm_1}{r_1} + \frac{Gm_2}{r_2}\right), \\
\ddot{z} = -Gm_1\frac{z}{r_1^3} - Gm_2\frac{z}{r_2^3} &= \frac{\partial}{\partial z}\left(\frac{Gm_1}{r_1} + \frac{Gm_2}{r_2}\right).
\end{aligned} \tag{5.9}$$

It is convenient to normalize units such that the distance between the two primaries, their angular velocity, and the sum of their masses are equal to one. With these dimensionless units, the equations of motion depend on one parameter only, namely the mass parameter, defined as

$$\mu = \frac{m_2}{m_1 + m_2}. \tag{5.10}$$

The value of the mass parameter for typical three-body problems in the solar system are listed in Table 5.1

Table 5.1: Mass parameters μ for some RTBP in the solar system.

	μ
Earth-Moon	0.012150582
Sun-Earth	$3.0034\ 10^{-6}$
Sun-Mars	$3.2268\ 10^{-7}$

With this choice $G = 1$, and the positions of the primaries are $\boldsymbol{r_1} = [-\mu, 0, 0]^T$ and $\boldsymbol{r_2} = [1 - \mu, 0, 0]^T$. Referring to Figure 5.1, the spacecraft distances from the primaries are

$$r_1 = \sqrt{(x + \mu)^2 + y^2 + z^2}, \tag{5.11}$$

$$r_2 = \sqrt{(x + \mu - 1)^2 + y^2 + z^2}. \tag{5.12}$$

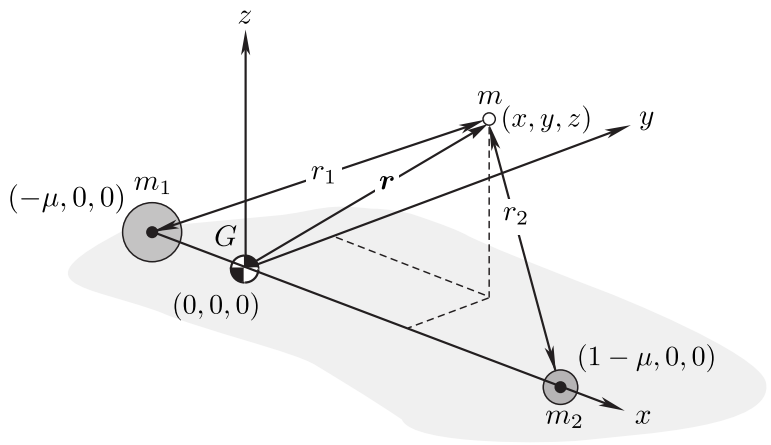

Figure 5.1: Three-body problem.

The dimensionless equation of the CRTBP are

$$\begin{aligned} \ddot{x} - 2\dot{y} &= \Omega_x, \\ \ddot{y} + 2\dot{x} &= \Omega_y, \\ \ddot{z} &= \Omega_z, \end{aligned} \tag{5.13}$$

where the subscripts denote the partial derivatives of the auxiliary function

$$\Omega(x, y, z) = \frac{1}{2}(x^2 + y^2) + \frac{1-\mu}{r_1} + \frac{\mu}{r_2} + \frac{1}{2}\mu(1-\mu) \tag{5.14}$$

written in Szebehely's coordinates [58]. Equations (5.13) can be rewritten in the explicit form

$$\begin{aligned} \ddot{x} &= 2\dot{y} + x - (1-\mu)\frac{(x+\mu)}{r_1^3} - \mu\frac{(x-1+\mu)}{r_2^3}, \\ \ddot{y} &= -2\dot{x} + y - \frac{(1-\mu)y}{r_1^3} - \mu\frac{y}{r_2^3}, \\ \ddot{z} &= -\frac{(1-\mu)z}{r_1^3} - \mu\frac{z}{r_2^3}, \end{aligned} \tag{5.15}$$

and the resulting ODEs system describing the low-thrust motion, expressed in the first-order form, is

$$\begin{cases} \dot{\boldsymbol{r}} &= \boldsymbol{v}, \\ \dot{\boldsymbol{v}} &= \boldsymbol{g}(\boldsymbol{r}) + \boldsymbol{h}(\boldsymbol{v}) + c_1\dfrac{u}{m}\boldsymbol{\alpha}, \\ \dot{m} &= -c_2 u, \end{cases} \tag{5.16}$$

where the expressions of $\boldsymbol{g}$ and $\boldsymbol{h}$ specific to the CRTBP are given by

$$\boldsymbol{g}(\boldsymbol{r}) = \begin{bmatrix} x - (1-\mu)\dfrac{(x+\mu)}{r_1^3} - \mu\dfrac{(x-1+\mu)}{r_2^3} \\ y - \dfrac{(1-\mu)y}{r_1^3} - \mu\dfrac{y}{r_2^3} \\ -\dfrac{(1-\mu)z}{r_1^3} - \mu\dfrac{z}{r_2^3} \end{bmatrix}, \tag{5.17}$$

$$\boldsymbol{h}(\boldsymbol{v}) = \begin{bmatrix} 2v_y \\ -2v_x \\ 0 \end{bmatrix}. \tag{5.18}$$

The CR3BP, expressed by (5.13) has five equilibrium points in the x, y-plane, known as Lagrangian or libration points. Three of them (L_1, L_2 and L_3) are *collinear* with the primaries, whereas the remaining two (L_4 and L_5) form equilater triangles with the primaries.

5.2 Boundary Conditions

System (5.16) is solved together with the following boundary conditions:

$$\boldsymbol{\psi}_0(\boldsymbol{x}(t_0); t_0) = \begin{bmatrix} \boldsymbol{r}(t_0) - \boldsymbol{r}_0 \\ \boldsymbol{v}(t_0) - \boldsymbol{v}_0 \\ m(t_0) - m_0 \end{bmatrix} = 0. \tag{5.19}$$

In the previous two-body model, we introduced the concept of sphere of influence and assumed that the spacecraft position coincides with the departure planet position. The initial state could be easily determined by considering the ephemeris and the only difference was in term of initial ΔV.

In the CRTBP the state of the spacecraft no longer coincides with one of the primaries at departure and at arrival. To this purpose, an orbital frame is instantaneously defined by the unit vectors $\hat{\boldsymbol{r}} - \hat{\boldsymbol{\theta}} - \hat{\boldsymbol{h}}$, where $\hat{\boldsymbol{r}}$ vector is parallel to the position vector, $\hat{\boldsymbol{h}}$ is parallel to the instantaneous angular momentum vector and finally $\hat{\boldsymbol{\theta}}$ completes the right-handed set.

Let us consider for instance a spacecraft departing from a circular orbit, so the initial

conditions in this frame are

$$\begin{aligned} \boldsymbol{r}^0_{orb} &= [r_0, 0, 0]^T, \\ \boldsymbol{v}^0_{orb} &= [0, v_0, 0]^T, \end{aligned}$$

where r_0 is the nominal radius of the initial orbit, set by the user, whereas $v_0 = \sqrt{(1-\mu)/r_0} + \Delta V$.
However a transformation in the $\hat{\boldsymbol{x}} - \hat{\boldsymbol{y}} - \hat{\boldsymbol{z}}$ synodic frame is required: it can be achieved by first transforming the initial state from the orbital frame to the inertial frame $\hat{\boldsymbol{i}} - \hat{\boldsymbol{j}} - \hat{\boldsymbol{k}}$, centered at the primary the spacecraft is orbiting around, throught the matrix

$$\boldsymbol{R} = \begin{bmatrix} (\cos\theta\cos\Omega - \cos i \sin\Omega \sin\theta) & (\cos\theta \sin\Omega + \cos i \cos\Omega \sin\theta) & \sin i \sin\theta \\ (-\sin\theta\cos\Omega - \cos i \sin\Omega \cos\theta) & (-\sin\theta \sin\Omega + \cos i \cos\Omega \cos\theta) & \sin i \cos\theta \\ \sin i \sin\Omega & -\sin i \cos\Omega & \cos i \end{bmatrix},$$

where Ω is the right ascension of the ascending node, i represents the inclination between the spacecraft and the primaries orbital plane, and θ stands for the argument of latitude. All angles are measured positive counterclockwise. The initial state in the inertial reference frame is therefore

$$\begin{aligned} \boldsymbol{r}^0_{iner} &= \boldsymbol{R}^T \boldsymbol{r}^0_{orb}, \\ \boldsymbol{v}^0_{iner} &= \boldsymbol{R}^T \boldsymbol{v}^0_{orb}. \end{aligned}$$

The synodic frame rotates with respect to the inertial frame with an angular velocity equal to the mean motion. A second transformation from the inertial to the rotating frame must therefore be performed: it is defined by the rotation matrix $\boldsymbol{T} = \boldsymbol{T}(t)$

$$\boldsymbol{T}(t) = \begin{bmatrix} \cos t & \sin t & 0 \\ -\sin t & \cos t & 0 \\ 0 & 0 & 1 \end{bmatrix}.$$

The dimensionless positions and velocities in the synodic reference frame can be expressed as

$$\boldsymbol{r}^0_{syn} = \boldsymbol{T} \boldsymbol{r}^0_{iner}, \tag{5.20}$$

$$\boldsymbol{v}^0_{syn} = \boldsymbol{T} \boldsymbol{v}^0_{iner} + \dot{\boldsymbol{T}} \boldsymbol{r}^0_{iner}, \tag{5.21}$$

where

$$\dot{\boldsymbol{T}} = \begin{bmatrix} -\sin t & \cos t & 0 \\ -\cos t & -\sin t & 0 \\ 0 & 0 & 1 \end{bmatrix}.$$

The coordinates in the synodic frame will have the same origin as the inertial frame. Therefore a final translation equal to the distance between the primary the spacecraft is orbiting around and the barycenter of the synodic frame is necessary. In the followings, we will consider transfer trajectories departing from some Earth parking orbits and the traslation will be described by the vector

$$\boldsymbol{s} = \begin{bmatrix} -\mu \\ 0 \\ 0 \end{bmatrix}. \tag{5.22}$$

The initial constraints finally read

$$\boldsymbol{\psi}_0(\boldsymbol{x}(t_0), t_0) = \begin{bmatrix} \boldsymbol{r}(t_0) - \boldsymbol{r}^0_{syn}(\Omega, i, \theta) \\ \boldsymbol{v}(t_0) - \boldsymbol{v}^0_{syn}(\Omega, i, \theta) \\ m(t_0) - m_0 \end{bmatrix} = 0. \tag{5.23}$$

Initial conditions may also be slightly modified to include more general classes of conics, defined by an initial set of complete orbital elements. Such initial conditions may be useful, for example, if a spacecraft is placed into a geosynchronous trasfer orbit (GTO). This orbit is particularly interesting because several low-cost spacecrafts (e.g. SMART-1) are launched as secondary payloads and so put in GTO orbits. The altitudes of the pericenter and the apocenter are respectively $h_p = 200$ km and $h_a = 35841$ km. Follows that the semimajor axis a and the eccentricity e are known; moreover the inclination i is typically small for such transfers so that it can be assumed to be equal to zero. Therefore, a simplified approach can be adopted for such orbits. It involves only two parameters: one angle ω, that is the argument of the periapsis of the initial GTO with respect to x-axis of the synodic frame, $0 \leq \omega \leq 2\pi$, and the initial excess velocity ΔV. The rotation matrix R from orbital to inertial Earth-centered frame is defined simply as

$$R = \begin{bmatrix} \cos\omega & \sin\omega & 0 \\ -\sin\omega & -\cos\omega & 0 \\ 0 & 0 & 1 \end{bmatrix}.$$

The initial point is assumed to correspond with the perigee of the GTO, in order to obtain the maximum increments of the apogee distance.

Trying to determine the solutions for these transfer trajectories however, appears to be very difficult: the long duration of the transfer combined with the need of very small values of initial Lagrange multipliers, consequent to the reduced distance from the primary at starting point (see eq. (5.42)-(5.43)), traduces into numerical difficulties regarding the computation of the shooting function and its Jacobian and inducing a very small convergence radius. Nevertheless, we noted that specially in the first part of the trajectory, the thrust vector is closely aligned with the velocity vector, whereas it shifts direction in the second part of the transfer to meet the state at the final point. This is not surprising since tangential thrust leads to the fastest change of the Jacobi constant as reported in [59]. A new approach is consequently adopted, presented also in [38], in which the first phase of the transfer is designed assuming the control magnitude at the maximum allowable level, aligned with the velocity of the spacecraft, viewed with respect to the synodic frame

$$\boldsymbol{u}(t) = c_1 \frac{\boldsymbol{v}(t)}{v(t)}. \tag{5.24}$$

The resulting trajectory is a spiral orbit around the Earth, that depends uniquely on the variables ω and ΔV. Moreover, this allows us to neglect the costate dynamics in the first phase, with great benefits on the optimization process, since it reduces the numerical difficulties previous mentioned. The trajectory is therefore subdivided into two different phases: the initial spiral phase, that, at this point, can be removed from the optimal control problem and optimized aside; and the second trajectory leg comprised between the initial spiral orbit and the prescribed halo orbit. A new design parameter τ_s is introduced: it is a time-like variable, taken along the spiral orbit, so that integrating from the starting conditions (the perigee of the GTO orbit) to the instant $t = \tau_s$ it is possible to identify a point on the spiral orbit that represents the initial boundary condition for the optimal control problem. The initial conditions in this case read

$$\boldsymbol{\psi}_0(\boldsymbol{x}(t_0), t_0) = \begin{bmatrix} \boldsymbol{r}(t_0) - \boldsymbol{r}^0_{syn}(\tau_s) \\ \boldsymbol{v}(t_0) - \boldsymbol{v}^0_{syn}(\tau_s) \\ m(t_0) - m_0 \end{bmatrix} = 0. \tag{5.25}$$

As far as the final boundary conditions are concerned, they can be expressed in the general form

$$\boldsymbol{\psi}_f(\boldsymbol{x}(t_f), t_f) = \begin{bmatrix} \boldsymbol{r}(t_f) - \boldsymbol{r}_f \\ \boldsymbol{v}(t_f) - \boldsymbol{v}_f \end{bmatrix} = 0. \tag{5.26}$$

Arrival orbits considered in this work are three-dimensional periodic orbits about the collinear libration points, also known as halo orbits, defined through the out-of-plane amplitude A_z. This is due to the fact that a growing interest for the periodic solutions about the collinear librations points has taken place in the last few years, and, among them, halo orbits appear to be the most promising. Their constant relative position with respect to the primaries, indeed, can be exploited for example by communication satellites or space telescopes.

Target halo orbits are constructed numerically in the synodic reference frame, by means of a sixth-order accurate scheme developed by Armellin et al. [3], starting by an analytical initial guess, based on the third-order Richardson expansion [48].

The values of $\boldsymbol{r}_f$ and $\boldsymbol{v}_f$ correspond to the position and velocity, in the synodic frame, of a final point that lies on the nominal halo orbit. However, this optimal final point is not fixed, but rather determined by the optimization process. Introducing a time variable $\tau_h \in [0, T_{halo}]$, taken along the orbit, each point y_h on the halo, can be uniquely identified by simply integrating the uncontrolled system (5.16) (with $\boldsymbol{u} = 0$), from the initial conditions $y_{h,0}$, necessary to generate the halo orbit, to the final instant $t = \tau_h$ as highlighted in Figure 5.2.

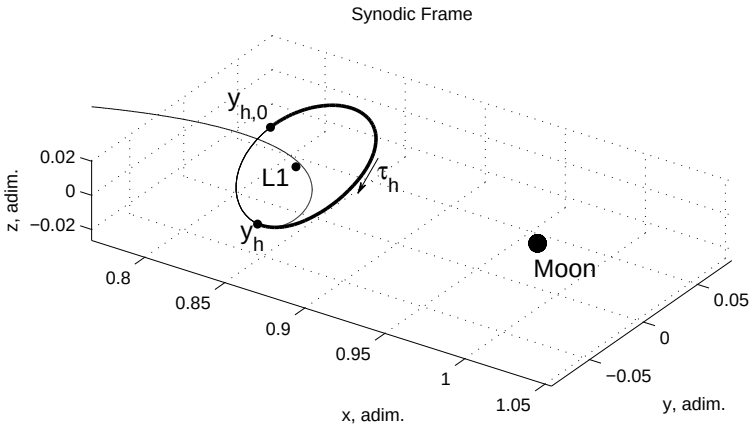

Figure 5.2: Halo orbit final conditions.

The final constriants can be rewritten as

$$\boldsymbol{\psi}_f(\boldsymbol{x}(t_f); t_f) = \begin{bmatrix} \boldsymbol{r}(t_f) - \boldsymbol{r}_f(\tau_h) \\ \boldsymbol{v}(t_f) - \boldsymbol{v}_f(\tau_h) \end{bmatrix} = 0. \tag{5.27}$$

5.3 Optimal Control Problem

As in the previous two-body formulation, we are looking for a solution that minimizes the propellant amount required for the transfer from the initial to the final boundaries. This request can be mathematically translated by introducing a performance index

$$\mathcal{J} = c_2 \int_{t_0}^{t_f} u dt. \tag{5.28}$$

At this point it is advantageous to adjoint the constraints (5.23)-(5.27) as well as the dynamics (5.16) to the performance index. All the following passages hold in the synodic reference frame.

$$\begin{aligned}\mathcal{J} = {\boldsymbol{\nu_1}}^T\big[\boldsymbol{r}(t_0) - \boldsymbol{r}_0(\Omega,i,\theta)\big] + {\boldsymbol{\nu_2}}^T\big[\boldsymbol{v}(t_0) - \boldsymbol{v}_0(\Omega,i,\theta)\big] + \\ \nu_3\big[m(t_0) - m_0\big] + {\boldsymbol{\nu_4}}^T\big[\boldsymbol{r}(t_f) - \boldsymbol{r}_f(\tau_h)\big] + {\boldsymbol{\nu_5}}^T\big[\boldsymbol{v}(t_f) - \boldsymbol{v}_f(\tau_h)\big] + \\ \int_{t_0}^{t_f}\big\{\mathcal{H} - \boldsymbol{\lambda}^T\dot{\boldsymbol{x}}\big\}dt,\end{aligned} \tag{5.29}$$

where the Hamiltonian is still defined as reported in (2.51)

$$\mathcal{H} = \mathcal{L} + \boldsymbol{\lambda}^T\boldsymbol{f} + \boldsymbol{\mu}^T\boldsymbol{C}(\boldsymbol{u},t), \tag{5.30}$$

which can be written explicitly as

$$\mathcal{H} = \boldsymbol{\lambda_r}\cdot\boldsymbol{v} + \boldsymbol{\lambda_v}\cdot\Big(\boldsymbol{g(r)} + \boldsymbol{h(v)} + c_1\frac{u}{m}\boldsymbol{\alpha}\Big) - \lambda_m c_2 u + c_2 u + \boldsymbol{\mu}^T\boldsymbol{C}(\boldsymbol{u}). \tag{5.31}$$

Taking the first variation of $\mathcal{J}$ and integrating by parts we obtain

$$\begin{aligned}\delta\mathcal{J} = {\boldsymbol{\nu_1}}^T\delta\boldsymbol{r}\big|_{t_0} - {\boldsymbol{\nu_1}}^T\frac{\partial\boldsymbol{r}_0(\Omega,i,\theta)}{\partial\Omega}\delta\Omega - {\boldsymbol{\nu_1}}^T\frac{\partial\boldsymbol{r}_0(\Omega,i,\theta)}{\partial i}\delta i - {\boldsymbol{\nu_1}}^T\frac{\partial\boldsymbol{r}_0(\Omega,i,\theta)}{\partial\theta}\delta\theta + \\ {\boldsymbol{\nu_2}}^T\delta\boldsymbol{v}\big|_{t_0} - {\boldsymbol{\nu_2}}^T\frac{\partial\boldsymbol{v}_0(\Omega,i,\theta)}{\partial\Omega}\delta\Omega - {\boldsymbol{\nu_2}}^T\frac{\partial\boldsymbol{v}_0(\Omega,i,\theta)}{\partial i}\delta i - {\boldsymbol{\nu_2}}^T\frac{\partial\boldsymbol{v}_0(\Omega,i,\theta)}{\partial\theta}\delta\theta + \\ \nu_3\delta m\big|_{t_0} + {\boldsymbol{\nu_4}}^T\delta\boldsymbol{r}\big|_{t_f} - {\boldsymbol{\nu_4}}^T\frac{\partial\boldsymbol{r}_f(\tau_h)}{\partial\tau_h}\delta\tau_h + {\boldsymbol{\nu_5}}^T\delta\boldsymbol{v}\big|_{t_f} - {\boldsymbol{\nu_5}}^T\frac{\partial\boldsymbol{v}_f(\tau_h)}{\partial\tau_h}\delta\tau_h + \\ \int_{t_0}^{t_f}\big\{\big(\mathcal{H}_x + \dot{\boldsymbol{\lambda}}\big)^T\delta\boldsymbol{x} + \mathcal{H}_u^T\delta\boldsymbol{u} + \big(\mathcal{H}_\lambda - \dot{\boldsymbol{x}}\big)^T\delta\boldsymbol{\lambda}\big\}dt + \\ \boldsymbol{\lambda}^T\delta\boldsymbol{x}\big|_{t_0} - \boldsymbol{\lambda}^T\delta\boldsymbol{x}\big|_{t_f}.\end{aligned} \tag{5.32}$$

Since $\delta\mathcal{J}$ must be zero, we obtain the first order necessary conditions

$$\begin{cases} \boldsymbol{\lambda}_{\boldsymbol{r}_0}^T = -\boldsymbol{\nu_1}^T \\ \boldsymbol{\lambda}_{\boldsymbol{v}_0}^T = -\boldsymbol{\nu_2}^T \\ \lambda_{m_0} = -\nu_3 \end{cases} \qquad \begin{cases} \boldsymbol{\lambda}_{\boldsymbol{r}_f}^T = \boldsymbol{\nu_4}^T \\ \boldsymbol{\lambda}_{\boldsymbol{v}_f}^T = \boldsymbol{\nu_5}^T \\ \lambda_{m_0} = 0 \end{cases} \tag{5.33}$$

and

$$\boldsymbol{\nu_1}^T \frac{\partial \boldsymbol{r}_0}{\partial \Omega} + \boldsymbol{\nu_2}^T \frac{\partial \boldsymbol{v}_0}{\partial \Omega} = 0, \tag{5.34}$$

$$\boldsymbol{\nu_1}^T \frac{\partial \boldsymbol{r}_0}{\partial i} + \boldsymbol{\nu_2}^T \frac{\partial \boldsymbol{v}_0}{\partial i} = 0, \tag{5.35}$$

$$\boldsymbol{\nu_1}^T \frac{\partial \boldsymbol{r}_0}{\partial \theta} + \boldsymbol{\nu_2}^T \frac{\partial \boldsymbol{v}_0}{\partial \theta} = 0, \tag{5.36}$$

$$\boldsymbol{\nu_4}^T \frac{\partial \boldsymbol{r}_0}{\partial \tau_h} + \boldsymbol{\nu_5}^T \frac{\partial \boldsymbol{v}_0}{\partial \tau_h} = 0. \tag{5.37}$$

Substituting eq.(5.33) into eqs. (5.34)-(5.37) , we obtain

$$\begin{bmatrix} \frac{\partial \boldsymbol{r}_0^T}{\partial \Omega} & \frac{\partial \boldsymbol{v}_0^T}{\partial \Omega} \\ \frac{\partial \boldsymbol{r}_0^T}{\partial i} & \frac{\partial \boldsymbol{v}_0^T}{\partial i} \\ \frac{\partial \boldsymbol{r}_0^T}{\partial \theta} & \frac{\partial \boldsymbol{v}_0^T}{\partial \theta} \end{bmatrix} \begin{Bmatrix} \boldsymbol{\lambda}_{\boldsymbol{r}_0} \\ \boldsymbol{\lambda}_{\boldsymbol{v}_0} \end{Bmatrix} = 0 \tag{5.38}$$

and

$$\boldsymbol{\lambda}_{\boldsymbol{r}_f}^T \frac{\partial r_f}{\partial \tau_h} + \boldsymbol{\lambda}_{\boldsymbol{v}_f}^T \frac{\partial v_f}{\partial \tau_h} = 0, \tag{5.39}$$

that is

$$\boldsymbol{\lambda}_{\boldsymbol{r}_f}^T \boldsymbol{v}_{\tau_h} + \boldsymbol{\lambda}_{\boldsymbol{v}_f}^T \left(\boldsymbol{g}_{\tau_h} + \boldsymbol{h}_{\tau_h} \right) = 0. \tag{5.40}$$

Therefore, initial and final values of position and velocity costates should satisfy the relations (5.38)-(5.40). However, in order to simplify the formulation of the optimal control problem, we elect to treat initial and final states as fixed, ignoring these relations with the presumption that they are implicity driven to zero by the optimization process. The trasversality conditions reduces to the eqs. (5.33), in which initial and final costates are free. Ω, i, θ and τ_h still represent design variables, but their optimization is left to a parametric optimization rather to the optimal control theory. Similarly in the case of a GTO starting orbit, the transversality conditions depend on the derivatives with

respect to τ_s.

$$\boldsymbol{\lambda}_{\boldsymbol{r}\,0}^{\boldsymbol{T}}\boldsymbol{v}_{\tau_s} + \boldsymbol{\lambda}_{\boldsymbol{v}\,0}^{\boldsymbol{T}}\left(\boldsymbol{g}_{\tau_s} + \boldsymbol{h}_{\tau_s}\right) = 0. \tag{5.41}$$

However, as mentioned before, we neglect those variables in the optimal control problem, and assume the initial and final state to be fixed. The optimization is restored numerically through Matlab's optimization toolbox, adjoining τ_s to the optimization vector.
In both cases the initial mass multiplier is free and positive, while final conditions requires that its final value is equal to zero.

From eq.(5.32) we derive also the Euler-Lagrange equations. In particular, the costate differential equations in this case are slightly different since we have

$$\dot{\boldsymbol{\lambda}}_{\boldsymbol{r}} = -\boldsymbol{G}^T\boldsymbol{\lambda}_{\boldsymbol{v}}, \qquad \dot{\boldsymbol{\lambda}}_{\boldsymbol{v}} = -\boldsymbol{\lambda}_{\boldsymbol{r}} - \boldsymbol{H}^T\boldsymbol{\lambda}_{\boldsymbol{v}}, \qquad \dot{\lambda}_m = -c_1\frac{u}{m^2}\lambda_v, \tag{5.42}$$

where $\boldsymbol{G}(\boldsymbol{r})$ and $\boldsymbol{H}(\boldsymbol{v})$ represent the gradients $\frac{\partial \boldsymbol{g}}{\partial \boldsymbol{r}}$ and $\frac{\partial \boldsymbol{h}}{\partial \boldsymbol{v}}$, respectively.

$$\begin{aligned}
G_{1,1} &= 1 - \frac{(1-\mu)}{r_1^3} + 3(1-\mu)\frac{(x+\mu)^2}{r_1^5} - \frac{\mu}{r_2^3} + 3\mu\frac{(x-1+\mu)^2}{r_2^5} \\
G_{2,2} &= 1 - \frac{(1-\mu)}{r_1^3} + 3(1-\mu)\frac{y^2}{r_1^5} - \frac{\mu}{r_2^3} + 3\mu\frac{y^2}{r_2^5} \\
G_{3,3} &= -\frac{(1-\mu)}{r_1^3} + 3(1-\mu)\frac{z^2}{r_1^5} - \frac{\mu}{r_2^3} + 3\mu\frac{z^2}{r_2^5} \\
G_{1,2} &= 3(1-\mu)\frac{(x+\mu)y}{r_1^5} + 3\mu\frac{(x-1+\mu)y}{r_2^5} \\
G_{1,3} &= 3(1-\mu)\frac{(x+\mu)z}{r_1^5} + 3\mu\frac{(x-1+\mu)z}{r_2^5} \\
G_{2,3} &= 3(1-\mu)\frac{yz}{r_1^5} + 3\mu\frac{yz}{r_2^5} \\
G_{2,1} &= G_{1,2} \\
G_{3,1} &= G_{1,3} \\
G_{3,2} &= G_{2,3}
\end{aligned} \tag{5.43}$$

$$\boldsymbol{H} = \begin{bmatrix} 0 & 2 & 0 \\ -2 & 0 & 0 \\ 0 & 0 & 0 \end{bmatrix}. \tag{5.44}$$

Finally, it is interesting to note that the optimality conditions are the same as for the two-body model formulation. Thus, Lawden's primer vector control law (2.64) is still in force.

5.4 Numerical Techniques

Once we have defined the boundary conditions and the design variables, we need to explain how the optimization is carried out. We specify right now that, contrarily to recent approaches [43], the proposed method does not make explicit use of invariant manifolds.

As mentioned previously in the two-body model formulation, one of the most difficult aspects in obtaining a solution to an Euler-Lagrange formulation of the problem, is generating an accurate initial guess for the costate variables. This time, however, the previous approach, based on the solution of a minimum-energy problem is not effective, due to the complexity and high nonlinearity of the vector field: indeed we note that the solution drastically changes passing from the energy-optimal to the fuel-optimal problem.

The main difficulty in estimating the initial costates values is the lack of physical meaning. Dixon and Biggs [16] first introduced the idea to estimate physical control variables and their derivatives instead of the initial costates in order to reduce problem sensitivity and provide more of a physical significance. In particular Ranieri [46] developed a mapping procedure based on the transformation in the spacecraft velocity frame. As a result, the initial angles for the thrust unit vector α, β and their derivatives $\dot{\alpha}$, $\dot{\beta}$ are introduced to map the initial costates into more physically realizable parameters using the Adjoint Control Transformation (ACT).

Consider a reference frame centered at the spacecraft and defined by the unit vectors $\hat{\boldsymbol{v}} - \hat{\boldsymbol{w}} - \hat{\boldsymbol{h}}$, where $\hat{\boldsymbol{v}}$ axis is aligned with the velocity vector $\boldsymbol{v}$. The $\hat{\boldsymbol{h}}$ axis is parallel to the instantaneous angular momentum vector $\boldsymbol{r} \times \boldsymbol{v}$. Finally, the $\hat{\boldsymbol{w}}$ axis is defined to complete a right-handed system. These unit vectors, and the associated time derivatives are defined as

$$\hat{\boldsymbol{v}} = \frac{\boldsymbol{v}}{v}, \qquad \hat{\boldsymbol{h}} = \frac{\boldsymbol{r} \times \boldsymbol{v}}{\|\boldsymbol{r} \times \boldsymbol{v}\|}, \qquad \hat{\boldsymbol{w}} = \hat{\boldsymbol{h}} \times \hat{\boldsymbol{v}} \tag{5.45}$$

$$\dot{\hat{\boldsymbol{v}}} = \dot{\boldsymbol{v}}/v - \boldsymbol{v}\dot{v}/v^2, \tag{5.46}$$

$$\dot{\hat{\boldsymbol{h}}} = \dot{\boldsymbol{h}}/h - \boldsymbol{h}\dot{h}/h^2, \tag{5.47}$$

$$\dot{\hat{\boldsymbol{w}}} = \dot{\hat{\boldsymbol{h}}} \times \hat{\boldsymbol{v}} + \hat{\boldsymbol{h}} \times \dot{\hat{\boldsymbol{v}}}, \tag{5.48}$$

where the following relations must be considered to fully determine the previous equations

$$\dot{v} = \boldsymbol{v} \cdot \dot{\boldsymbol{v}}/v, \tag{5.49}$$

$$\dot{h} = \boldsymbol{h} \cdot \dot{\boldsymbol{h}}/h. \tag{5.50}$$

The thrust-direction unit vector in this frame is

$$\hat{\boldsymbol{u}}_{vwh} = [\cos\alpha\cos\beta \qquad \sin\alpha\cos\beta \qquad \sin\beta]^T. \tag{5.51}$$

Its time derivative is

$$\dot{\hat{\boldsymbol{u}}}_{vwh} = \begin{bmatrix} -\dot{\alpha}\sin\alpha\cos\beta - \dot{\beta}\cos\alpha\sin\beta \\ \dot{\alpha}\cos\alpha\cos\beta - \dot{\beta}\sin\alpha\sin\beta \\ \dot{\beta}\cos\beta \end{bmatrix}. \tag{5.52}$$

Because the equations of motion are integrated in the barycentric rotating frame, a rotation matrix is required to transform the thrust direction $\hat{\boldsymbol{u}}_{vwh}$ and $\dot{\hat{\boldsymbol{u}}}_{vwh}$:

$$\boldsymbol{R} = \begin{bmatrix} \hat{\boldsymbol{i}}\cdot\hat{\boldsymbol{v}} & \hat{\boldsymbol{i}}\cdot\hat{\boldsymbol{w}} & \hat{\boldsymbol{i}}\cdot\hat{\boldsymbol{h}} \\ \hat{\boldsymbol{j}}\cdot\hat{\boldsymbol{v}} & \hat{\boldsymbol{j}}\cdot\hat{\boldsymbol{w}} & \hat{\boldsymbol{j}}\cdot\hat{\boldsymbol{h}} \\ \hat{\boldsymbol{k}}\cdot\hat{\boldsymbol{v}} & \hat{\boldsymbol{k}}\cdot\hat{\boldsymbol{w}} & \hat{\boldsymbol{k}}\cdot\hat{\boldsymbol{h}} \end{bmatrix}, \qquad \dot{\boldsymbol{R}} = \begin{bmatrix} \hat{\boldsymbol{i}}\cdot\dot{\hat{\boldsymbol{v}}} & \hat{\boldsymbol{i}}\cdot\dot{\hat{\boldsymbol{w}}} & \hat{\boldsymbol{i}}\cdot\dot{\hat{\boldsymbol{h}}} \\ \hat{\boldsymbol{j}}\cdot\dot{\hat{\boldsymbol{v}}} & \hat{\boldsymbol{j}}\cdot\dot{\hat{\boldsymbol{w}}} & \hat{\boldsymbol{j}}\cdot\dot{\hat{\boldsymbol{h}}} \\ \hat{\boldsymbol{k}}\cdot\dot{\hat{\boldsymbol{v}}} & \hat{\boldsymbol{k}}\cdot\dot{\hat{\boldsymbol{w}}} & \hat{\boldsymbol{k}}\cdot\dot{\hat{\boldsymbol{h}}} \end{bmatrix}. \tag{5.53}$$

The derivative of the thrust unit vector is expressed in the sinodic frame as

$$\dot{\hat{\boldsymbol{u}}}_{ijk} = \dot{\boldsymbol{R}}\hat{\boldsymbol{u}}_{vwh} + \boldsymbol{R}\dot{\hat{\boldsymbol{u}}}_{vwh}. \tag{5.54}$$

Thus, from eq. (2.60)

$$\boldsymbol{\lambda_v} = -\lambda_v \hat{\boldsymbol{u}}_{ijk}. \tag{5.55}$$

For the position costate instead

$$\boldsymbol{\lambda_r} = -\dot{\boldsymbol{\lambda}}_{\boldsymbol{v}} - \boldsymbol{H^T}\boldsymbol{\lambda_v}. \tag{5.56}$$

The derivative of the primer vector $\dot{\boldsymbol{\lambda}}_{\boldsymbol{v}}$ can be obtained by differentiating eq.(5.55)

$$\dot{\boldsymbol{\lambda}}_{\boldsymbol{v}} = -\dot{\lambda}_v \hat{\boldsymbol{u}}_{ijk} - \lambda_v \dot{\hat{\boldsymbol{u}}}_{ijk}. \tag{5.57}$$

Following this process, we replace the unknown values of the initial position and velocity costates with the physically meaningful quantities α, $\dot{\alpha}$, β, $\dot{\beta}$, λ_{v0} and $\dot{\lambda}_{v0}$. However,

the adjoint control transformation is only used to initialize the position and velocity costates, whereas the computation of costates at successive times is obtained as always by directly integrating eq. (5.42).
Consequently, the optimization process is summarized as follows:

1. Inizialize the optimization vector

$$X_0 = [TOF, \Omega_0, i_0, \theta_0, \alpha_0, \dot{\alpha}_0, \beta_0, \dot{\beta}_0, \lambda_{v_0}, \dot{\lambda}_{v_0}, \tau_h, \lambda_{m_0}, m_f]$$

   or

$$X_0 = [TOF, \tau_s, \alpha_0, \dot{\alpha}_0, \beta_0, \dot{\beta}_0, \lambda_{v_0}, \dot{\lambda}_{v_0}, \tau_h, \lambda_{m_0}, m_f]$$

   depending on the initial orbit around the Earth (circular or GTO);

2. input upper and lower bounds for each of the optimization variables;

3. calculate initial and final state $\boldsymbol{r}_0$, $\boldsymbol{v}_0$, $\boldsymbol{r}_f$ and $\boldsymbol{v}_f$;

4. apply the adjoint control transformation to compute $\boldsymbol{\lambda_{r_0}}$ and $\boldsymbol{\lambda_{v_0}}$;

5. set the initial value for the continuation parameter and integrate spacecraft state and costate according to the derived control structure;

6. evaluate the constraint violations;

7. search for optimal values of optimization variables to reduce the constraint violations and minimize the performance index;

8. iterate on the continuation parameter, using the solution found as first guess for the next iteration;

9. solve the discontinuous problem.

A further consideration regards the case of initial GTO orbit. Indeed we have seen that the initial spiral trajectory is not comprised in the optimal control problem, but should be optimized aside. To this purpose a possibility is by means of genetic algorithms. The values of ω and ΔV are sought in order to maximize the spacecraft energy with respect to the Earth in a given interval of time.

5.5 Results

5.5.1 Circular to Halo Orbits Transfers

The first example is an Earth-to-Halo transfer starting by an initial high circular orbit with a radius equal to $r_0 = 125000$ km to an $A_z = 8000$ km halo orbit around L1. Moreover, the initial mass is 1500 kg, while the maximum thrust assumed to be available is $T_{max} = 0.33$ N with a $I_{sp} = 3800$ s. Tables 5.2-5.3 show the search space for the optimization parameters, while Figures 5.3(a)-5.3(b) present the optimal trajectory in both the synodic and the inertial reference frame. In this example the time of flight is ≈ 49 days, and the final mass is about 1481.5 kg with a propellant mass fraction of 1.233%. Figure 5.3(c)-5.3(d) show the thrust magnitude and the mass consumption.

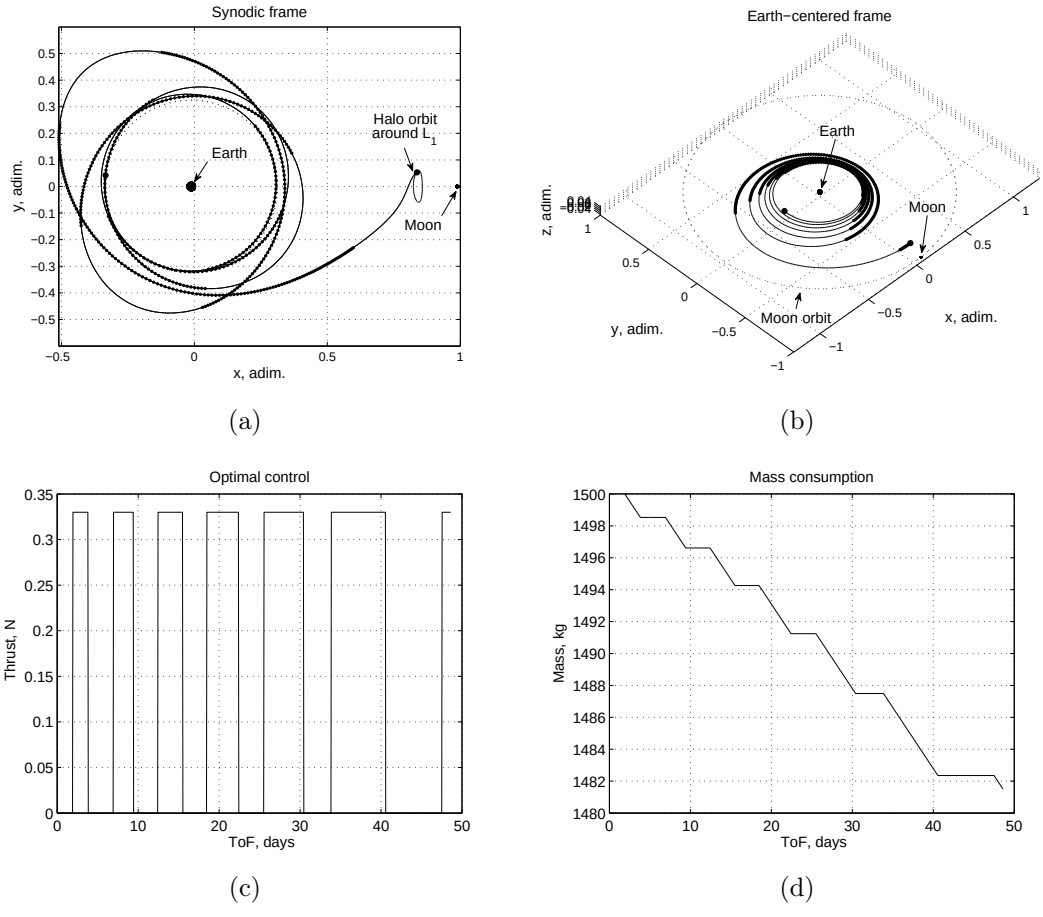

Figure 5.3: Low-thrust transfer to a $A_z = 8000$ km L_1 halo orbit, departing from a $r_0 = 125000$ km circular orbit: (a) Synodic frame; (b) Inertial frame; (c) Thrust profile; (d) Mass consumption.

Table 5.2: Search space and solution for circular to L_1 halo orbit transfer (I).

	TOF [days]	Ω_0 [rad]	i_0 [rad]	θ_0 [rad]	τ_h [TU]	λ_{m_0}	m_f [%m_0]
upper	50	2π	$\pi/2$	2π	T_h	1	1
lower	30	0	$-\pi/2$	0	0	0	0.5
solution	48.62	2.85	0.04	0.1326	3.33	0.02	0.988

Table 5.3: Search space and solution for circular to L_1 halo orbit transfer (II).

	α_0 [rad]	$\dot{\alpha}_0$ [rad/TU]	β_0 [rad]	$\dot{\beta}_0$ [rad/TU]	λ_{v_0}	$\dot{\lambda}_{v_0}$
upper	2π	∞	2π	∞	∞	∞
lower	0	$-\infty$	0	$-\infty$	0	$-\infty$
solution	2.25	-0.0063	0.1224	-0.3656	0.0038	0.0529

Previously we assumed that the conditions (5.38)-(5.40), on the initial and final values of the costates, could be neglected in order to simplify the optimal control formulation. It is interesting now to evaluate those relations for the obtained solution, in order to quantify the committed error. Table 5.4 reports the violations of the transversality conditions. As can be seen the violations are very small and their influence on the optimal solution is negligible, justifying our assumption.

Table 5.4: Transversality conditions violations.

condition	complete optimal control formulation	simplified optimal control formulation
eq. (5.38)	$[0, 0, 0]^T$	$[0.4940, -0.6457, 0.4366]^T\ 10^{-3}$
eq. (5.40)	0	$-8.9690\ 10^{-4}$

5.5.2 GTO to Halo Orbits Transfers

The second example is again an Earth-to-Halo transfer, this time starting from an initial GTO orbit with perigee and apogee altitudes equal to $h_p = 400$ km and $h_a = 35864$ km, respectively. The spacecraft is characterized by an initial mass of about 1000 kg, with a propulsion system capable to provide a maximum of 0.5 N, with a $I_{sp} = 3000$ s. This example is taken from [38]. In order to reproduce the reference solution the angle

ω and initial excess velocity ΔV are fixed and equal to $\pi/2$ and 0, respectively. Figures 5.4(a)-5.4(b) illustrate the solution obtained. The final mass is about 907.16 kg with a propellant mass fraction m_p/m_0 of 9.28%, whereas the total time of flight is 77.88 days. Tables 5.5-5.6 report the search space and the optimal values for the optimization variables. Figures 5.4(c)-5.4(d) show instead the thrust amplitude and the propellant mass consumption: as can be seen, in the first part of the transfer the engine is on duty at the maximum level and the trajectory consists in a tangential spiral arc. In the last part, the optimal control problem is solved and the bang-bang structure of the control law becomes visible.

Again, evaluating the violations of the transversality conditions, we find small errors equal to -0.001667 for eq.(5.41) and -0.007293 for eq.(5.40).

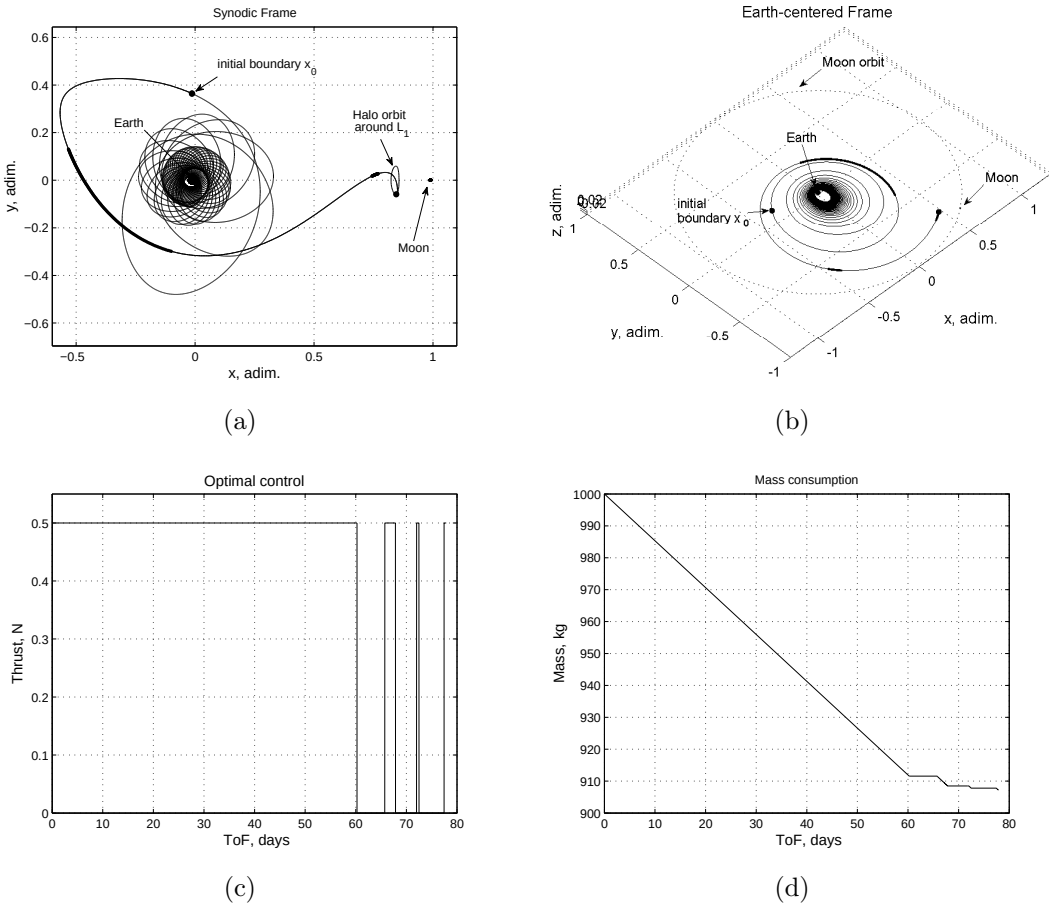

Figure 5.4: Low-thrust transfer to the $A_z = 8000$ km L_1 halo orbit, departing from a GTO: (a) Synodic frame; (b) Inertial frame; (c) Thrust profile; (d) Mass consumption.

Table 5.5: Search space and solution for GTO to L_1 halo orbit transfer (I).

	TOF [days]	τ_s [TU]	τ_h [TU]	λ_{m_0}	m_f [%m_0]
upper	25	14.95	T_h	1	1
lower	10	0	0	0	0.5
solution	17.65	13.85	8.81	5.3e-3	0.907

Table 5.6: Search space and solution for GTO to L_1 halo orbit transfer (II).

	α_0 [rad]	$\dot{\alpha}_0$ [rad/TU]	β_0 [rad]	$\dot{\beta}_0$ [rad/TU]	λ_{v_0}	$\dot{\lambda}_{v_0}$
upper	0.5	10	0.5	10	0.1	0.1
lower	-0.5	-10	-0.5	-10	0	-0.1
solution	-0.324	-0.751	-0.175	-3.864	0.0244	-0.0831

Figures 5.5(a)-5.5(d) illustrate a transfer from the same initial GTO orbit to the $A_z =$ 8000 km halo orbit around L_2. The corresponding solution is reported in Tables 5.7-5.8. The propellant mass fraction m_p/m_0 in this case is about 9.51%, whereas the total time of flight is approximately 85.43 days.

Table 5.7: Search space and solution for GTO to L_2 halo orbit (I).

	TOF [days]	τ_s [TU]	τ_h [TU]	λ_{m_0}	m_f [%m_0]
upper	35	14.95	T_h	1	1
lower	5	0	0	0	0.5
solution	23.24	14.27	2.48	4.6e-3	0.905

Table 5.8: Search space and solution for GTO to L_2 halo orbit (II).

	α_0 [rad]	$\dot{\alpha}_0$ [rad/TU]	β_0 [rad]	$\dot{\beta}_0$ [rad/TU]	λ_{v_0}	$\dot{\lambda}_{v_0}$
upper	0.5	10	0.5	10	0.1	0.1
lower	-0.5	-10	-0.5	-10	0	-0.1
solution	-0.4561	0.6337	0.3457	0.0836	0.0395	-0.0606

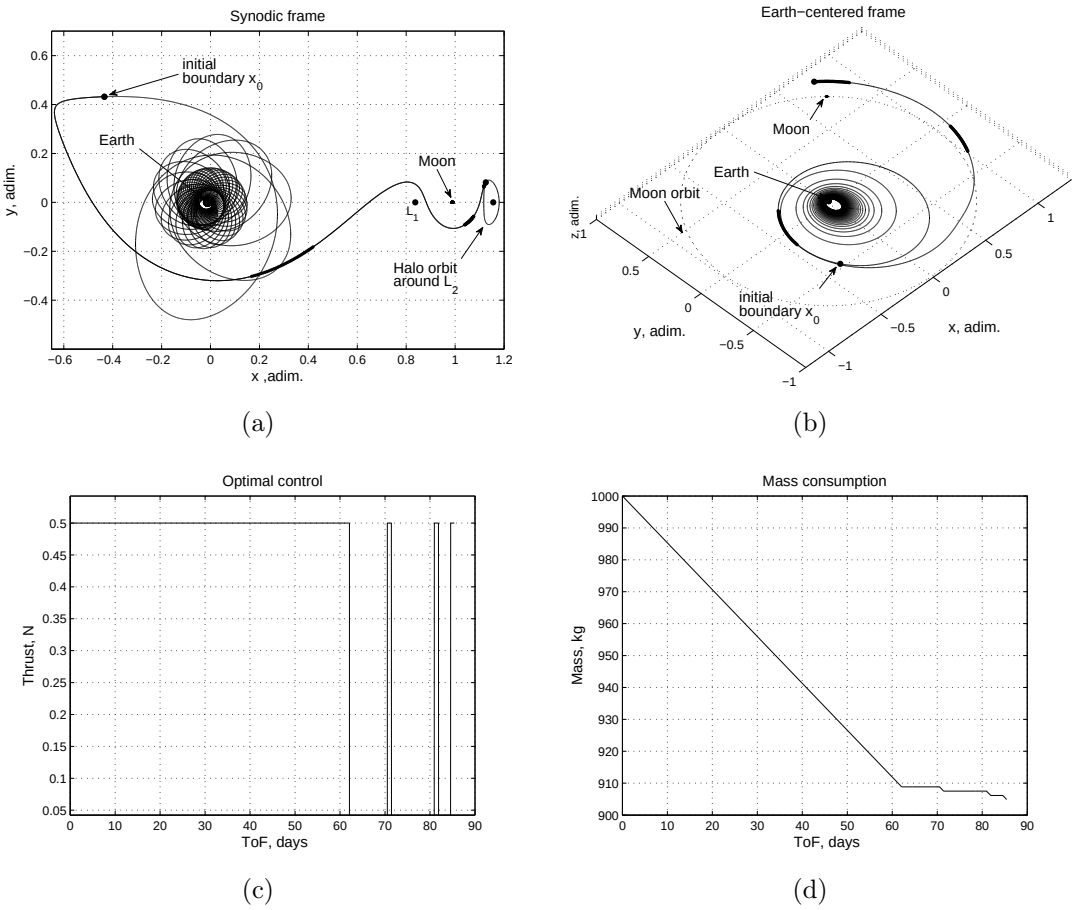

Figure 5.5: Low-thrust transfer to the $A_z = 8000$ km L_2 halo orbit, departing from a GTO: (a) Synodic frame; (b) Inertial frame; (c) Thrust profile; (d) Mass consumption.

It is worth investigating how the solution changes if the values of ω, which characterizes the orientation of the initial spiral leg, is optimized through genetic algorithms, as suggested in section 5.4. The search interval is $[0, 2\pi]$ rad, while the value of ΔV is still forced to be zero. The optimal value obtained is $\omega = 0.078$ rad. The optimal transfer is reported in Figures 5.6(a)-5.6(d), while Tables 5.9-5.10 summarize the values obtained for the optimization variables. In particular, both the propellant mass fraction m_p/m_0, equal to 9.25%, and the total transfer time, approximately 77.11 days, are slightly lower than the previous case.

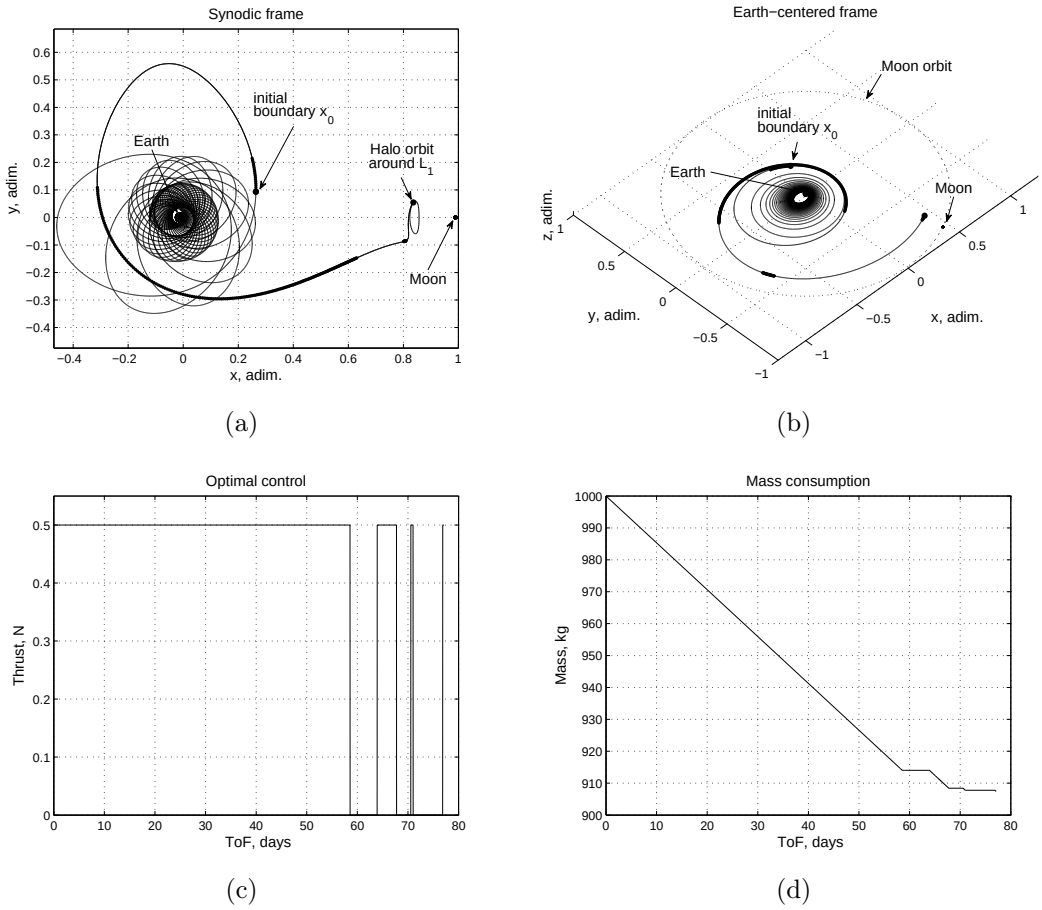

Figure 5.6: Low-thrust transfer to the $A_z = 8000$ km L_1 halo orbit, departing from a GTO with a initial ω of 0.078 rad: (a) Synodic frame; (b) Inertial frame; (c) Thrust profile; (d) Mass consumption.

Table 5.9: Search space and solution for GTO to L_1 halo orbit transfer with free initial ω (I).

	TOF [days]	τ_s [TU]	τ_h [TU]	λ_{m_0}	m_f [%m_0]
upper	35	18.39	T_h	1	1
lower	10	0	0	0	0.5
solution	18.89	13.39	2.38	1.1e-2	0.9074

Table 5.10: Search space and solution for GTO to L_1 halo orbit transfer with free initial ω (II).

	α_0 [rad]	$\dot{\alpha}_0$ [rad/TU]	β_0 [rad]	$\dot{\beta}_0$ [rad/TU]	λ_{v_0}	$\dot{\lambda}_{v_0}$
upper	0.5	10	0.5	10	0.1	0.1
lower	-0.5	-10	-0.5	-10	0	-0.1
solution	0.298	-0.875	-0.500	-0.024	0.032	0.020

Let us consider now an initial ΔV at the perigee of the GTO orbit, with a maximum value of 0.2 km/s. The search intervals for ω and ΔV are $[0, 2\pi]$ rad and $[0, 0.2]$ km/s respectively. Using genetic algorithms, the solution obtained is $\omega = 2.216$ rad and $\Delta V = 0.2$ km/s: obviously the maximum admissible value for the initial ΔV is selected. The solution slightly changes, as can be seen in Figures 5.7(a)-5.7(b).

Table 5.11: Search space and solution for GTO to L_1 halo orbit transfer with initial $\Delta V = 0.2$ km/s (I).

	TOF [days]	τ_s [TU]	τ_h [TU]	λ_{m_0}	m_f [$\%m_0$]
upper	35	14.95	T_h	1	1
lower	10	0	0	0	0.5
solution	27.96	11.94	8.838	6.8e-3	0.918

Table 5.12: Search space and solution for GTO to L_1 halo orbit transfer with initial $\Delta V = 0.2$ km/s (II).

	α_0 [rad]	$\dot{\alpha}_0$ [rad/TU]	β_0 [rad]	$\dot{\beta}_0$ [rad/TU]	λ_{v_0}	$\dot{\lambda}_{v_0}$
upper	0.5	10	0.5	10	0.1	0.1
lower	-0.5	-10	-0.5	-10	0	-0.1
solution	-0.14	-1.218	0.467	-0.988	0.0288	0.0238

As can be seen in Tables 5.11-5.12, the final mass is higher and equal to 918.01 kg, which means a propellant mass fraction m_p/m_0 of 8.198%, whereas the total time of flight is approximately 79.88 days, almost comparable with the previous cases. However, it should be noted that the initial spiral phase, in this case, is shorter than the previous

solution, while a longer final optimal controlled phase is needed to match the final state.

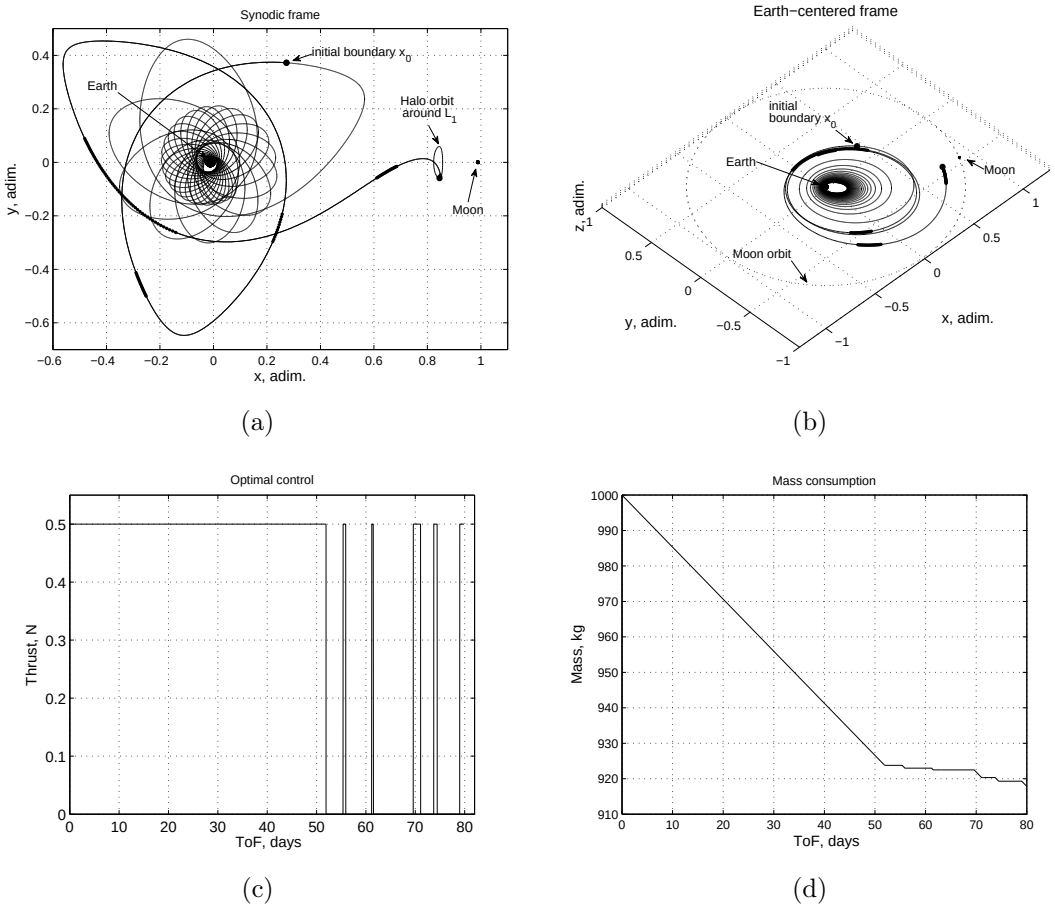

Figure 5.7: Low-thrust transfer to the $A_z = 8000$ km L_1 halo orbit, departing from a GTO with a initial ΔV of 0.2 km/s: (a) Synodic frame; (b) Inertial frame; (c) Thrust profile; (d) Mass consumption.

The previous solutions are characterized by a maximum admissible thrust value of 0.5 N, that could require a considerable amount of power. In order to obtain more attractive solutions, a transfer from GTO to $A_z = 8000$ km L_1 halo orbit with a $T_{max} = 0.33$ N is considered in the next example. The obtained values for ω is $0.724792480468750\ 10^{-4}$, whereas the initial ΔV has been forced to zero. All other optimization variables are listed in Tables 5.13-5.14, along with their search space. The corresponding trajectory is depicted in Figures 5.8(a)-5.8(d). As can be seen the lower value of thrust involve an higher transfer time, equal to 123.62 days. The propellant mass fraction instead is 9.97%.

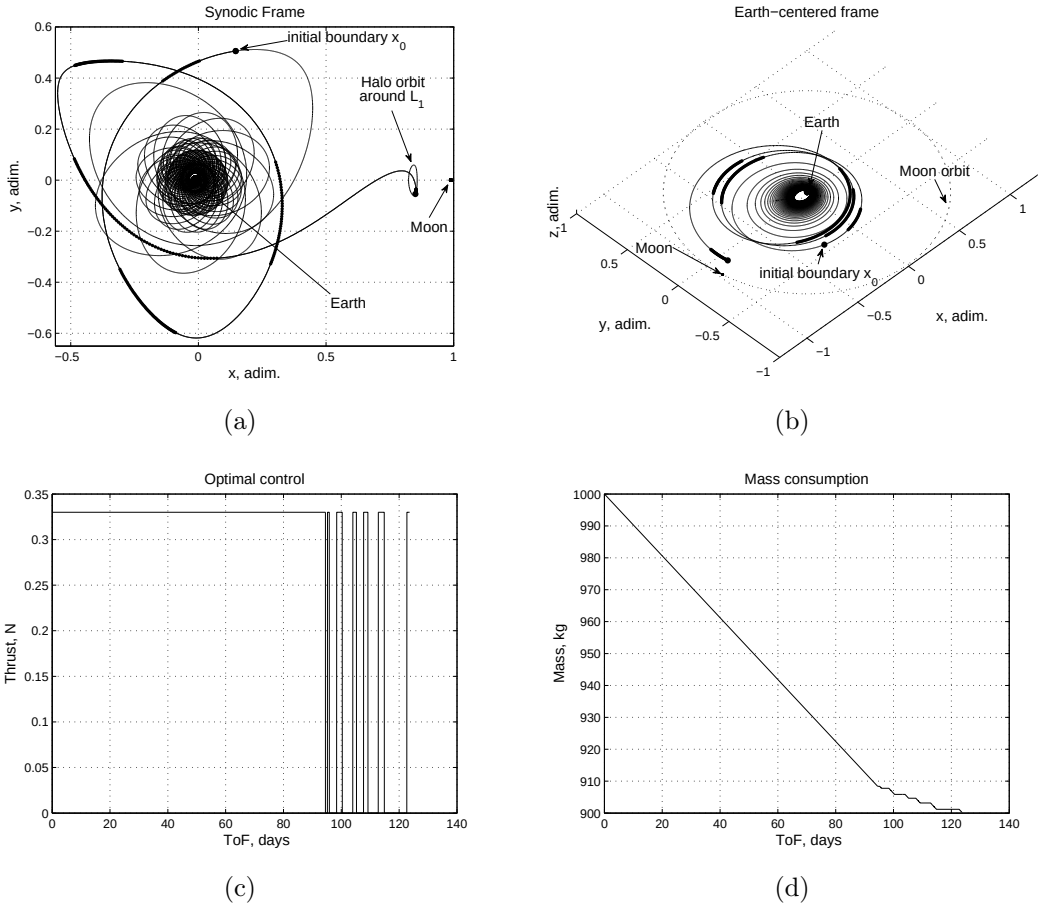

Figure 5.8: Low-thrust transfer to the $A_z = 8000$ km L_1 halo orbit, departing from a GTO with a maximum admissible thrust of 0.33 N: (a) Synodic frame; (b) Inertial frame; (c) Thrust profile; (d) Mass consumption.

Table 5.13: Search space and solution for GTO to L_1 halo orbit transfer with maximum admissible thrust of 0.33 N (I).

	TOF [days]	τ_s [TU]	τ_h [TU]	λ_{m_0}	m_f [$\%m_0$]
upper	35	14.95	T_h	1	1
lower	10	0	0	0	0.5
solution	29.094	21.739	8.224	0.010	0.9003

Table 5.14: Search space and solution for GTO to L_1 halo orbit transfer with maximum admissible thrust of 0.33 N (II).

	α_0 [rad]	$\dot{\alpha}_0$ [rad/TU]	β_0 [rad]	$\dot{\beta}_0$ [rad/TU]	λ_{v_0}	$\dot{\lambda}_{v_0}$
upper	0.5	10	0.5	10	0.1	0.1
lower	-0.5	-10	-0.5	-10	0	-0.1
solution	0.024	-1.843	0.101	0.690	0.027	0.037

5.5.3 L_1 Halo to L_2 Halo Transfers

As last example, we consider a transfer from a L_1 halo orbit to a L_2 halo orbit in the Earth-Moon three-body system. Both halos have an amplitude $A_z = 8000$ km. The spacecraft is characterized by an initial mass of 1000 kg, with a maximum thrust of 0.5 N and $I_{sp} = 3000$.

The starting point is sought follow the same strategy illustrated for the final point, thus we have two time variables τ_{h1} and τ_{h2} for initial and final halo orbit respectively.

The fuel-optimal solution consists in approximately 13.5 days transfer with an overall propellant consumption of about 0.265%. More information of the obtained solution are listed in Tables 5.15-5.16, whereas the corresponding trajectory is presented in Figures 5.9(a)-5.9(d). The transfer starts with the engine on duty, in order to depart from the initial halo orbit. At the arrival, a small thrust arc is required instead to match the state on the final halo orbit.

Table 5.15: Search space and solution for the transfer trajectory from L_1 halo orbit to L_2 halo orbit (I).

	TOF [days]	τ_{h1} [TU]	τ_{h2} [TU]	λ_{m_0}	m_f [%m_0]
upper	35	2.7459	3.4086	1	1
lower	5	0	0	0	0.5
solution	13.48	0.3451	1.4874	2.8e-3	0.9974

Table 5.16: Search space and solution for the transfer trajectory from L_1 halo orbit to L_2 halo orbit (II).

	α_0 [rad]	$\dot{\alpha}_0$ [rad/TU]	β_0 [rad]	$\dot{\beta}_0$ [rad/TU]	λ_{v_0}	$\dot{\lambda}_{v_0}$
upper	0.5	10	0.5	10	0.1	0.1
lower	-0.5	-10	-0.5	-10	0	-0.1
solution	-0.4561	0.6337	0.3457	0.0836	0.0395	-0.0606

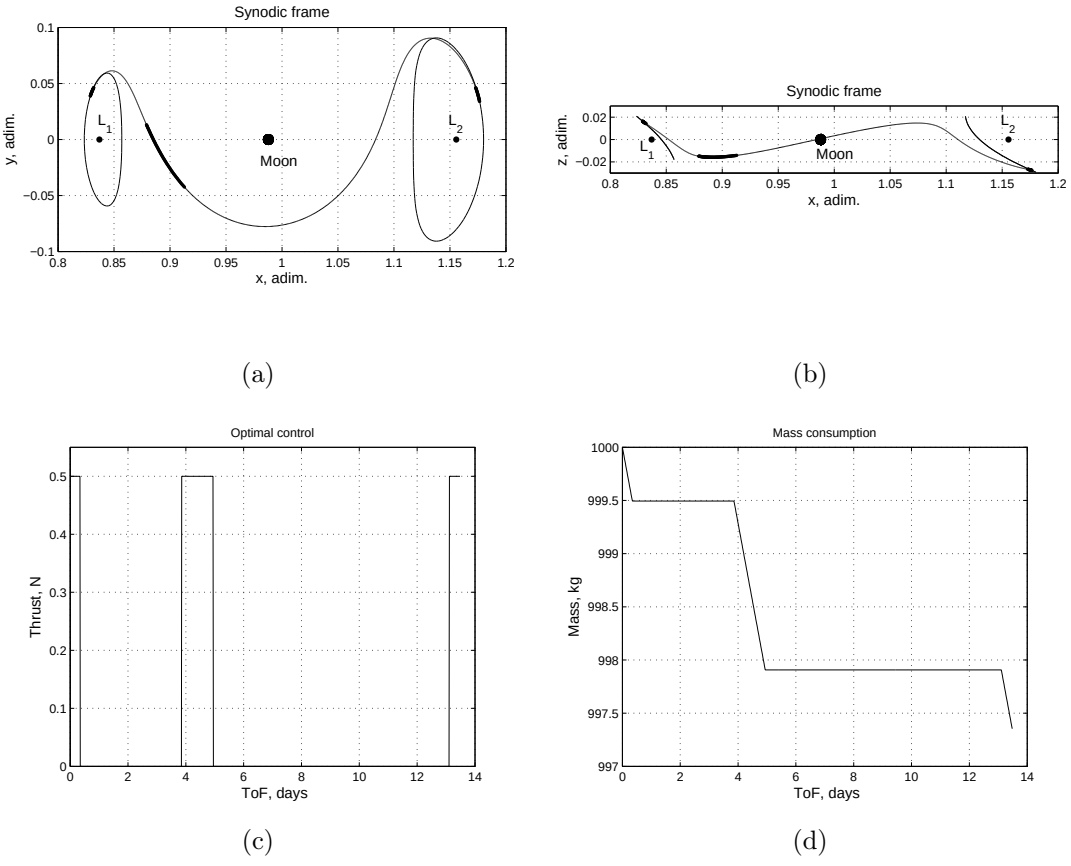

Figure 5.9: Low-thrust transfer from a $A_z = 8000$ km L_1 halo orbit to a $A_z = 8000$ km L_2 halo orbit: (a) Synodic frame, xy plane; (b) Synodic frame, xz plane; (c) Thrust profile; (d) Mass consumption.

Chapter 6

Conclusions and Future Developments

Final considerations on the performed work and suggestions for future improvements are reported in this chapter.

6.1 Conclusions

The main purpose of this thesis was the development and the assessment of the performances of an efficient and robust method, aimed at designing low-thrust trajectories in the two-body and three-body dynamics.
The first part of the thesis is focused on the design of optimal low-thrust interplanetary transfers in the two-body dynamics. In this context, the optimal control theory has been introduced and the related first order necessary conditions were derived, through the calculus of variations. Significant effort was spent in deriving the trasversality conditions for different kind of intermediate constraints and in implementing a method for the solution of the associated multi-point boundary value problem. In particular, the proposed computational scheme consists of different steps: firstly, a trajectory optimization tool based on genetic algorithms is used to find an approximate reference solution. Subsequently, the MPBVP, associated to the indirect method, is solved with parametric optimization, whose additional goal is optimizing those variables neglected in the formulation of the optimal control problem. However, first-guesses for the optimization variables are required, specially for the initial costate values. To this aim, an energy-optimal problem, characterized by a simplified control law, has been introduced

and easily solved. Starting from this energy-optimal solution, a continuation method is exploited to favor the convergence of the algorithm by smoothly approximating the behaviour of the bang-bang control law, and then obtaining the discontinuous solution of the fuel-optimal problem.
In the second part of the thesis, the system description based on two-body model has been replaced with the circular restricted three-body problem (CRTBP), in order to widen the set of mission scenarios. The equations of motion of the CRTBP are moderately complex and give rise to an extremely challenging optimal control problem, that emphasizes the numerical difficulties in obtaining an optimal solution. Within this context, the optimal control problem is still transcribed into a parameter optimization problem. However the energy-optimal problem turned out to be unsuitable in this case, and it has been replaced with an adjoint control trasformation, whose aim is to introduce new and more physically meaningful optimization variables. The fuel-optimal problem is faced, as in the two-body problem, by means of a continuation process, to approximate the discontinuous profile of the control law.
The performances of the algorithm have been evaluated in an intensive test phase, that proved the efficiency of the algorithm in finding accurate solutions to the fuel-optimal problem in both two-body and three-body dynamics. In particular, test cases show that the optimization process implemented is able to compute a wide range of trajectories of increasing complexity, obtaining comparable results with existing solutions.

6.2 Developments

Clearly, the implemented algorithm is not free of further possible improvements. First of all, the path of the continuation parameter is still heuristic and varies depending on the case considered. A more accurate implementation could therefore be developed, possibly based on an adaptive scheme, that autonomously selects the most suitable values for this parameter.
Furthermore, the analytical computation of the Jacobian of the constraints could help the convergence of the numerical algorithm, specially for high-dimensional problems. The formulation used, in fact, leads to a simplified structure of the Jacobian that can be conveniently constructed providing the requested partial derivatives in an analytical way. Although not implemented here, the sensitivity issues, common to indirect shooting methods, clearly encourage the use of analytic derivatives rather than estimating them numerically. Nonetheless, this task is nontrivial and further considerations are required for a careful implementation, specially when gravity assist maneuvers are in-

cluded.

Significant improvements could be obtained also with the use of a parallel implementation, in which all the transfer phases are computed and propagated in parallel for the constraints evaluation.

Moreover, various extensions of the currently used dynamical models offer opportunities and challenges for future works. The gravitational attraction of the Sun and its perturbative effects, for example, should be considered, thus leading to a more complete dynamical formulation. The application of different kinds of intermediate constraints, such as powered gravity assists or deep space maneuvers with the corresponding first order necessary conditions, should be investigated. Additional path constraints on the state or control variables (e.g. a variable maximum thrust level, depending on the power available) could be included. The minimization of alternative performance criteria could also be investigated in order to develop a more general optimization software.

Finally, a question rises spontaneously: what happens if the adjoint control transformation is exploited also in the two-body formulation? How are the algorithm performances affected? The answers are to be sought in future developments, together with the search for more efficient techniques to obtain accurate first guesses for the optimization variables.

Lastly, the proposed design method in CRTBP does not make explicit use of invariant manifolds. Thus, a further possible development is the inclusion of the invariant manifolds associated to the final halo orbits in the algorithm, in order to obtain solutions that combine the benefits associated to a low-energy transfer with those of a low-thrust trajectory.

List of Symbols and Acronyms

Latin symbols:

a	Semimajor axis
e	Eccentricity
g_0	Gravitational acceleration at sea level
h_a	Apocenter altitude
h_p	Pericenter altitude
i	Inclination
i, j, k	Integer numbers
m	Mass
m_p	Propellant mass
$m_{1,2}$	Masses of the primaries
n	Angular velocity of the primaries
p	Continuation parameter
q	Integer number
r	Position
$r_{1,2}$	Distance between the spacecraft and the primaries in synodic frame
r_{ph}	Pericenter radius of the hyperbolic trajectory
t	Time
t_0	Initial time
t_f	Final time
t_i^+	Intermediate time just after the encounter
t_i^-	Intermediate time just before the encounter
u	Engine thrust ratio
v	Velocity
v_∞	Relative velocity amplitude at the sphere of influence
$y_{h,0}$	Halo orbit initial conditions
$\boldsymbol{f}$	Force vector
$\boldsymbol{r}$	Position vector
$\boldsymbol{r}_{1,2}$	Position of the primaries in synodic frame
$\boldsymbol{s}$	Translation vector

$\boldsymbol{u}$	Control vector
$\boldsymbol{u}_{\alpha,\delta}$	Unit vector of polar angles α and δ
$\boldsymbol{v}$	Velocity vector
$\boldsymbol{v}_\infty$	Relative velocity vector at the sphere of influence
$\boldsymbol{x}$	State vector
A_z	Halo out-of-plane z-amplitude
I_{sp}	Specific impulse
R_i	Distance between the spacecraft and the primaries in inertial frame
R_{ij}	Distance between i-th and j-th mass particles in inertial frame
T_{halo}	Period of the halo orbit
T_{max}	Maximum admissible thrust
U	Potential energy or Domain of feasible controls
$\boldsymbol{C}_i$	Initial conditions vector at i-th node
$\boldsymbol{R}$	Spacecraft position vector in inertial reference frame or Rotation matrix
$\boldsymbol{R}_i$	Position vector of i-th mass particle in inertial frame
$\boldsymbol{T}$	Transformation matrix from inertial to synodic reference frame
$\mathcal{H}$	System Hamiltonian
$\mathcal{J}$	Performance index
$\mathcal{L}$	Accumulated cost function

Greek symbols:

α	Thrust direction
δ_{ga}	Turn angle of the gravity assist
θ	Argument of latitude
λ_m	Mass costate
μ	Gravitational constant or Mass parameter of the three-body system
ρ	Switching function
τ_h	Time variable on halo orbit
τ_s	Time variable on initial spyral orbit
ω	Argument of the periapsis
$\boldsymbol{\lambda}$	Costate vector
$\boldsymbol{\lambda_r}$	Position costate vector
$\boldsymbol{\lambda_v}$	Velocity costate vector
$\boldsymbol{\mu}$	Control conditions Lagrange multipliers
$\boldsymbol{\nu}$	Boundary conditions Lagrange multiplier
$\boldsymbol{\xi}^i$	Optimization variables vector at i-th node

$\boldsymbol{\pi}$	Intermediate boundary conditions Lagrange multipliers
$\boldsymbol{\chi}$	Intermediate boundary conditions
$\boldsymbol{\psi}^0$	Initial boundary conditions
$\boldsymbol{\psi}^f$	Final boundary conditions
$\boldsymbol{\psi}_i$	Intermediate boundary conditions
$\boldsymbol{\omega}$	Angular velocity vector
ΔV	Instant velocity variation
Ω	Right ascension of the ascending node
$\boldsymbol{\Xi}^{\boldsymbol{i}}$	Optimized decision vector at i-th node
$\boldsymbol{\Upsilon}$	Global optimization vector
$\boldsymbol{\Psi}_i$	Constraints vector at i-th node

Acronyms:

ACT	Adjoint Control Transformation
AU	Astronomical Unit
CR3BP	Circular-Restricted Three-Body Problem
GA	Genetic Algorithms
GTO	Geosynchronous trasfer orbit
GTOC	Global Trajectory Optimization Competition
MGA	Multiple Gravity Assist
MJD2000	Modified Julian Date 2000
MPBVP	Multi-Point Boundary Value Problem
NLP	Nonlinear programming
ODE	Ordinary Differential Equation
PMP	Pontryagin Maximum Principle
ToF	Time of Flight
TPBVP	Two Point Boundary Value Problem
TU	Time unit

Bibliography

[1] K. Alemany and R.D. Braun. Survey of Global Optimization Methods for Low-Thrust, Multiple Asteroid Tour Missions. 2007.

[2] R. Armellin, P. Di Lizia, A. Morselli, M. Lavagna, and F. Bernelli Zazzera. Space Trajectory Optimisation Under Uncertainties. *Ariadna study 10/4101.*

[3] R. Armellin and F. Topputo. A Sixth-Order Accurate Scheme for Solving Two-Point Boundary Value Problems in Astrodynamics. *Celestial Mechanics and Dynamical Astronomy*, 96(3):289–309, 2006.

[4] E Belbruno. Lunar Capture Orbits, a Method of Constructing Earth-Moon Trajectories and the Lunar GAS Mission. In *AIAA, DGLR, and JSASS, International Electric Propulsion Conference, 19 th, Colorado Springs, CO*, page 1987, 1987.

[5] R. Bertrand and R. Epenoy. New Smoothing Techniques for Solving Bang-Bang Optimal Control Problems-Numerical Results and Statistical Interpretation. *Optimal Control Applications and Methods*, 23(4):171–197, 2002.

[6] J.T. Betts. Survey of Numerical Methods for Trajectory Optimization. *Journal of Guidance, Control, and Dynamics*, 21(2), 1998.

[7] M. Bramanti, C.D. Pagani, and S. Salsa. *Matematica: calcolo infinitesimale e algebra lineare.* Zanichelli, 2000.

[8] A.E. Bryson and Y.C. Ho. *Applied Optimal Control: Optimization, Estimation, and Control.* Hemisphere Pub, 1975.

[9] P. Carrara. Strategia per l'Ottimizzazione di Trasferimenti Spaziali. Master's thesis, Politecnico di Milano, 2007.

[10] L. Casalino and G. Colasurdo. Optimization of δv Earth-Gravity-Assist Trajectories. *Journal of Guidance, Control, and Dynamics*, 21(6):991–995, 1998.

[11] L. Casalino and G. Colasurdo. Optimization of Variable-Specific-Impulse Interplanetary Trajectories. *Journal of Guidance, Control, and Dynamics*, 27(4):678–684, 2004.

[12] L. Casalino, G. Colasurdo, and D. Pastrone. Optimization Procedure for Preliminary Design of Opposition-Class Mars Missions. *Journal of Guidance, Control, and Dynamics*, 21(1):134–140, 1998.

[13] L. Casalino, D. Pastrone, and G. Colasurdo. Optimal Low-Thrust Escape Trajectories Using Gravity Assist. *Journal of Guidance, Control, and Dynamics*, 22(5):637–642, 1999.

[14] G. Colasurdo and L. Casalino. Missions to Asteroids Using Solar Electric Propulsion. *Acta Astronautica*, 50(11):705–711, 2002.

[15] Politecnico di Torino. Global Trajectory Optimization Competition, 2007. `http://areeweb.polito.it/eventi/gtoc3/`.

[16] LCW Dixon and MC Biggs. *The Advantages of Adjoint-Control Transformations when Determining Optimal Trajectories by Pontryagin's Maximum Principle*. Numerical Optimisation Centre, Hatfield Polytechnic, 1969.

[17] D.P.S. Dos Santos, L. Casalino, G. Colasurdo, and A.F.B.D.A. Prado. Optimal Trajectories Using Gravity Assisted Maneuver and Solar Electric Propulsion (Sep) Towards Near-Earth-Objects.

[18] P. Enright and B. Conway. Discrete Approximations to Optimal Trajectories Using Direct Transcription and Nonlinear Programming. *Journal of Guidance, Control, and Dynamics*, 15(4):994–1002, 1992.

[19] Y. Gao and CA Kluever. Low-Thrust Interplanetary Orbit Transfers Using Hybrid Trajectory Optimization Method with Multiple Shooting. *AIAA/AAS Astrodynamics Specialist Conference and Exhibit*, 16-19 August 2004.

[20] G. Gómez, A. Jorba, J. Masdemont, and C. Simó. Study of the Transfer From the Earth to a Halo Orbit Around the Equilibrium Point L1. *Celestial Mechanics and Dynamical Astronomy*, 56(4):541–562, 1993.

[21] K. Graichen and N. Petit. A Continuation Approach to State and Adjoint Calculation in Optimal Control Applied to the Reentry Problem. In *Proceeding of the 17th World Congress the International Federation of Automatic Control, Seoul, Korea*, pages 14307–14312, 2008.

[22] I.S. Grigoriev and K.G. Grigoriev. Conditions of the Maximum Principle in the Problem of Optimal Control over an Aggregate of Dynamics Systems and Their Application to Solution of the Problem of Optimal Control of Spacecraft Motion. *Cosmic Research*, 41(3):285–209, 2003. Translated from Kosmicheskie Issledovaniya, Vol.41, No. 3, 2003, pp. 307-331.

[23] M. Guelman. Earth-to-Moon Transfer with a Limited Power Engine. *Journal of Guidance, Control, and Dynamics*, 18(5):1133–1138, 1995.

[24] T. Haberkorn, P. Martinon, J. Gergaud, et al. Low Thrust Minimum-Fuel Orbital Transfer: A Homotopic Approach. *Journal of Guidance, Control, and Dynamics*, 27(6):1046–1060, 2004.

[25] CR Hargraves and SW Paris. Direct Trajectory Optimization Using Nonlinear Programming and Collocation. *Journal of Guidance, Control and Dynamics*, 10(4):338–342, 1987.

[26] R.F. Hartl, S.P. Sethi, and R.G. Vickson. A Survey of the Maximum Principles for Optimal Control Problems with State Constraints. *SIAM review*, pages 181–218, 1995.

[27] KC Howell, DL Mains, and BT Barden. Transfer Trajectories from Earth Parking Orbits to Sun-Earth Halo Orbits. *Spaceflight mechanics 1994*, pages 399–422, 1994.

[28] D.J. Jezewski. Primer Vector Theory and Applications. *NASA TR R-454*, Nov. 1975.

[29] F. Jiang, H. Baoyin, and J. Li. Practical Techniques for Low-Thrust Trajectory Optimization with Homotopic Approach. *Journal of Guidance, Control, and Dynamics*, 35(1):245–258, 2012.

[30] J.A. Kechichian. Optimal Low-Earth-Orbit-Geostationary-Earth-Orbit Intermediate Acceleration Orbit Transfer. *Journal of Guidance, Control, and Dynamics*, 20(4):803–811, 1997.

[31] H. Kuninaka, K. Nishiyama, I. Funaki, T. Yamada, Y. Shimizu, and J. Kawaguchi. Asteroid Rendezvous of Hayabusa Explorer Using Microwave Discharge Ion Engines. In *29th International Electric Propulsion Conference, number IEPC-2005-10*, Princeton University, 2005.

[32] M. La Mantia and L. Casalino. Indirect Optimization of Low-Thrust Capture Trajectories. *Journal of Guidance, Control, and Dynamics*, 29(4):1011–1014, 2006.

[33] D.F. Lawden. *Optimal Trajectories for Space Navigation*. Butterworths, London, 1963.

[34] J.P. Marec. *Optimal Space Trajectories*. Elsevier, Amsterdam, 1979.

[35] C.A.L. Martell and A. John. Adjoint Variable Solutions via an Auxiliary Optimization Problem. *Journal of Guidance, Control, and Dynamics*, 18:1267–1271, 1995.

[36] P. Martinon and J. Gergaud. Using Switching Detection and Variational Equations for the Shooting Method. *Optimal Control Applications and Methods*, 28(2):95–116, 2007.

[37] G. Mengali and A.A. Quarta. Trajectory Design with Hybrid Low-Thrust Propulsion System. *Journal of Guidance, Control, and Dynamics*, 30(2):419–426, 2007.

[38] G. Mingotti, F. Topputo, and F. Bernelli-Zazzera. Low-Thrust, Invariant-Manifolds Trajectories to Halo Orbits.

[39] K. Muinonen and E. Bowell. Asteroid Orbit Determination Using Bayesian Probabilities. *Icarus*, 104(2):255–279, 1993.

[40] Sir Isaac Newton. *Philosophiae Naturalis Principia Mathematica*. London, I edition, 1687.

[41] C. Ocampo. An Architecture for a Generalized Spacecraft Trajectory Design and Optimization System. In *Libration Point Orbits and Applications Proceedings of the Conference*, pages 529–571. World Scientific Publishing Co. Pte. Ltd., 2003.

[42] J.T. Olympio. Optimal Control Problem for Low-Thrust Multiple Asteroid Tour Missions. *Journal of Guidance, Control, and Dynamics*, 34(6):1709–1719, 2011.

[43] MT Ozimek and KC Howell. Low-Thrust Transfers in the Earth-Moon System, Including Applications to Libration Point Orbits. *Journal of Guidance, Control, and Dynamics*, 33(2):533, 2010.

[44] A.E. Petropoulos and J.M. Longuski. Shape-Based Algorithm for Automated Design of Low-Thrust, Gravity-Assist Trajectories. *Journal of Spacecraft and Rockets*, 41(5):787–796, 2004.

[45] L.S. Pontryagin, V.G. Boltyanskiy, R.V. Gamkrelidze, and E.F. Mishchenko. *The Mathematical Theory of Optimal Processes*. Wiley-Interscience, 1 edition, 1962.

[46] C.L. Ranieri and C.A. Ocampo. Optimization of Roundtrip, Time-Constrained, Finite Burn Trajectories via an Indirect Method. *Journal of Guidance, Control, and Dynamics*, 28(2):306–314, 2005.

[47] M.D. Rayman, P. Varghese, D.H. Lehman, and L.L. Livesay. Results from the Deep Space 1 Technology Validation Mission. *Acta Astronautica*, 47(2-9):475–487, 2000.

[48] D.L. Richardson. Analytic Construction of Periodic Orbits About the Collinear Points. *Celestial Mechanics and Dynamical Astronomy*, 22(3):241–253, 1980.

[49] S.M. Roberts and J.S. Shipman. Two-Point Boundary Value Problems: Shooting Methods. 1972.

[50] CT Russel, CA Raymond, TC Fraschetti, MD Rayman, CA Polanskey, KA Schimmels, and SP Joy. Dawn Mission and Operations. In *International Astronomical Union Symposium on Asteroids, Comets, and Meteors*, Rio de Janeiro, Brazil, 7-12 August 2005.

[51] R.P. Russell. Primer Vector Theory Applied to Global Low-Thrust Trade Studies. *Journal of Guidance, Control, and Dynamics*, 30(2):460–472, 2007.

[52] C.G. Sauer Jr. Optimization of Multiple Target Electric Propulsion Trajectories. *AIAA Paper 73-205*, Jan. 1973.

[53] J. Schoenmaekers, D. Horas, and J.A. Pulido. SMART-1: With Solar Electric Propulsion to the Moon. In *16th International Symposium on Space Flight Dynamics, Pasadena, California*, volume 3, 2001.

[54] H. Seywald and R.R. Kumar. Method for Automatic Costate Calculation. *Journal of Guidance, Control, and Dynamics*, 19(6):1252–1261, 1996.

[55] YC Sim, SB Leng, and V. Subramaniam. A Combined Genetic Algorithms-Shooting Method Approach to Solving Optimal Control Problems. *International Journal of Systems Science*, 31(1):83–89, 2000.

[56] J.A. Sims and S.N. Flanagan. Preliminary Design of Low Thrust Interplanetary Missions. *Astrodynamics 1999*, pages 583–592, 2000.

[57] T.F. Starchville. Optimal Low-Thrust Trajectories to Earth-Moon L2 Halo Orbits (Circular Problem). *Astrodynamics 1997*, pages 1741–1756, 1997.

[58] V.G. Szebehely. Theory of Orbits, the Restricted Problem of Three Bodies. 1967.

[59] F. Topputo. *Low-thrust Non-Keplerian Orbits: Analysis, Design and Control*. PhD thesis, Politecnico di Milano, 2007.

[60] F. Topputo, M. Vasile, and F. Bernelli-Zazzera. Low Energy Interplanetary Transfers Exploiting Invariant Manifolds of the Restricted Three-Body Problem. *Journal of the Astronautical Sciences*, 53(4):353–372, 2005.

[61] SR Vadali and RS Nah. Fuel-Optimal, Low-Thrust, Three-Dimensional Earth-Mars Trajectories. *Journal of Guidance, Control and Dynamics*, 24(6):1100–1107, 2001.

[62] O. von Stryk and R. Bulirsch. Direct and Indirect Methods for Trajectory Optimization. *Annals of Operations Research*, 37(1):357–373, 1992.

[63] C.H. Yam, T.T. McConaghy, K.J. Chen, and J.M. Longuski. Preliminary Design of Nuclear Electric Propulsion Missions to the Outer Planets. In *AIAA/AAS Astrodynamics Specialist Conference, AIAA Paper*, volume 5393, pages 16–19, 2004.